X-RAY CRYSTALLOGRAPHIC STUDIES ON SOME NON-CODED AMINO ACID-BASED PEPTIDES

A THESIS
SUBMITTED FOR THE DEGREE OF
DOCTOR OF PHILOSOPHY IN THE
FACULTY OF SCIENCE, JADAVPUR UNIVERSITY

2025

BY

DEETI JYOTHI

CSIR-INDIAN INSTITUTE OF CHEMICAL BIOLOGY
INFECTIOUS DISEASES AND IMMUNOLOGY DIVISION
4, RAJA S. C. MULLICK ROAD, JADAVPUR
KOLKATA-700 032, INDIA

सी.एस.आई.आर–भारतीय रासायनिक जीवविज्ञान संस्थान
वैज्ञानिक तथा औद्योगिक अनुसंधान परिषद की एक इकाई
विज्ञान एवं प्रौद्योगिकी मंत्रालय के अधीन, एक स्वायत्त निकाय, भारत सरकार
4, राजा एस. सी. मल्लिक रोड, यादवपुर, कोलकाता - 700 032
CSIR - INDIAN INSTITUTE OF CHEMICAL BIOLOGY
A Unit of Council of Scientific & Industrial Research
An Autonomous Body, under Ministry of Science & Technology, Government of India
4, Raja S. C. Mullick Road, Jadavpur, Kolkata-700 032

CERTIFICATE FROM THE SUPERVISOR

This is to certify that the thesis entitled **"X-RAY CRYSTALLOGRAPHIC STUDIES ON SOME NON-CODED AMINO ACID-BASED PEPTIDES"** submitted by **Smt. DEETI JYOTHI**, who got her name registered on 08.08.2019 [Registration no. **SLSBT1100919**, Index no. **9/19/Lifesc./26**] for the award of Ph.D. (Science) degree of **Jadavpur University**, is based upon her own work under the supervision of **Dr. UMESH PRASAD SINGH** and that neither this thesis nor any part of it has been submitted for either any degree/diploma or any other academic award anywhere before.

उमेश सिंह
28/02/2025

(Signature of supervisor & date with official Seal)

DR. UMESH PRASAD SINGH (Sr. Principal Scientist)
Infectious Diseases and Immunology Division
CSIR-Indian Institute of Chemical Biology
Jadavpur, Kolkata-700032, India

डॉ. उमेश प्रसाद सिंह / Dr. Umesh Prasad Singh
वरिष्ठ प्रधान वैज्ञानिक / Senior Principal Scientist
सीएसआईआर-भारतीय रासायनिक जीवविज्ञान संस्थान
(वैज्ञानिक तथा औद्योगिक अनुसंधान परिषद)
CSIR - Indian Institute of Chemical Biology
(Council of Scientific & Industrial Research)
४, राजा एस. सी. मल्लिक रोड / 4, Raja S. C. Mullick Road
कोलकाता-७०००३२ / Kolkata-700032

DECLARATION

I, **Deeti Jyothi,** hereby declare that the work emphasized in this thesis entitled "**X-RAY CRYSTALLOGRAPHIC STUDIES ON SOME NON-CODED AMINO ACID-BASED PEPTIDES**" is my own work and carried under the guidance of Dr. Umesh Prasad Singh, senior principal scientist, CSIR-Indian Institute of Chemical Biology, Jadavpur, Kolkata, India. I have duly acknowledged all the sources of information which have been used in this thesis. To the best of my knowledge and belief, this work is original and has not been submitted in part or full, in any degree or diploma of this or any other university.

DEETI JYOTHI
(JU Registration ID: SLSBT1100919)
Infectious Diseases and Immunology Division
CSIR-Indian Institute of Chemical Biology
Jadavpur, Kolkata-700032, India

ABSTRACT

Non-coded amino acid-based synthetic peptides have gained significant interest due to their potential applications in various fields, such as therapeutics, nanotechnology, antibacterial activity, vaccine development research, etc. Because of their huge importance in various fields, designing new peptides based on non-coded amino acids in different structures is always challenging, as is synthesizing other peptides for applications.

Chapter 1 includes a brief introduction and background study of non-coded amino acid-based peptides (*α*, *β,* and *γ* hybrid peptides) and their potential uses in various fields were discussed through X-ray crystallographic studies.

Chapter 2 contains methodology studies, including peptide crystallization and stepwise single crystal crystal XRD studies of non-coded amino acid-based peptides.

Chapter 3 contains a study that elucidates the conformational characteristics of the achiral α/β hybrid peptide Boc-[Gly-tBuβ3,3Ac6c]4-OMe(P1) through a single crystal XRD study. Mixed intra-molecular C_{12}, $C_{22,}$ and C_{26} type H-bonds and solvent molecules (water) mediated H-bonds stabilize the overall structure of the octapeptide **P1**. Adding bulky groups like tBu$\beta^{3,3}$Ac$_6$c in *β*-residues leads to specific preferences for the (ϕ, θ, ψ) torsion angles of the β-peptide, which leads to overall conformational preferences in the *α*/*β* hybrid peptide. We have discovered a unique paper clamp-like fold, observed in **P1**, which has not been reported in natural or any synthetic non-coded amino acid-based peptides.

Chapter 4 deals with a study that elucidates the conformational characteristics of chiral α-L-amino acid and *β*3,3Ac$_6$c dimeric repeats in *α*/*β* hybrid peptide, Boc-[Leu-$\beta^{3,3}$Ac$_6$c]$_4$-OMe(**P2**) through a single XRD study. Four molecules are present in the triclinic space group due to solvent-mediated symmetry breaking. The self-assembly of peptide **P2** forms channels filled with solvent molecules (dioxane and ethanol) that present interesting patterns in the crystal packing. This comparison with the previously published similar structures of tetrapeptides and pentapeptides containing *α*/*β* hybrid peptides confirms that there are specific preferences for the (ϕ, θ, ψ) torsion angles for $\beta^{3,3}$Ac$_6$c peptides and such *α*/*β* hybrid dimeric repeats can indeed lead to helical folds stabilized by C_{11}/C_9 H-bond even in much longer peptides.

Chapter 5 contains a study that elucidates the conformational and supramolecular interaction studies of α/γ hybrid tripeptides, Boc-X-γ^{4L}Phe-^{L}Val-OMe (**P3-P7**) where X is an *L/D* amino acid (^{D}F/^{L}F/^{D}A/^{D}L, and ^{L}P) through a single crystal XRD study. We have discovered a tri-peptide-based β-hairpin fold that is stable without any intramolecular H-bonded interactions, which is normally observed in such β-hairpin fold. This fold remains stable even with changes in the sequence of the tri-peptide by varying the first amino acid with the L/D configuration in the sequence.

Keywords**:** α-, β-, and γ-hybrid peptides, chiral/achiral amino acids, *L/D* amino acids, H-bonds, helical structures, β-hairpin, conformational analysis, Single crystal X-ray crystallography.

SINCERE THANKS
AND DEVOTED
TO
MY FAMILY AND GOD

~Deeti Jyothi

ACKNOWLEDGMENT

As this may be my only opportunity to thank these individuals in writing, I may be a bit more verbose in my thanks than necessary.

It gives me great pleasure to express my gratitude toward all the people who contributed to the completion of this thesis. First and foremost, I want to thank my advisor and mentor Dr. Umesh Prasad Singh, Senior Principal Scientist, Infectious Diseases & Immunology Division, Indian Institute of Chemical Biology, Kolkata, whose innovative thinking, high perception of knowledge, practical insight, and experience in the subject have resulted in the success of the entire attempt. I am very lucky to have such a caring, patient, encouraging, and experienced supervisor who ensured all the positive inputs to cross all the toughest hurdles during this journey. I will always remember his encouraging stories and brainstorming discussions that changed my way of thinking and learned some important life lessons.

I sincerely thank the CSIR-Indian Institute of Chemical Biology for giving me the platform to carry on my research. I take this opportunity to sincerely acknowledge the Council of Scientific & Industrial Research, Government of India, New Delhi, for providing financial assistance in the form of a fellowship which buttressed me to perform my work comfortably. I want to acknowledge ex-directors Prof. Samit Chattopadhyay, Prof. Arun Bandyopadhyay, and the present director of CSIR-IICB, Prof Vibha Tandon for allowing me to be a part of this institute and for providing the necessary facilities to carry out my research work.

I thank Jadavpur University for my Ph.D. registration in the Lifesciences & Biotechnology department.

I would like to thank each member and staff of the CIF Department of CSIR-IICB for helping me conduct various experiments and process the data.

Also, I would like to thank all the members of the canteen, cleaning, security, and gardening, who wished me a pure smile every single day of my entire Ph.D. period which gave me positive vibes for that day.

I am indebted to all the seniors and juniors of my lab, thanks to Dr. Nitin Kishore, Mr. Purna Chandra Pal, Yasmin Begum di, and Sudesna Das for their unconditional efforts to teach me life lessons more than the research work whenever possible which showed impact on my life.

I would also like to thank other seniors from IICB, Dr. Kill Sunil Kumar (late), Dr. Chandrasekhar Kadaiahgadi, Dr. Ravuri Srinath, Dr. Saswati Ghosh, Dr. Prashanth, Dr. Ratnam Mallesh, Dr. Yatam Priyanka, Dr. Kasarla Varalaxmi, Dr. Rajeev Kumar, Dr. Debo, Atanu and Bidisha Di for their kind support and help. They helped me out in every possible manner whether it was related to research or any other problem of my life and they treated me like their own younger sister. I would like to especially thank Abhi, Arindam, Subhankar, Kaushik, Arpan, Asikul, Yogita Dahat, Sunnapu Prasad, Pathi Vijay Babu, Mohammed Rafi, Nipun Abhinav, Dr. Akriti di, Subhajit, Sudip, Bedabrata Ray, Supratim, and Shubham for making my stay in this city easier and more joyful which helped me a lot to release the stress of this hectic life throughout my Ph.D. journey.

Although there are so many people who directly or indirectly helped me throughout my Ph.D. journey, I would like to mention my beloved friend from iicb who helped me a lot Dr. Asharani Prusty (and also Jagannath da). The friendship between us flourished with scientific and non-scientific talks, celebrating festivals, and exploring Kolkata together giving us memorable days and endless bonding.

I thank Dr. Yalamanda Vadlamudi and Dr. Uttam Pal for their help and suggestions during my Ph.D. They both have great capability to help others with positivity.

I am grateful to our collaborators from different institutes for their contribution to several projects during this journey Dr. Rajkishor Rai (CSIR-IIIM, Jammu), Dr. Snehasikta Swarnakar (CSIR-IICB, Kolkata), Dr. Ramanand Rai (BHU, Varanasi), Dr. Saravanan Matheshwaran (IIT, Kanpur), and Dr. Krishna Gopal (CSIR-IMTCH, Chandigarh).

Last on the list but first in my mind, I pay my deep sense of admiration to my parents Mr. and Mrs. Deeti Sathaiah-Pushpalatha for bringing me up to this academic field and believing in me. I want to thank my most loved siblings Deeti Santhosh Kumar Patel-Soujanya and Madasu Suvarna-Mallesh who always believed in me when no one else had and supported me in all my decisions in life. I am also grateful to my other family members (In-laws) Mr. and Mrs. Bhagyanagaram Rajababu-Rajeshwari and Navajyothi for their silent blessings, constant support, love, and encouragement during my thesis writing. I feel blessed to have Saadhvi, Pranvi, Sai Keerthana, Dhruvansh, Nishwi, and Manvith in my life as stressbusters. I am always grateful to my other family members who constantly pray for me.

Above all, I thank my lord for giving me the strength to complete this phase in my life and same time for beginning a new phase of life by blessing me with the best company of my husband Mr. Bhagyanagaram Ranjith Kumar (A return gift from the lord for all my prayers) who enabled me to reach my destiny with his patience, positivity, and sacrifice of his comfort zone to give company in my loneliness to face my hurdles.

Thank you.

~ ***Deeti Jyothi***

Infectious Diseases and Immunology Division

CSIR-Indian Institute of Chemical Biology, Kolkata, India

TABLE OF CONTENTS

CHAPTER-1

Role of Single Crystal XRD Studies for α/β and γ-Hybrid Peptides

1.1 Introduction and Literature of α/β hybrid peptides

In the era of peptidomimetics, there has been significant progress in the synthesis and structural characterization of peptide foldamers.(1–3) Peptide foldamers are oligomers of natural/unnatural amino acids that adopt well-defined structural motifs similar to that observed in proteins.(Hill et al. 2001; Guichard and Huc 2011a; “Horne-et-al-2009; Seebach et al. 1997) Oligomers of β- and γ-amino acids and their hybrids with α-amino acids can adopt various secondary structures as found in structures of peptides and proteins. Characterization of various hybrid structures demonstrated that α/β residues could be accommodated into helical folds, which have driven great interest in the chemistry and biology of peptides.(3,8) Among unnatural peptides, α/β hybrid peptides consisting of alternating α- and β-amino acid residues are among the most studied. For α/β hybrid peptides, several types of helical conformations have been reported similar to the natural 3_{10}-helix and the α-helix structures, analogous to protein secondary structures.(Sharma et al. 2014; Roy-et-al-2004; Dong-et-al-2012; Choudhary-et-al-2012) Un-natural α/β-amino acid residues have been used as valuable building blocks in the construction of varieties of folded structures by introducing them into peptide sequences that display structural diversity with similar molecular divergence.(Gellman 1998b; Seebach, et al 2004; Baldauf et al 2006; Gardiner-Seebach-2008) β-amino acids in peptide sequences have a promising strategy to obtain analogs that exhibit properties of high interest for medicinal chemistry applications.(Datta and Roy 2021; Fülöp, Martinek, and Tóth 2006; “Shin-Gellman-2018; They can be combined with α-amino acids, which result in backbone architectures with well-defined structures. β-amino acids stabilize a given conformation and confer functionality through groups typically present in the side chains of α-amino acids. In α/β-peptides, C_{11}/C_9-helix is a non-traditional helical

structure, in which C_9-ring and C_{11}-ring H-bond with residue alternation and has been found to be among the most stable helices.(“Hofmann-et-al-2006) To date, several types of β-amino acids have been reported to promote C_{11}/C_9-helical folding: β^2-, β^3-, $\beta^{2,2}$-, $\beta^{2,3}$-, $\beta^{3,3}$-, and cyclic β-amino acids with a ring constraint.(Shahmohammadi and Fülöp 2020; Kiss, Mándity, and Fülöp 2017; Sharma, Venkateshwarlu, et al. 2015; Sharma, Sridhar, et al. 2015; Legrand et al. 2014; Kudo, Miyanaga, and Eguchi 2014; Sleebs, Nguyen, and Hughes 2013; Lee-et-al-2017; Liang et al. 2021) In the previous studies by Wani et al. 2017 and Vasudev et al. 2008,(8,31), they reported C11/C9 helical folding in the α/β hybrid peptides containing 1-amino cyclohexane acetic acid (β3,3Ac6c), which is a homologue of the conformationally constrained amino acid 1-aminocyclohexane-1-carboxylic acid, Ac_6C. Research in this area aimed at how alternating sequences of α- and β- residues facilitate unique folding behaviours. For instance, 1-amino-cyclohexane acetic acid (Ac_6C) or its derivatives influence backbone torsion angles and foster helical motifs such as the C_{11}/C_9 helix. In another study, we replaced the leucine residue with an achiral amino acid glycine. Then, we investigated the effect of conformationally flexible achiral glycine residue on the backbone conformation in α/β-hybrid peptides(32) through x-ray crystallographic studies. According to their research, the β-amino acids with Ac_6c derivatives are helping in maintaining helical conformations, and glycine residues may have an impact on folding behavior and backbone flexibility due to its small backbone structure.

1.1.1 Unnatural amino acids

Peptides composed of non-coded amino acids, also known as non-proteinogenic amino acids, have a vital role in structural biology and therapeutic applications due to their enhanced stability, which are naturally incorporated into proteins during translation, unlike the other well-known twenty standard amino acids.(Lee et al 2017;

Kudo et al 2014; Gellman et al 1998; Gardiner Seebach 2008; Conlon et al 2004; Koehbach and Craik 2019; Datta and Roy 2021) These non-coded amino acids are either modified or synthesized separately. They play a critical role in expanding the structural and functional diversity of peptides due to their folding properties, which increase stability and biological activity, offering tremendous opportunities in peptide design and structural manipulation.(“Karle et al 1996.; Choudhary et al 2012; Sang and Cai 2023; Guichard and Huc 2011)

1.1.2 Structure and Function

The non-coded amino acids can be incorporated into peptides to create novel structures with improved stability, bioavailability, biological activity, and therapeutic potential, as reported by Schneider and DeGrado (1998).(Degrado-Schneider 1998; Schneider et al 1998) To increase the use of peptides in biomedical research, the present literature review investigates how these amino acids can help create foldamers, which are designed and followed by synthesized artificial compounds made to resemble the folding characteristics of genuine biomolecules. The effect of non-coded amino acids on structure and function numerous studies have been conducted on the impact of non-standard amino acids on a peptide structure. In continuation, Goodman *et al.* (2007)(40) showed how the foldamers containing non-coded amino acids contribute to making flexible structures that enable the new generation molecules with specific forms and functions.(Beke et al 2003) The effect of α-helix or beta β-sheet mimics enhanced resistance to proteolysis, which is a crucial step for drug stability. Further research delivered more information related to foldamers and their potentiality for self-assembly and molecular recognition in their report. Their research mainly focused on the function of peptides with stable secondary structures like alpha helices and beta sheets formed by non-coded amino acids in biological

systems.(Gellman 1998; Baldauf et al 2006) Divya Sahu *et al.* (2012)(Sahu et al-2012) further explained the significance of non-coded amino acids in peptide drug discovery. They mainly highlighted how non-coded amino acids can be used to produce stable peptides with better pharmacokinetics and resistance to enzyme degradation, which makes them promising candidates for clinical use.

1.1.3 Peptides Folding and Chirality

The torsion angles mainly govern the overall folding and structural stability inside the peptides. The turn-effect of non-coded amino acids on torsion angles inside the peptide backbone is primarily involved in the overall structure and folding behaviour as described by Martinek and Fulop (2012)(42). Ranganathan et al. (1998)(43) also reported that their N-terminus chirality effects mainly determine the peptide conformations. Due to their unique nature, the non-coded amino acids can provide different folding motifs and C12-type helices. Interestingly, Seebach and Matthews (1997)(Seebach and Matthews 1997; Gardiner Seebach 2008; Koert 1997) reported the folding dynamics of β-peptides, the non-coded amino acids at the β-position in the peptides showing unique secondary structures including α-helices and β-sheets, which were not seen in α-position non-coded amino acid-based peptides.

1.2 Introduction and Literature of X-ray crystallography

The X-ray crystallography technique is the most reliable and powerful method for determining the peptide as well as protein structures at their atomic resolution level.(47) In the context of peptides that are based on non-coded amino acids, crystallography offers a tremendous amount of information on how modified or synthetic residues affect the peptide structure, folding, and interactions. Non-coded amino acids include those that are not part of the standard amino acid code or have

been chemically modified (for example, β-amino acids, residues containing cyclohexane, or D-amino acids). These can create specific functionalities like enhanced stability, modified folding patterns, and novel functionalities.

1.3 Implications of SCXRD in Drug Design and Biotechnology

The usefulness of Single Crystal XRD study is evidenced by several publications that have clearly established the importance of the X-ray crystallography technique in peptide structure analysis.(48–51) Glusker *et al.* (1996)(52) provided key insights into crystal structure analysis techniques to understand hydrogen-bond networks in small peptides and modified small peptides that incorporated non-coded amino acids. Also, the X-ray crystallographic technique used in finding unique folding properties such as β-sheets and C_{12} type helices for hybrid peptides containing both standard and non-standard amino acids using X-ray crystallography, as reported by Aravinda et al. (2003) and Bucci (2019).(53,54) In addition, Choi *et al.* (2010)(Choi, S. H. 2010) reported the relative information about torsion angles and folding dynamics in peptides containing β-amino acids which are different from their alpha-amino counterparts. The overall x-ray crystallographic studies from different reports provided thorough information about how the non-coded amino acids affect the overall peptide structure. The review by Balaram et. al. (1996)(53) explained different applications for non-coded amino acid-based peptides in molecular design. They concluded that the incorporation of non-standard amino acids into peptide scaffolds creates tremendous opportunities for various fields like bio-molecular engineering, targeted drug delivery, and peptide vaccines. The incorporation of non-coded amino acids into peptides to increase their overall structure stability and bioavailability was highlighted in a report by Adessi and Soto (2002).(56) Their research mainly explains how non-coded amino acids enhance the peptide's resistance to proteolysis hence, usefulness as pharmaceutical

compounds. Further, Patgiri *et al.* (2012) and Han *et al.* (2024) explained the effect of designed non-standard amino acid-based peptide inhibitors interfering in some protein-protein interactions with an experiment of Ras-protein and Ras-associated protein interaction in cancer treatment.(57,58) Due to their more stability and higher selectivity, the non-coded amino acid-based peptides are now potentially useful therapeutic medicines. Banta *et al.* (2010)(59) also investigate the application of non-coded amino acid-based peptides in the field of nanotechnology. The non-coded amino acids were used in protein engineering to produce functional hydrogels and some other drug-delivery materials. Their technique helps to create biomaterials with improved mechanical qualities and targeted drug release by utilizing the special qualities of non-coded amino acids.

1.4 Challenges and future directions

The non-coded amino acid-based peptides might be challenging to crystallize to get high-quality x-ray data and structures due to the non-standard side chains of β-amino acids in the peptide sequence and their higher flexibility in α-, β- and γ-hybrid peptides.(60) Dezotti *et al.* (2012)(61) initially reported that the crystallization for non-coded amino acids containing peptides was difficult due to their flexibility in nature and conformational heterogeneity. The existence of disordered areas may create problems during X-ray diffraction data (electron density) interpretation. Kabsch(2010)(62) and team further reported a few key points to overcome the difficulties by using advanced software of x-ray diffraction studies (XDS) for processing x-ray diffraction data, essential software for getting high-resolution structures of peptides with unconventional residues. Future research will probably concentrate on designing computationally non-coded amino acids containing peptides and developing techniques to study their dynamic behaviour in solution. The incorporation of non-

standard amino acids into peptides, followed by dynamic behavioural studies, would increase their applicability in the field of biomaterials, bio-sensing, and drug discovery**.** Guichard and Huc (2011)(63) mentioned core points in their report for future research, to create novel computational methods and crystallographic techniques to understand the performance of non-coded amino acid-based peptides in both crystalline and solution states. In addition, efforts are being made to produce non-standard amino acids containing peptides with unique features for use in bio-sensing, nanotechnology, and immunotherapy techniques.

CHAPTER-2

Methodology for Single Crystal XRD studies

2.1. Peptide Synthesis

All the peptides were designed and synthesized with Dr. Rajkishor Rai, a peptide chemist and senior scientist at CSIR-IIIM, Jammu. While synthesizing designed peptides, tertiary butoxy carbonyl (BOC) and methoxy (OMe) were used as protective groups at the N-terminus and C-terminus, respectively.(64),(65)

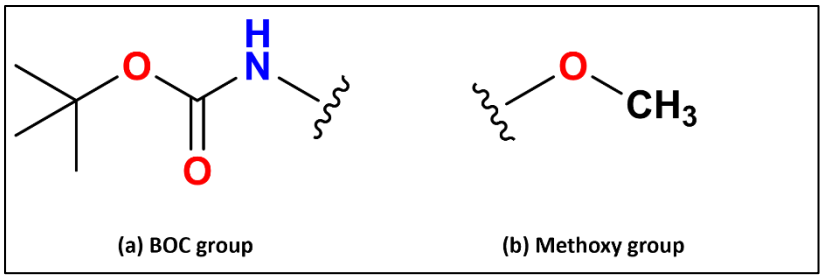

Figure 2.1: Scheme of functional groups. (a) Boc and (b) OMe.

The synthesized peptides were crystallized and analyzed further. Our methodology ensures accuracy and reproducibility in the production of peptides (P 1-7) crystal structures by offering a methodical approach to crystallographic studies shown in Figure 2.2.

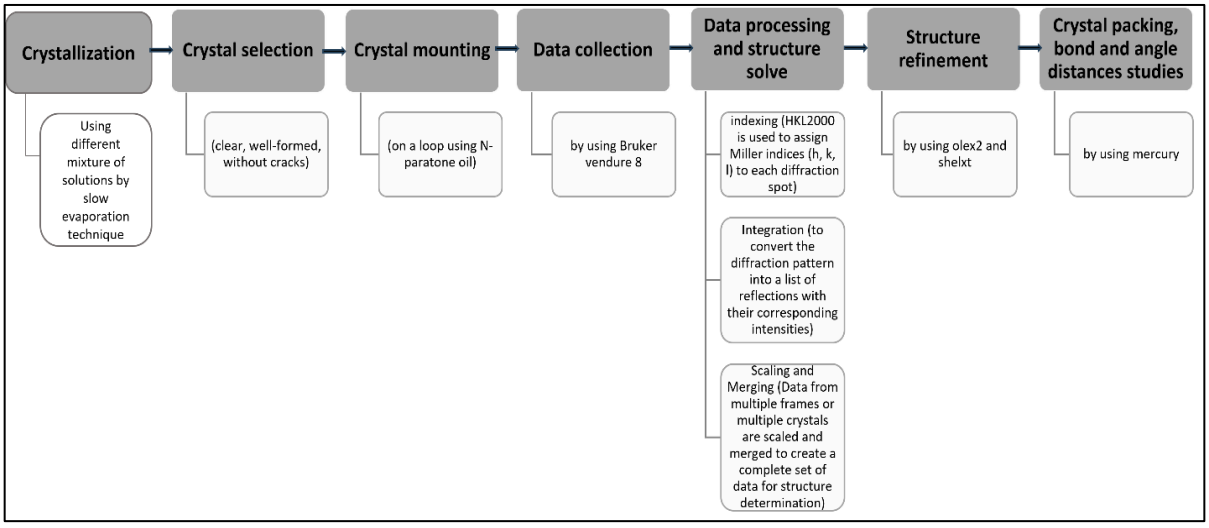

Figure 2.2: Workflow of single crystal XRD.

2.2. Crystallization

Single crystals of peptides (P1-7) were obtained by using slow evaporation of different solution mixtures of peptides as shown in Figure 2.3.(66) Different solutions of peptides were taken in a small test tube (5 mL) and covered with parafilm with minimal holes for slow evaporation of solvents. Crystal formation starts slowly when the solution gets close to supersaturation due to solvent evaporation. The crystallization details of all peptides are listed in Table 2.1.

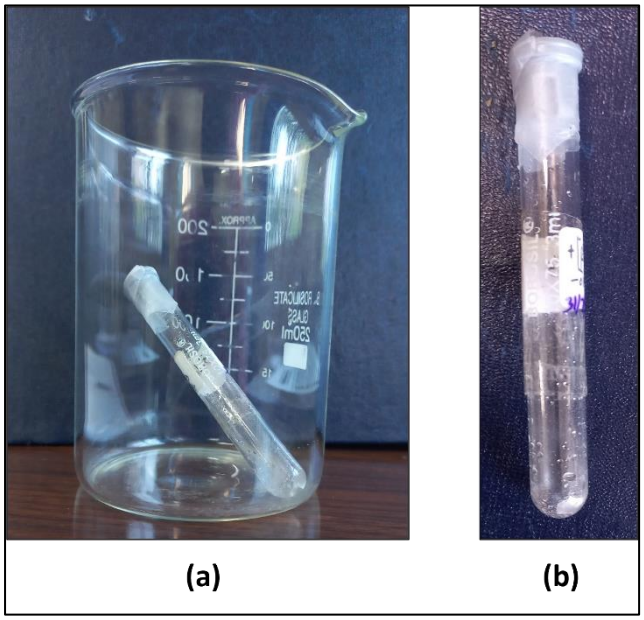

Figure 2.3: Peptide crystallization procedure. (a) Solution of peptide in a small test tube (5mL) placed inside the beaker. (b) Test tube containing crystals and peptide solution.

Table 2.1: Crystallization details of peptides (P1-7).

S. No	Peptide	Solution	Solvent mixture ratio (%)	Time for first appearance of crystals (in days)
1	**P1**	Methanol	100%	90
2	**P2**	Dioxane: Water	4:1	10-15
3	**P3**	Methanol: Water	1:1	15-30
4	**P4**	Methanol: Dioxane	1:1	15-30
5	**P5**	Methanol: Water	1:1	15-30
6	**P6**	Methanol: Water	1:1	15-30
7	**P7**	Methanol: Water	1:8	15-30

2.3. X-ray diffraction studies

2.3.1. Principle of X-ray diffraction

X-ray diffraction is a powerful analytical method for the analysis of crystalline materials to determine their molecular structure. (67,68)(69) The interaction of X-rays with the crystal lattice is the foundation of XRD. When an X-ray beam hits a crystalline sample, it interacts with the electrons of the atoms in the sample, scattering the X-rays in different directions. When conditions are met, the dispersed X-rays experience constructive interference, resulting in a diffraction pattern shown in Figure 2.4. Bragg's Law explains this phenomenon.(70,71)

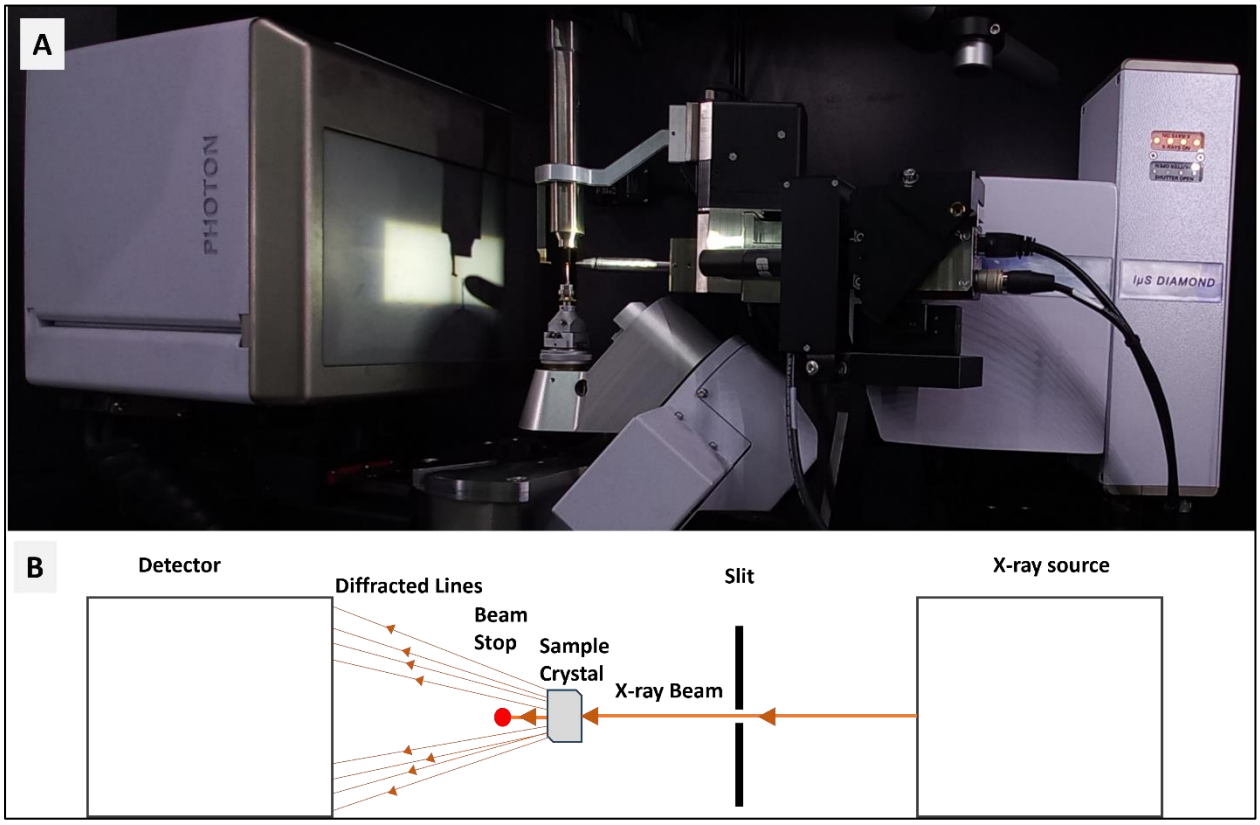

Figure 2.4: Scheme of X-ray Diffraction. (a) XRD pattern is shown in a Bruker Venture 8 diffractometer and (b) The same in cartoon representation.

2.3.2. The Bragg's Law

W. L. Bragg developed an equation in 1913, building on the research of Freidrich, Knipping, and Laue.(72) This study supported Laue's theory that crystals may diffract X-rays, which was sparked by Ewald.(73) The diffraction geometry of X-rays by crystals is still quantitatively explained by the Bragg equation $n\lambda = 2d \sin \theta$ today where *n* is an integer that represents the order of reflection, λ is the wavelength of the X-ray radiation,

d is the spacing between the crystal layers (planes), and θ is the angle between the incident ray and the scatter plane shown in Figure 2.5. According to the equation, crystals are made up of several parallel planes of atoms that are only slightly apart. It is believed that the planes can reflect the X-rays in a way that makes the angle of incidence and angle of reflection identical. Subsequent planes will contribute in phase, meaning that the path length difference between waves must be only at specific angles (integer number of wavelengths).(68,74)

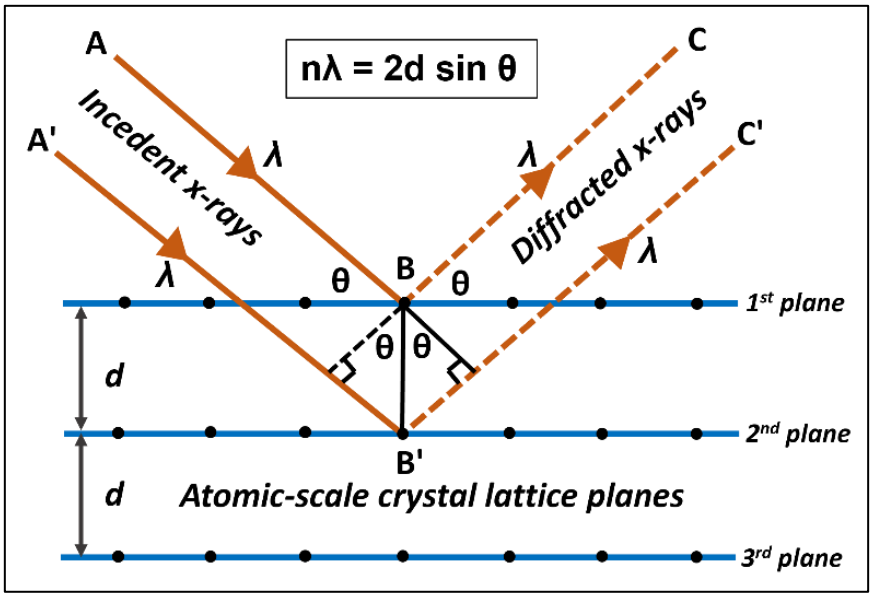

Figure 2.5: A pictorial depiction of the relationships that constitute Bragg's equation.

Therefore, only when the Bragg equation is satisfied can constructive interference and the creation of diffraction maxima take place. The Bragg equation is the first equation. Destructive inference will happen if the waves are out of phase. This is a typical scenario since the majority of a diffraction pattern is made up of space. Diffraction spots can reveal just as much information when they are absent as when they are present. For instance, systematically absent reflections can be used to allocate space groups.

Laue also came up with a trio of less popular equations that describe the same result.

2.3.3. Crystal selection

Crystals are composed of a regular, repeating arrangement of units. To perform single XRD studies, we need to select crystal to mount based on different factors(75) including:

- Quality of Crystals: The crystals were carefully selected based on their physical appearance. The criteria for selection included clarity, well-formed structure, and the absence of visible cracks. Selecting high-quality crystals is essential to obtain reliable diffraction patterns and structure determination results. The size (bigger the better but within the beam size) and quality of the crystal directly affect the resolution of the data and, therefore, the accuracy of the final structure shown in Figure 2.6.

- Temperature Control: Molecules can be sensitive to temperature and x-ray radiation damage, so cryoprotection is often used to maintain crystal integrity during data collection.

- Symmetry and Disorder: Some molecules exhibit crystallographic disorders (thermal or position disoeders) or high symmetry, which may complicate structure solution and refinement.

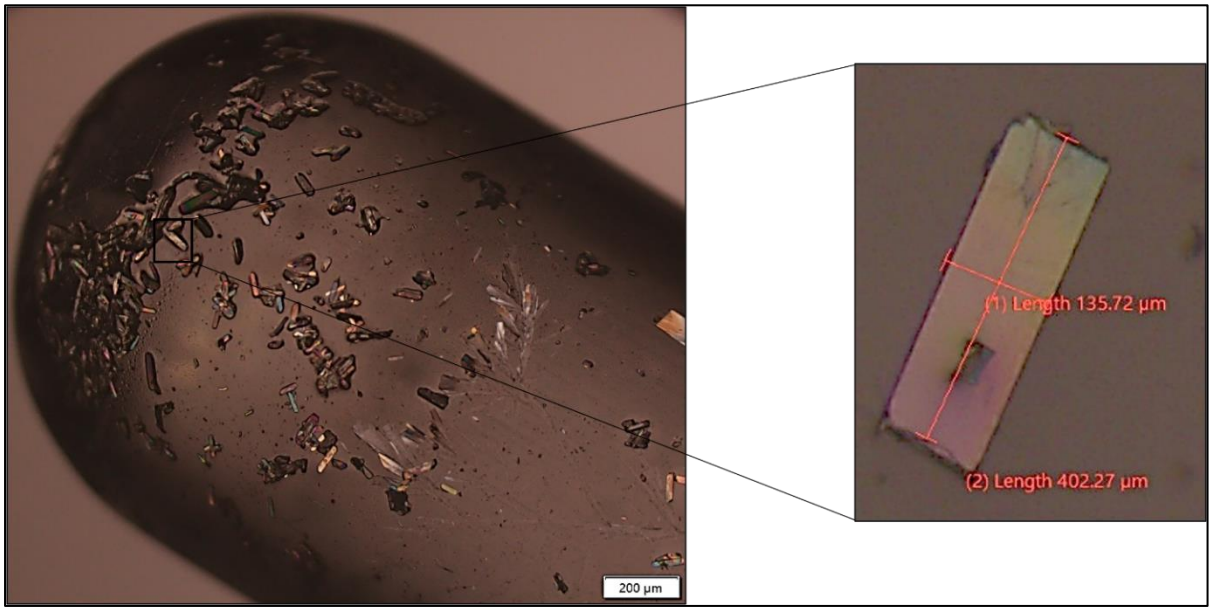

Figure 2.6: Example of crystal selection for data collection. (left) large no of crystals grown in a test tube and (right) a selected rectangular plate-shaped crystal with well-defined margins and its measurements during microscopic examination shown in zoomed view. Note the selected crystal's highest dimension (402 µM) is less than that of the beam size of 500 µM used in the diffractometer.

2.3.4. Crystal Mounting

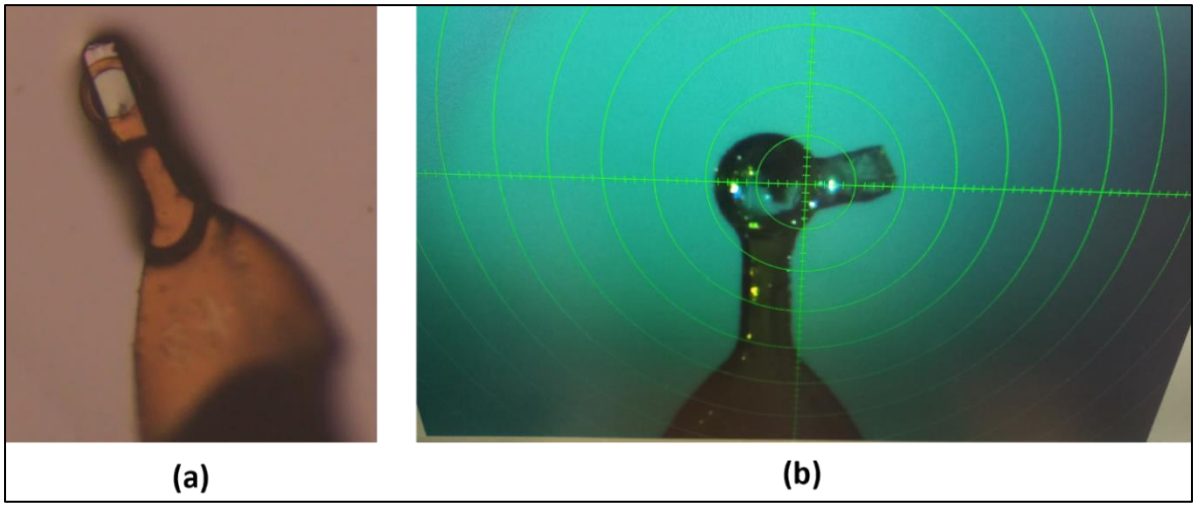

Figure 2.7: An Example of crystal pickup within a loop held in place with a viscous N-paratone oil pictured via a high magnification camera (a) in the microscope and (b) mounted on the diffractometer.

The selected crystals were mounted on a polymeric loop using N-paratone oil**,** which ensures minimal damage to the crystal due it its inert nature and protects it from environmental moisture by forming a film around the crystal as shown in Figure 2.7. The process of crystal, mounting is critical for obtaining high-quality diffraction data. Proper mounting minimizes the impact of air scattering and ensures that the crystal remains stable (thermally as well as in position) which is crucial to maintain the integrity of the crystal during data collection.(76)

2.3.5. Data Collection and Processing

Data collection was performed using a Bruker diffractometer.(77) The instrument generates high-resolution diffraction patterns, essential for accurately determining the crystal structure. This step involves rotating the crystal to collect reflections from various angles.(67,74,78) Data collection consists of recording the diffraction pattern produced when X-rays interact with the crystal lattice. The resulting data set contains reflections that can be processed to elucidate the crystal structure**.** APEX2 or 3 software suite(79) was used for data acquisition and processing of single-crystal X-ray diffraction data and XDS was **u**sed for data reduction and integration of X-ray diffraction images shown in Figure 2.8.

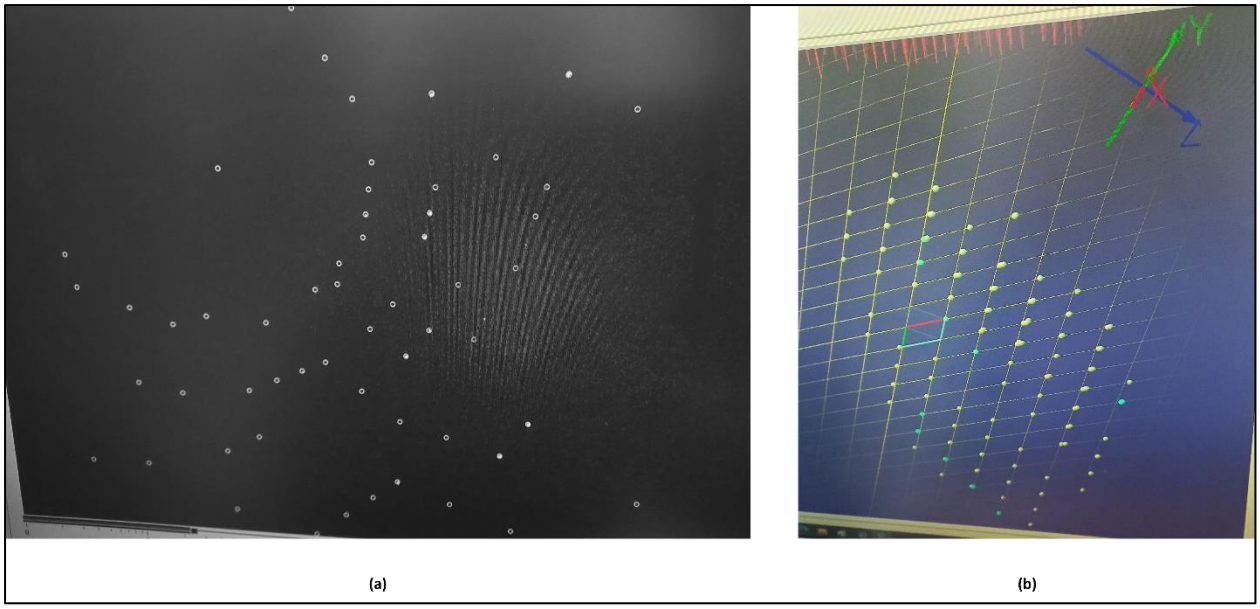

Figure 2.8: An example of a diffraction pattern. The particular position and symmetry of the spots are illustrated in addition to the varying intensities of the spots. Demonstration of the reciprocal crystal lattice, created by representing the constituent diffraction with points.

2.3.6. Structure Solution and Refinement

Direct Method is used to solve most of the peptide structures as most of the data for small peptides (<15-20 residues) is available in atomic resolution. These algorithms exploit the phase relationships of the diffracted beams to generate initial estimates of the electron density. SHELXL program(80,81) is normally used for structure solutions via direct methods. The preliminary structure solution is obtained and refined using Olex2 2-1.5 software suite (http://www.olexsys.org)(82) which uses SHELXT software(83). Olex2 suite is also used for visualization and various crystallographic calculations as shown in Figure 2.9s. All the relevant crystallographic data collection parameters and structure refinement details for the peptides are summarized, cif files are generated and submitted to the Cambridge Crystallographic Data Centre (CCDC) (Advancing Structural Science | CCDC (cam.ac.uk)).(84)

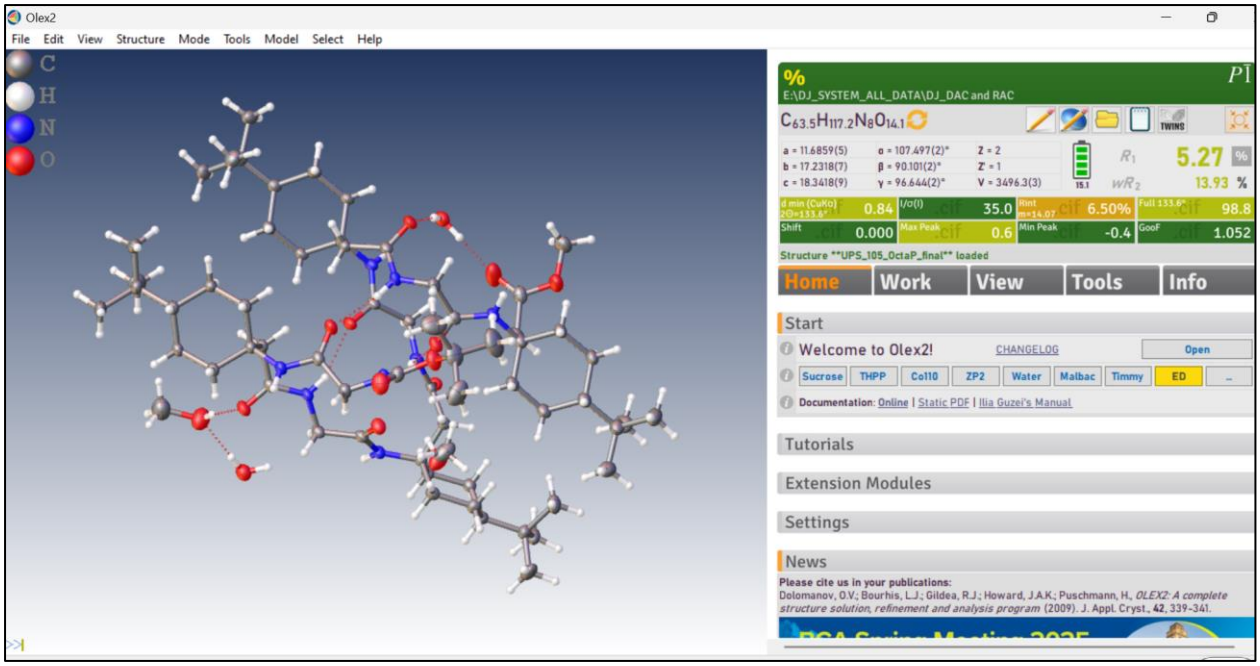

Figure 2.9: Example of the structure solution and refinement by using Olex2 software suite(82).

2.3.7 Crystal packing, bond-length, and bond-angle calculations

Crystal packing studies investigate how molecules are arranged in the crystal lattice, affecting properties like solid-state stability and reactivity. Analyzing intermolecular interactions can provide insights into the packing efficiency and potential void spaces within the crystal. The final structures, after refinement, were analyzed using Mercury software22 (V 2024.2.0. 8) to study crystal packing, bond length and bond-angle calculations. Understanding hydrogen bonding and their pattern and torsion angles within the molecules is crucial for analyzing molecular conformation and stability. **PLATON** software(85) is used for geometry checks and hydrogen bond analysis. Hydrogen bonds influence crystal packing and molecular interactions. These analyses provide insight into the molecular interactions and structural stability of the compounds.

2.3.8. Visualization and Image Generation

Chimera (Version 1.18)(86) and Pymol (The PyMOL Molecular Graphics System, Version 2.3.2, Schrodinger, LLC.) software were used to superimpose peptides and analyze the comparative studies. The GIMP program was used to generate all the images.

CHAPTER-3

Intramolecular H-bonded Helical Foldings in Achiral *α/β* Hybrid Peptides Containing Glycine and Tertiary butyl-1-Aminocyclohexaneaceticacid (tBu$\beta^{3,3}$Ac$_6$c)

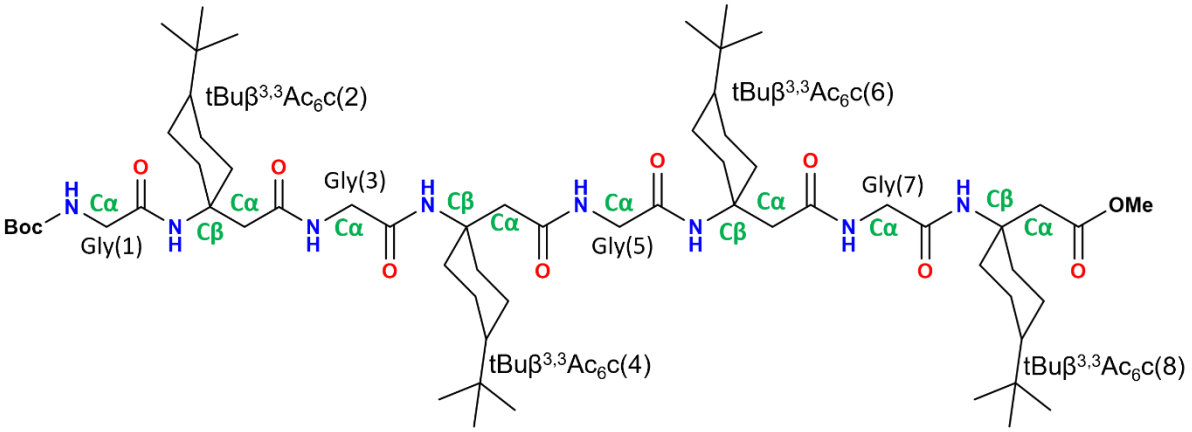

α/β hybrid peptide: Boc-[Gly-tBu$\beta^{3,3}$Ac$_6$c]$_4$-OMe

3.1. Graphical Abstract

Stable helices: Mixed intramolecular C_{12}, C_{22}, and C_{26} type H-bonds and solvent molecules (water and methanol) mediated stabilization of the helical conformation in achiral *α*/*β* hybrid peptide leading to a paper clamp-like unique fold

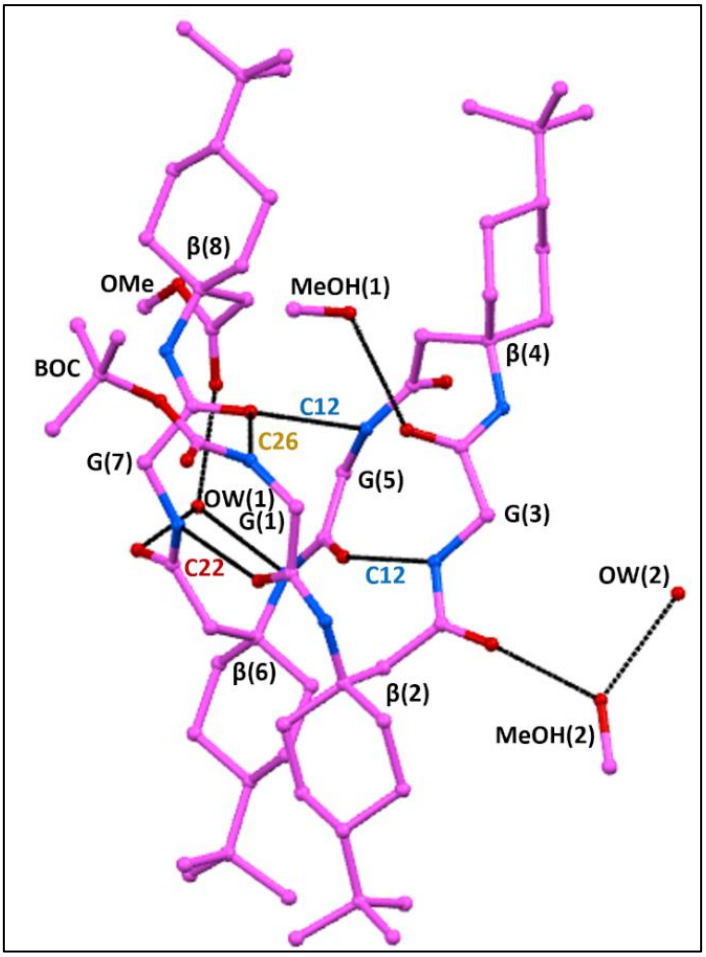

3.2. Abstract

This study elucidates the conformational characteristics of achiral *α*/*β* hybrid peptide Boc-[Gly-tBu$\beta^{3,3}$Ac$_6$c]$_4$-OMe (**P1**) through X-ray crystallography. Octapeptide **P1** adopts folded conformations with stable C_{12}, C_{22}, and C_{26}-type intramolecular H-bonded folded conformations. A water molecule also helps stabilize the helical conformation of this peptide. Solvent molecules like water and methanol were observed to play crucial roles in stabilizing the crystal structure through solvent-mediated intramolecular and intermolecular H-bonds. The achiral ^{L}Gly residues seem to take φ, and ψ values around ±132.7(30.9)°, and ±155.7(13.3)° while the *β*-residues (tBu$\beta^{3,3}$Ac$_6$c) seem to take phi (φ), theta (θ), and psi (ψ) values around (±59.5(8)°, ±52.9(1.5)°, and ±106.3(20.5)°). It shows that the conformational preference of *β*-residues is the main determinant of the overall conformation of the octapeptide **P1**, while the ^{L}Gly residues show a lot of flexibility in their conformation and adjust to the overall requirement of peptide folding. The dimeric repeats of glycine and tBu$\beta^{3,3}$Ac$_6$c residues in this octapeptide, **P1** are observed to take a unique paper-clamp-like fold hitherto unreported in any natural or synthetic peptides.

Keywords: Achiral amino acids, *α*/*β* hybrid peptides, solvent molecules, hydrogen bonds, helices, conformational analysis, x-ray crystallography.

3.3. Introduction

This chapter presents the structural characteristics of achiral *α*/*β* hybrid peptide, Boc-[Gly-tBu$\beta^{3,3}$Ac$_6$c]$_4$-OMe (**P1**) in solid state studied by single crystal X-ray crystallography. The scheme of peptide **P1**: Boc-Gly-tBu$\beta^{3,3}$Ac$_6$c-Gly-tBu$\beta^{3,3}$Ac$_6$c-Gly-tBu$\beta^{3,3}$Ac$_6$c-Gly-tBu$\beta^{3,3}$Ac$_6$c-OMe is shown in Figure 3.1.

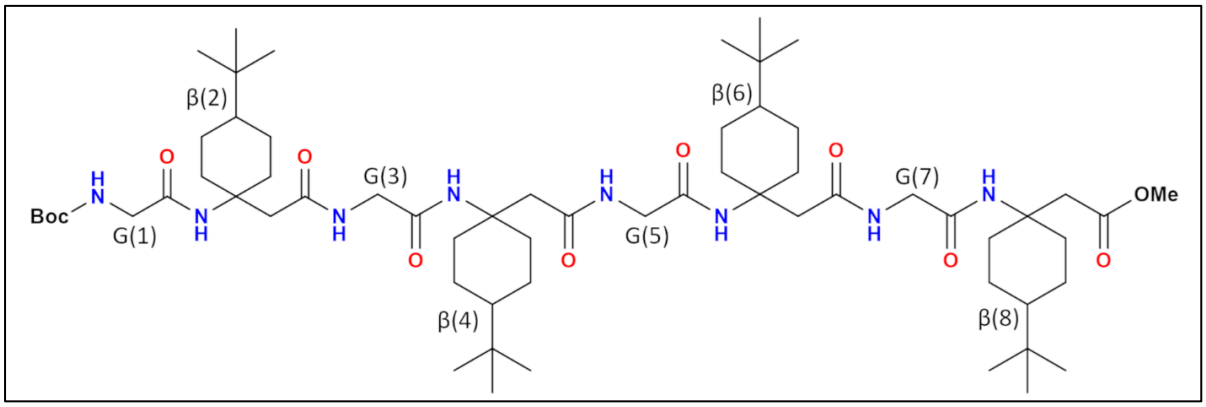

Figure 3.1. Scheme of peptide **P1,** Boc-[Gly-tBu$\beta^{3,3}$Ac$_6$c]$_4$-OMe.

In this octapeptide **P1,** dimeric repeats of achiral amino acids ^{L}Gly (glycine) and *β*-amino acid (tBu$\beta^{3,3}$Ac$_6$c) were taken to investigate the impact of the bulky side chain tBu (t-butyl cyclohexyl group) containing β-amino acid on the conformation of the peptide backbone. We also wanted to see if octapeptide **P1** can take a well-defined, rigid backbone and is capable of adopting a secondary structure stabilized by intramolecular hydrogen bonds.

3.4. Literature review

Establishing specific intramolecular hydrogen bonding interactions like C_{11}/C_9 and C_{11}/C_{12} types in synthesized peptides appears to be a multifaceted tool in managing secondary structures of peptides and small molecules.(87–89) Cyclohexyl-based residues can efficiently use C_{11} type intramolecular hydrogen bonds to stabilize *β*-turns in *α*/*β* hybrid peptide structures as reported by Krishnayan *et. al.* 2012. (1) They demonstrated that controlling peptide and protein folding requires the stability of *β*-

turns, which are ubiquitous structural motifs in proteins. Incorporating cyclohexyl groups in non-coded amino acids is probably helpful in improving the stability of these turns by adding steric effects that promote turn formation.(90),(91) Further, they have explored the creation of repeating C_{11}/C_9 type intramolecular hydrogen-bonded helical structures in peptides containing modified cyclohexyl group based *β*-amino acids. Introducing cyclohexyl groups in peptides helps maintain helical conformations in secondary structures. According to their study, adding cyclohexyl groups can affect the overall shape and encourage particular helical configurations in the *α*/*β* hybrid peptides.(92) Wani *et. al.* 2017 reported the stable intramolecular C_{11}/C_9 type H-bonded helices in short *α*/*β* hybrid peptides containing repeats of chiral ᴸLeu (leucine) and achiral *β* amino acids ($\beta^{3,3}$-Ac_6c) in their sequences.(93–95) The results demonstrated that the dimeric repeats of a chiral L-amino acid and achiral $\beta^{3,3}Ac_6c$ residues can stabilize helical structures, which are ubiquitous elements of folded proteins and may be useful in designing folded peptides. Such helical motifs probably have an extra layer of stability in peptides due to the particular C_{11}/C_9 type of intramolecular hydrogen bonds.(31) In our earlier studies of peptides containing achiral *α*/*β*-hybrid peptides like Boc-Gly-$\beta^{3,3}Ac_6c$-NHMe (P1'), Boc-Gly-$\beta^{3,3}Ac_6c$-Gly-OMe (P2'), and Boc-(Gly-$\beta^{3,3}Ac_6c$)2-OMe (P3') were studied.(32) These peptides demonstrated variable C_{11} or C_{12} type intramolecular H-bonded stable structures or intramolecular H-bonds were completely absent as in P3'. This was in contrast to stable C_9/C_{11} type of H-bonded helical structures in *α*/*β* hybrid peptides containing chiral ᴸLeu and achiral $\beta^{3,3}$-Ac_6c. Since it is known that the type of *β*-amino acids can affect the H-bonded pattern of *α*/*β* hybrid peptides,(96–100) hence we wanted to explore further changes in the peptide structure by incorporating tBu$\beta^{3,3}Ac_6c$ in our peptide. Since the smaller peptides may take unusual conformations due to packing

constraints in the solid state, we thought it wise to study a peptide of a reasonable length (octapeptide) to study its natural propensity.

3.5. Methodology

3.5.1. Single crystal x-ray crystallography

The single crystals of the octapeptide **P1** were grown by slow evaporation of the methanolic solution of the peptide. Crystallization of this peptide was difficult and crystals appeared only after repeating the crystallization process by dissolving the dried-out peptide sample each time after solvent evaporation. The block-shaped crystals were self-nucleated, grew, and reached their ideal size suitable for data collection in about 15 weeks. The single crystal X-ray data was collected using a Bruker Venture 8 diffractometer equipped with an IμS DIAMOND microfocus X-ray source (*Cu K/α*= 1.54178 Å) and fitted with a PHOTON III photon counting detector with mixed mode technology. The crystal diffraction data was collected using φ/ω scan up to θ_{max} = 133.628º. The APEX3 v2019.1-0 software(101) was used for data collection and integration, while the SADABS(102) program was used to apply the absorption correction. A least squares analysis on randomly collected reflections from a single rapid scan set with 0.5º wide oscillation (180 frames) evenly dispersed in reciprocal space provided the unit cell parameters of the crystal. An automated data collection technique was used to collect all data sets using 0.5º wide scans in multiple sets. The crystal-to-detector distance was kept fixed at 7.0 cm. The final unit-cell parameters were refined using all available reflections. The SHELXT(83) program was used to solve the structures, and the SHELXL(103),(80) program was used for refining using the Olex 2-1.5 (http://www.olexsys.org) program suite.(82) Mercury 4.2.0. (https://www.ccdc.cam.ac.uk/solutions/csd-system/components/mercury/)(104) was used to

calculate the hydrogen-bond distances, and torsion angles (φ, θ, ψ, and ω), and create crystal packing diagrams. All the images were compiled using GIMP 3.10.38.(105) Table 3.1 lists the crystallographic parameters of **P1**. The octapeptide **P1** cif file was submitted to The Cambridge Crystallographic Data Centre (CCDC) (Advancing Structural Science| CCDC (cam.ac.uk))(84) with CCDC no. **2369636.** These data are provided free of charge by the joint Cambridge Crystallographic Data Center and Fachinformationszentrum Karlsruhe http://www.ccdc.cam.ac.uk/structures Access Structures service.

3.6. Results and Discussion

3.6.1. Single crystal X-ray diffraction study

The octapeptide **P1** crystallized in the triclinic centrosymmetric space group $P\bar{1}$. The two molecules are present in the unit cell and are related by an inversion centre as the entire molecule is achiral. The peptide **P1** is co-crystallized with solvent molecules (two water and two methanol).The ORTEP diagram and molecular conformation of the peptide are shown in Figs 3.2 and 3.3, respectively. The X-ray crystallography parameters for peptides are listed in Table 3.1. The measured hydrogen-bond distances and backbone torsion angle parameters are listed in Tables 3.2 and 3.3, respectively.

3.6.2. Molecular structure

The octapeptide **P1** is well folded in the solid state. In all the four tBu-$\beta^{3,3}$-Ac$_6$c residues (β_2-β_8) in the peptide **P1,** the backbone amino groups, and the tBu groups are oriented equatorially, while the C_α carbons are oriented axially with respect to the mean plane

of cyclohexyl moieties, which are all in stable chair conformation (Figure 3.3 and Table 3.2).

Figure 3.2. ORTEP diagram of octapeptide **P1** drawn at 20%. All H-atoms are removed for sake of clarity. All N-atoms have been shown in blue while O-atoms are in red. All non-hydrogen atoms have been labeled. The co-crystallized solvent molecules (two water and two methanol) have also been labeled.

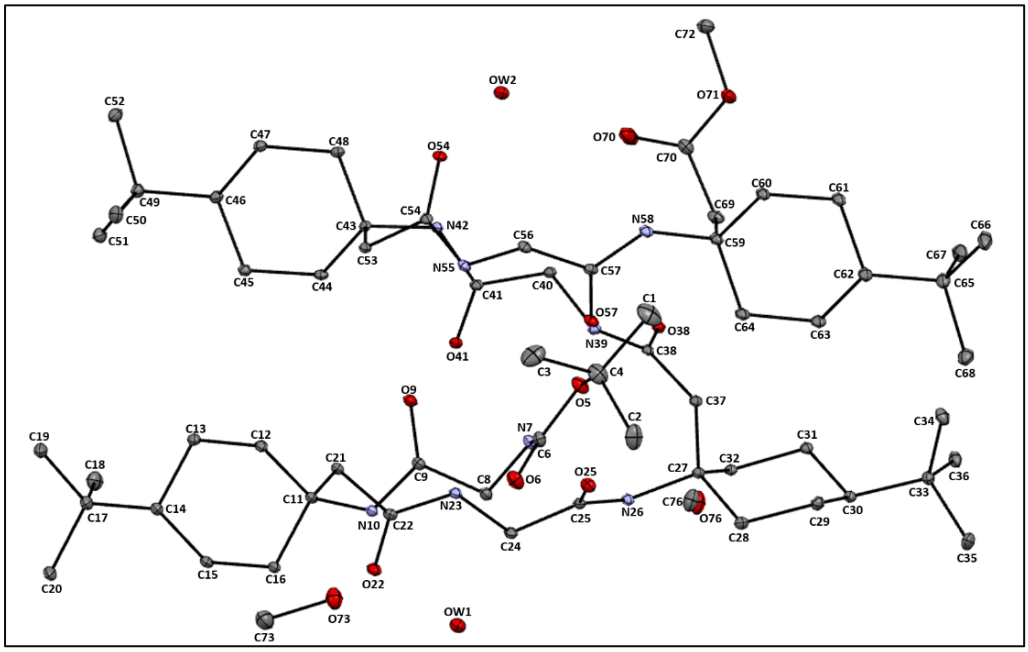

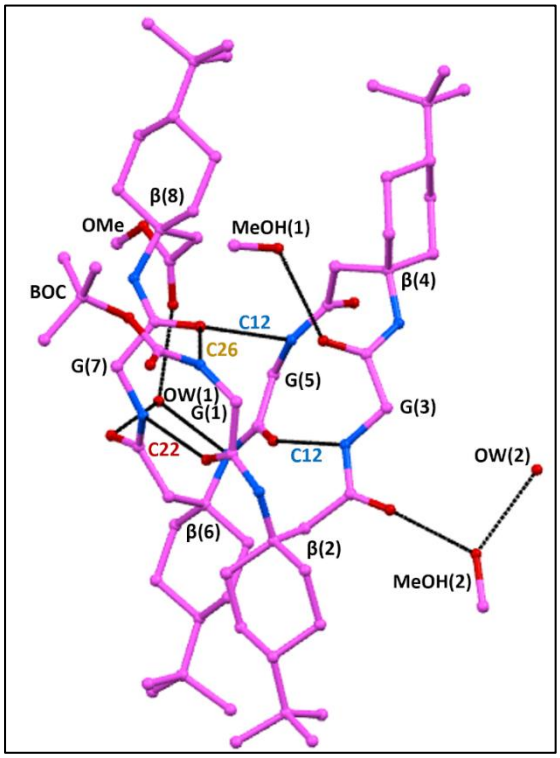

Figure 3.3. Crystallographic structure of octapeptide **P1**. All H-atoms have been removed for the sake of clarity. All the *α* and *β* amino acids as well as the N-terminal Boc and C-terminal methoxy (OMe) groups have been labelled. All putative intramolecular H-bonded interactions have been shown by dashed lines and are labeled showing the type of H-bond. All C-atoms are in magenta, N-atoms are in blue, and O-atoms are in red. The solvent molecules (two water and two methanol) have also been shown and labeled.

Table 3.1. Crystal x-ray diffraction data and structure refinement parameters of octapeptide **P1**.

Parameters	**Octapeptide P1**
Empirical formula	$C_{62}H_{108}N_8O_{11} \cdot 2(H_2O) \cdot 2(CH_4O)$
Formula weight	1218.86
Crystal habit	Block
Crystal size [mm]	0.52×0.09×0.08
Crystallizing solvent	Methanol (100%)
Temperature (K)	100.0
Wavelength	1.54178
Crystal system	Triclinic P
Space group	$P\bar{1}$
a [Å]	11.6859(5)
b [Å]	17.2318(7)
c [Å]	18.3418(9)
Angles [*α, β, γ*]°	*α* = 107.497(2)
	β = 90.101(2)
	γ = 96.644(2)
Volume [Å^3]	3496.3(3)
Z	2
Density [g/cm3] [calc.]	1.158
F (000)	1334.0
Radiation	*Cu K/α*
Θ Range [°]	5.056 to 133.628
Scan type	ω/φ
Independent reflections	12267
Measured reflections	172587
Observed reflections with I >= 2σ(I)	11337
R int	0.0650
Δ*ρmax* / Δ*ρmin* [e Å^{-3}]	0.65/-0.43
Goodness-of-fit on F2	1.052
Final *R* / wR_2 [%]	0.0527/ 0.1367
restraints/parameters	0/811
CCDC No.	2369636

Table 3.2. The configuration of different moieties of *β*-amino acids in peptide **P1**.

Sr. Number	Residue	NH_2	tBu	C*α*
1	tBu-$\beta^{3,3}$-Ac_6c (2)	equitorial	equitorial	axial
2	tBu-$\beta^{3,3}$-Ac_6c (4)	equitorial	equitorial	axial
3	tBu-$\beta^{3,3}$-Ac_6c (6)	equitorial	equitorial	axial
4	tBu-$\beta^{3,3}$-Ac_6c (8)	equitorial	equitorial	axial

In peptide **P1**, one intramolecular C_{12}-type hydrogen bond is present between N-H of Gly(3) and C=O of Gly(5) atoms with a distance of 2.90 Å**,** and another C_{12}-type intramolecular hydrogen bond is present between N-H of Gly(5) and C=O of Gly(7) atoms with a distance of 2.85 Å. A C_{22}-type intramolecular hydrogen bond forms between C=O of Gly(1) and N-H of Gly(7) atoms with a distance of 2.82 Å, A C_{26}-type intramolecular hydrogen bond forms at a distance of 3.0 Å between N-H of Gly(1) and C=O of Gly(7), These intramolecular H-bonds are mainly involving in peptide P1 folding (Figure 3.3, Table 3.4). The solvent molecules like water and methanol also form intermolecular and intramolecular hydrogen bonds with **P1**. The solvent mediated (OW2) three-centred intramolecular hydrogen bond in peptide **P1** between NH and C=O of β(6), and C=O of Gly(7) is helping to further stabilize the folding of the peptide as shown in Figure 3.3.

The intramolecular H-bonded interactions between achiral amino acids of *α*/*β* hybrid peptide are shown schematically in Figure 3.6.

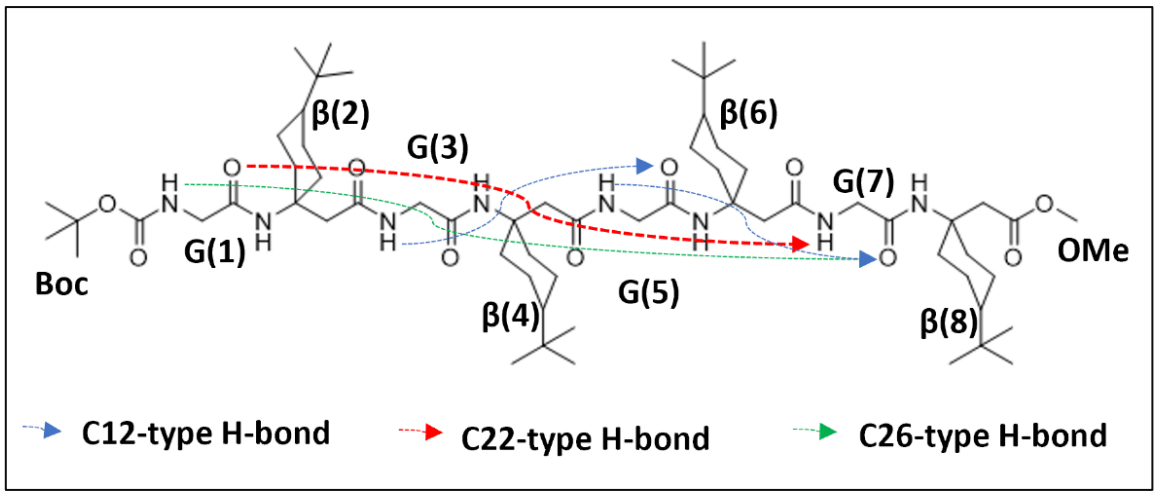

Figure 3.6. The scheme of intramolecular H-bonds observed in **P1.** The dashed lines indicate intramolecular H-bonds. All side chain residues have been labelled. C_{12}-type H-bonds are shown in blue, C_{22}-type H-bond are shown in red and C_{26}-type H-bond are shown in green colours.

A simplified view of folded backbone of **P1** is shown in Figure 3.7. The Overall backbone structure of octapeptide **P1** has a unique fold in *α*/*β* hybrid achiral peptide that looks similar to a paper-clamp, which has not been reported so far in natural amino acids-based peptides or synthetic non-coded amino acids-based peptides (Fig 3.8).

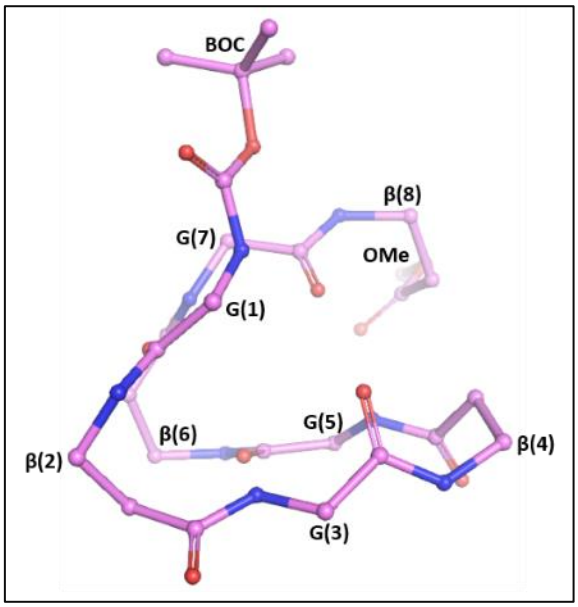

Figure 3.7. The molecular fold of peptide **P1.** All backbone residues have been labelled. All side chain residues and all H-atoms were removed for clarity. All C, N and O atoms have been shown in magenta, blue and red colours, respectively.

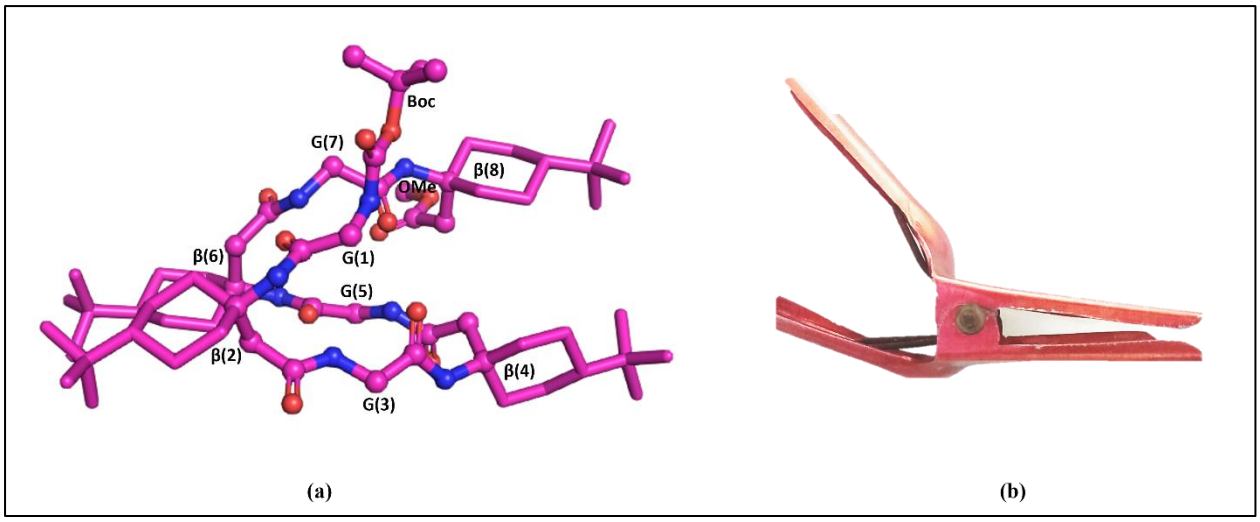

Figure 3.8. (a) Paper-clamp-like fold of peptide **P1** shown in ball and stick model. All C, N and O atoms have been shown in magenta, blue, and red colours, respectively. All hydrogens atoms have been removed for sake of clarity; **(b)** The paper-clamp image shown in a similar orientation for reference.

Table 3.3. Torsional angles (°) for octapeptide **P1**. Gly and tBu$\beta^{3,3}$Ac$_6$c refer to Glycine and tertiary butyl-1-amino cyclohexane acetic acid, respectively. The standard deviations are shown in parentheses.

Residue	**φ [°]**	**Θ [°]**	**ψ [°]**	**ω [°]**
Octapeptide **P1**				
Gly (1)	106.8(2)	--	-169.9(1)	-161.6(1)
tBu$\beta^{3,3}$Ac6c (2)	57.1(2)	54.5(2)	-104.4(2)	-179.5(1)
Gly (3)	-169.3(1)	--	-138.5(1)	179.7(1)
tBu$\beta^{3,3}$Ac6c (4)	-50.4(2)	-51.5(2)	116.3(2)	170.0(1)
Gly (5)	146.4(2)	--	161.2(1)	-175.2(1)
tBu$\beta^{3,3}$Ac6c (6)	60.9(2)	38.7(2)	-125.9(2)	179.6(1)
Gly (7)	-107.5(2)	--	153.2(1)	-178.1(1)
tBu$\beta^{3,3}$Ac6c (8)	69.6(2)	52.8(2)	78.4(2)	--

The measured torsion angles for all ^{L}Gly and *β*-amino acids are listed in Table 3.3. The Ramachandran plots were generated using all calculated torsion angles (φ and ψ) and are shown in Figure 3.4. All ^{L}Gly residues in the peptide backbone exhibit large variability in their φ and ψ values with an average of around ±132.7(30.9)° for φ while the ψ torsion angles are averaged around ±155.7(13.3)°. As shown by the Ramachandran plot in Figure 3.4 the φ, ψ values of all four Gly residues are distributed across all four quadrants and they fall within the allowed regions of the Ramachandran plot of Glycine. Gly(1) residue has φ, and ψ of 106.8°, and -169.9° suggesting some twisting in the peptide backbone but generally an extended *β*-sheet-like conformation. The deviation of its ω from the ideal 180° may be because of constraints of making intramolecular H-bonds by N-H and C=O of Gly(1) with C=O and N-H respectively of

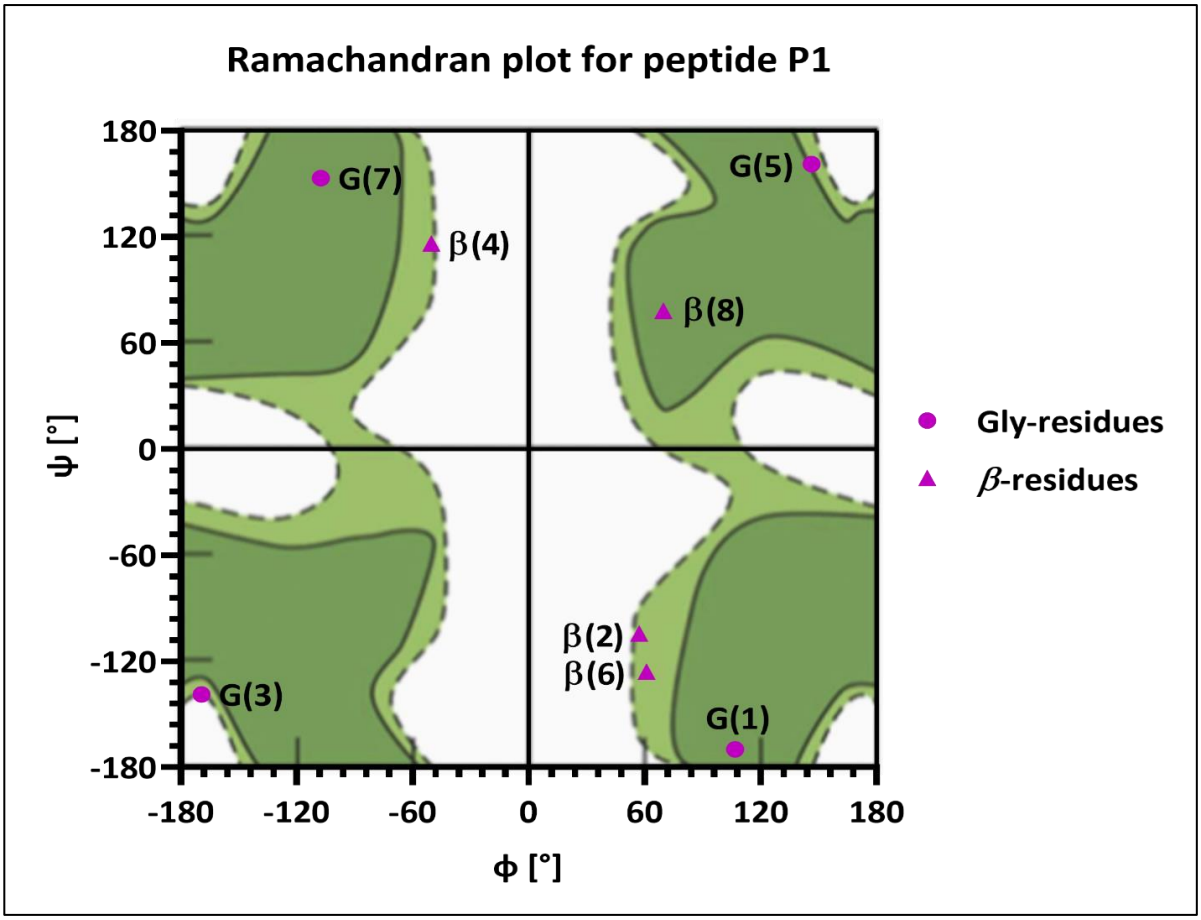

Figure 3.4. The Ramachandran plot for octapeptide **P1.** The green-colored area shows the allowed regions (continuous lines) and the generously allowed regions (dotted lines) for Gly residue in peptides/proteins (adapted from Ramakrishnan, 2001).(88),(106) Each point in the plot corresponds to a specific residue, and their positions indicate the dihedral angles of peptide **P1**. The dihedral angles of *β* residues are also shown for comparison.

Gly(7) (Figure 3.3). In the case of Gly(3), the torsion values are φ = -169.3°, and ψ = -138.5° showing an extended backbone conformation. Gly(5) residue has φ, ψ of 146.4(2)° 161.2(1)° and Gly(7) has φ, ψ values of about -107.5(2) and 153.2(1) respectively. Overall, all four Gly residues have extended *β*-sheet-like conformations.

All four *β* residues, *β*(2-8), adopt *gauche* conformation for φ torsion angles with an average of around ±59.5(8.0)° while their ψ torsion angles are averaged around ±106.3(20.5)° (Table 3,3). Generally, for all *β*-residues, the sign of (φ, θ, and ψ) is either (+, +, -) or it is (-, -, +) except for β(8), where it is (+, +, +). Since the C=O of *β*(8)

at one end is involved in water (OW1) mediated interaction with N-H and C=O of *β*(6) residue (Figure 3.3) and at the other end its methoxy O makes H-bond with N-terminal C=O of the Boc group of another symmetry-related molecule (translational along *a*-direction). Hence these H-bonding constraints may be forcing ψ of *β*(8) residue to take an unusual torsion angle value. All four *β*(2-8) residues adopt *gauche* conformation about the C_{β} - C_{α} bond either with positive (+) or negative (-) signs with θ-values about ±50(6.3)° (Table 3.3). The three of the *β*-residues have a very narrow range of θ values around ±52.9(1.5)°. Only *β*(6) shows a larger deviation from this average θ-value and has a low value around 38.7(2)°. Since N-H and C=O of *β*(6) are involved in water (OW1) mediated H-bonding with terminal carbonyl of *β*(6), this constrain may be responsible for its larger deviation from the average θ-value observed for the other three *β*-residues (Figure 3.3). It seems the bulky t-Bu substitution on the cyclohexyl rings, may restrict its flexibility, which in turn may lead to restriction of its (φ, θ, and ψ) values in a different region around [±59.5(8.0), ±50 (6.3), ± 106(20.5)] compared to the to [±73(9), ±58 (6), ± 91(6)] observed for $\beta^{3,3}$Ac6C observed in peptides containing chiral-achiral dimeric repeats like (^{L}Leu- $\beta^{3,3}$Ac6C) (Chapter 5). Hence, when combined with flexible achiral Gly residue, their dimeric repeats show unique folds, as observed for **P1**.

The ω values in all ^{L}Gly and *β* residues are consistently around ±175(7)°, which is close to ±180°, indicating that all peptide bonds adopt the *trans* configuration (a common feature for peptide bonds), which is more stable than the *cis* configuration. The varying torsion angles suggest regions of flexibility due to Gly residues, and the rigidity in *β*(2-8) residues allows the peptide to adopt different stable conformations and influence their behaviour in the crystal lattice. The peptide **P1** shows high

intramolecular hydrogen bonding, as shown by the hydrogen bond analysis, which is essential for maintaining its stability (Shown in Table 3.4).

Table 3.4. List of hydrogen bond and angle (°) distances of peptide **P1**. The standard deviations are shown in parentheses.

Type (Octapeptide P1)	Donor (D)	Acceptor (A)	D---A (Å)	H---A (Å)	<DH---A (°)
Intramolecular	NH (Gly (1))	CO (Gly (7))	3.0666(19)	2.20	167
Intermolecular	NH (tBu-$\beta^{3,3}$Ac$_6$c (2))	CO (OW (1))[e]	2.897(2)	2.04	165
Intramolecular	NH (Gly (3))	CO (Gly (5))	2.9052(18)	2.16	142
Intermolecular	NH (tBu-$\beta^{3,3}$Ac$_6$c (4))	CO (tBu-$\beta^{3,3}$Ac$_6$c (4))[b]	2.9248(18)	2.05	173
Intramolecular	NH (Gly (5))	CO (Gly (7))	2.8510(18)	2.17	134
Intermolecular	NH (tBu-$\beta^{3,3}$Ac$_6$c (6))	CO (OW (2))	2.931(2)	2.21	139
Intramolecular	NH (Gly (7))	CO (Gly (1))	2.8249(19)	1.96	169
Intermolecular	NH (tBu-$\beta^{3,3}$Ac$_6$c (8))	CO (tBu-$\beta^{3,3}$Ac$_6$c (6))[d]	2.8928(19)	2.04	162
Intermolecular	OH (MeOH (1))	CO (tBu-$\beta^{3,3}$Ac$_6$c (2))	2.692(2)	1.86	172
Intermolecular	OH (OW (1))	CO (MeOH (1))	2.739(2)	1.89	167
Intermolecular	OH (OW (1))	CO (tBu-$\beta^{3,3}$Ac$_6$c (4))	2.8880(18)	2.05	162
Intermolecular	OH (OW (2))	CO (tBu-$\beta^{3,3}$Ac$_6$c (8))	2.672(3)	1.82	166
Intermolecular	OH (OW (2))	CO (tBu-$\beta^{3,3}$Ac$_6$c (6))	2.849(2)	1.99	170
Intermolecular	CH (Boc)	OH (OW (2))[d]	3.359(4)	2.49	148
CH (Boc)	CH (Boc)	CO (Boc)	2.888(3)	2.36	113
Intramolecular	CH (Boc)	CO (Boc)	2.971(3)	2.38	118
Intramolecular	CH (Gly (1))	CO (Boc)	2.778(2)	2.37	104
Intramolecular	CH (Gly (1))	CO (Gly (5))	3.316(2)	2.50	139
Intramolecular	CH (tBu-$\beta^{3,3}$Ac$_6$c (2))	CO (Gly (1))	3.055(2)	2.49	116
Intramolecular	CH (tBu-$\beta^{3,3}$Ac$_6$c (2))	CO (tBu-$\beta^{3,3}$Ac$_6$c (2))	3.105(2)	2.45	123
Intramolecular	CH (tBu-$\beta^{3,3}$Ac$_6$c (2))	CO (Gly (1))	3.120(2)	2.55	116
Intramolecular	CH (tBu-$\beta^{3,3}$Ac$_6$c (2))	CO (Gly (5))	3.3709(19)	2.51	145
Intermolecular	CH (Gly (1))	CO (tBu-$\beta^{3,3}$Ac$_6$c (4))[b]	3.3979(19)	2.55	143
Intermolecular	CH (Gly (1))	CO (tBu-$\beta^{3,3}$Ac$_6$c (2))[a]	3.381(2)	2.41	167
Intermolecular	CH (tBu-$\beta^{3,3}$Ac$_6$c (4))	CO (MeOH (1))	3.330(4)	2.36	167
Intermolecular	CH (tBu-$\beta^{3,3}$Ac$_6$c (4))	CO (tBu-$\beta^{3,3}$Ac$_6$c (4))	3.108(2)	2.45	123
Intramolecular	CH (tBu-$\beta^{3,3}$Ac$_6$c (4))	CO (Gly (3))	2.935(2)	2.37	115
Intramolecular	CH (Gly (5))	CO (tBu-$\beta^{3,3}$Ac$_6$c (4))	2.788(2)	2.44	100
Intramolecular	CH (Gly (5))	CO (tBu-$\beta^{3,3}$Ac$_6$c (8))	3.425(3)	2.45	168
Intramolecular	CH (tBu-$\beta^{3,3}$Ac$_6$c (6))	CO (Gly (5))	2.988(2)	2.38	119
Intramolecular	CH (tBu-$\beta^{3,3}$Ac$_6$c (6))	CO (tBu-$\beta^{3,3}$Ac$_6$c (6))	3.181(2)	2.51	125
Intermolecular	CH (tBu-$\beta^{3,3}$Ac$_6$c (6))	CO CO (MeOH (2))[f]	3.533(4)	2.56	170
Intramolecular	CH (tBu-$\beta^{3,3}$Ac$_6$c (6))	CO (Gly (1))	3.279(2)	2.40	148
Intramolecular	CH (Gly (7))	CO (tBu-$\beta^{3,3}$Ac$_6$c (8))	2.786(2)	2.39	103
Intramolecular	CH (tBu-$\beta^{3,3}$Ac$_6$c (8))	O (OMe)	3.080(2)	2.48	119
Intermolecular	CH (tBu-$\beta^{3,3}$Ac$_6$c (8))	CO (Boc)[c]	3.418(2)	2.57	144
Intramolecular	CH (tBu-$\beta^{3,3}$Ac$_6$c (8))	CO (Gly (7))	2.999(2)	2.43	116
symmetry operations: a: -x,1-y,1-z; b:1-x,-y,1-z; c:1-x,1-y,1-z; d:1+x,y,z; e:1-x,1-y,-z; f:-1+x,y,z.					

3.6.3. Crystal packing

The packing of **P1** in the crystalline state is shown in Figure 3.5. There are two molecules in the unit cell which are related by an inversion centre. They interact by forming a pair of H-bonds between two symmetry-related molecule's *β*(4) residue where N-H and C=O of *β*(4) residue make intermolecular H-bonds with another C=O and N-H of inversion symmetry-related molecule's *β*(4) residue (Fig 35.a and d). Additionally, the C=O of the same *β*(4) residue makes water (OW1) and methanol (MeOH1) mediated H-bond with C=O of *β*(2) of the inversion symmetry-related molecule and vice versa. Thus, two pairs of H-bonds stabilize the dimer formed by the molecule and its inversion symmetry-related molecule (Fig 3.5a). This inversion symmetry-related H-bonded pair formation propagates roughly along the *c*-direction in the crystal, and they are joined together by a pair of H-bonds between C=O of β6 and NH β8 of one molecule with NH and C=O of β8′ and β6′, respectively, of a symmetry-related molecule (Fig 3.5 b and d). The C=O of *β*(8) residue through water-mediated interaction forms H-bond with N-H of *β*(2). This propagates the crystal along the *a*-direction (Figure 3.5d). No H-bond formation was observed along the *b*-direction (Figure 3.5c). The hydrophobic interaction between tBu-moieties of *β* residues helps to expand the crystal formation along the *b*-direction, and this interaction mimics leucine zipper-like interactions.

The molecules in peptide **P1** crystal are arranged in a parallel orientation in the overall crystal packing with two molecules inside the crystal unit cell and, one centre of inversion symmetry is present between two achiral molecules leading to every molecule to be inversely aligned with respect to the other molecule (Figureure 3.5d).

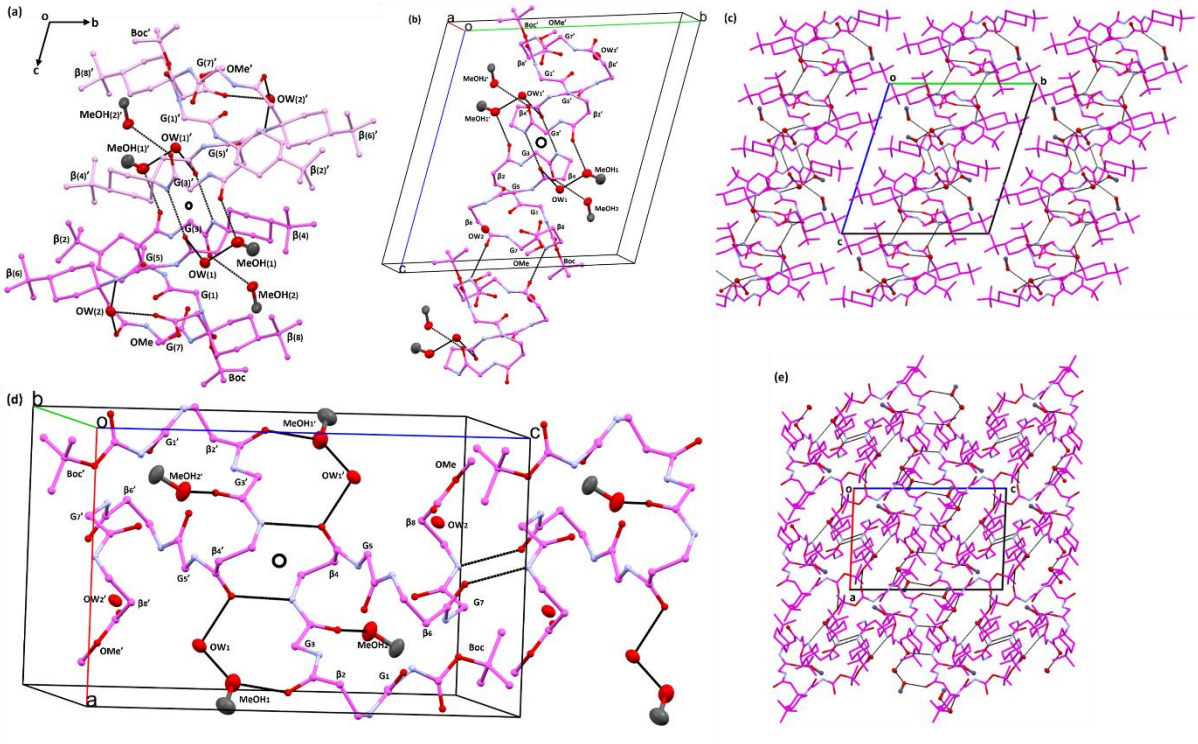

Figure 3.5. Crystal packing observed for peptide **P1**. **(a)** Interaction of two molecules of peptide **P1** in crystal unit cell viewed along a-axis shown in ball and stick model. Two molecules related by inversion symmetry are present in the unit cell. One molecule of peptide **P1** is shown in magenta and another inversion symmetry-related molecule is shown in light magenta for better understanding. The inversion centre is shown by an open circle between two molecules; **(b)** The same arrangement when viewed along the a-axis of unit cell in ball and stick model. All side chains are removed for the sake of clarity. The inversion centre is shown by an open circle between two molecules **(c)** The same viewed along the a-axis (in stick model); (d) Packing of the molecule of **P1** viewed along the b-axis (in ball and stick model). All side chains have been removed for the sake of clarity. The inversion centre is shown by open circle **(e)** The crystal packing viewed along the b-axis (in stick model). All the α and β amino acids as well as the N-terminal Boc and C-terminal methoxy (OMe) groups have been labelled. All putative intermolecular H-bonded interactions have been shown by dashed lines. All C, N and O-atoms are shown in magenta, blue, and red colours respectively. The solvent molecules (two water and two methanol) have also been shown in sphere model and are labelled.

The octapeptide **P1** adopts two C_{12}, one C_{24}, and one C_{26} types of intramolecular H-bond mediated folded conformations in their structures. A few putative H-bonds were also observed between **P1** and solvent molecules (water and methanol). Therefore,

they are crucial for defining the overall conformation and stability of **P1**. The schematic diagram of the peptide's intramolecular H-bonded pattern is shown in Figure 3.6.

A highly ordered crystal lattice by the peptide **P1** is produced by a combination of different factors like inter and intramolecular H-bonded interactions, weak wander wall interactions especially between tBu groups of *β*-amino acids, optimal torsional angles (φ, θ, ψ, and ω) of *β*-amino acids. It is additionally helped by interactions with solvent molecules (water and methanol).

3.7. Conclusions

- ✓ The octapeptide **P1** structure comprises dimeric repeats of achiral *α*- (standard amino acid, glycine) and *β*- (non-standard amino acid, tBu$\beta^{3,3}$Ac$_6$c) amino acids. Unique conformational properties were observed for tBu*β* residues, which introduces structural diversity in *α*/*β* hybrid peptides.
- ✓ It seems the bulky t-Bu substitution on the cyclohexyl rings, may restrict its flexibility, which in turn may lead to restriction of its (φ, θ, and ψ) values in a different region around [±59.5(8.0), ±50 (6.3), ± 106(20.5)] compared to the to [±73(9), ±58 (6), ± 91(6)] observed for $\beta^{3,3}$Ac6C observed in peptides containing chiral-achiral dimeric repeats like (^{L}Leu- $\beta^{3,3}$Ac6C). Hence, when combined with flexible achiral Gly residue, their dimeric repeats may show unique folds, as observed for **P1**.
- ✓ We have discovered a unique paper clamp-like fold in the *α*/*β* hybrid achiral peptide, which has not been reported so far in any natural or synthetic non-coded amino acids-based peptides.

CHAPTER-4

Conformation of α/β Hybrid Peptides Containing Achiral 1-Aminocyclohexaneacetic acid ($\beta^{3,3}$-Ac_6c)

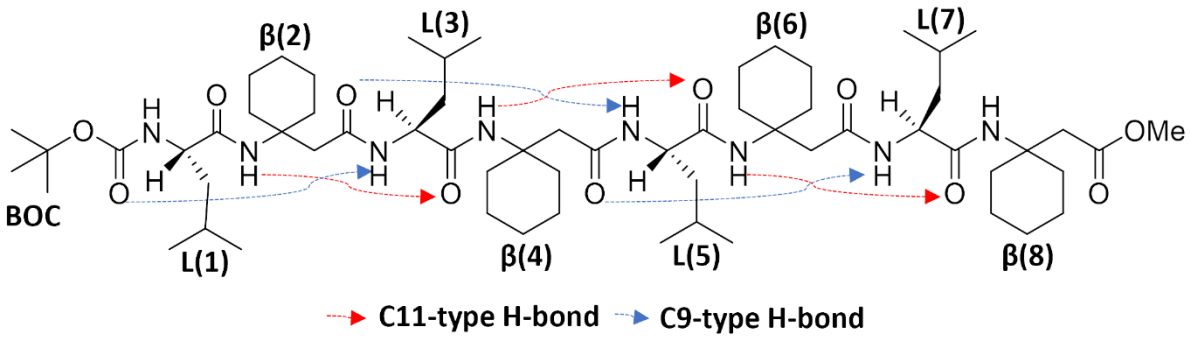

4.1 Graphical Abstract

Stable helices: Repeating mixed of C_{11}/C_9 intramolecular H-bonds with opposite directionalities stabilize the helical conformation in α/β hybrid peptides.

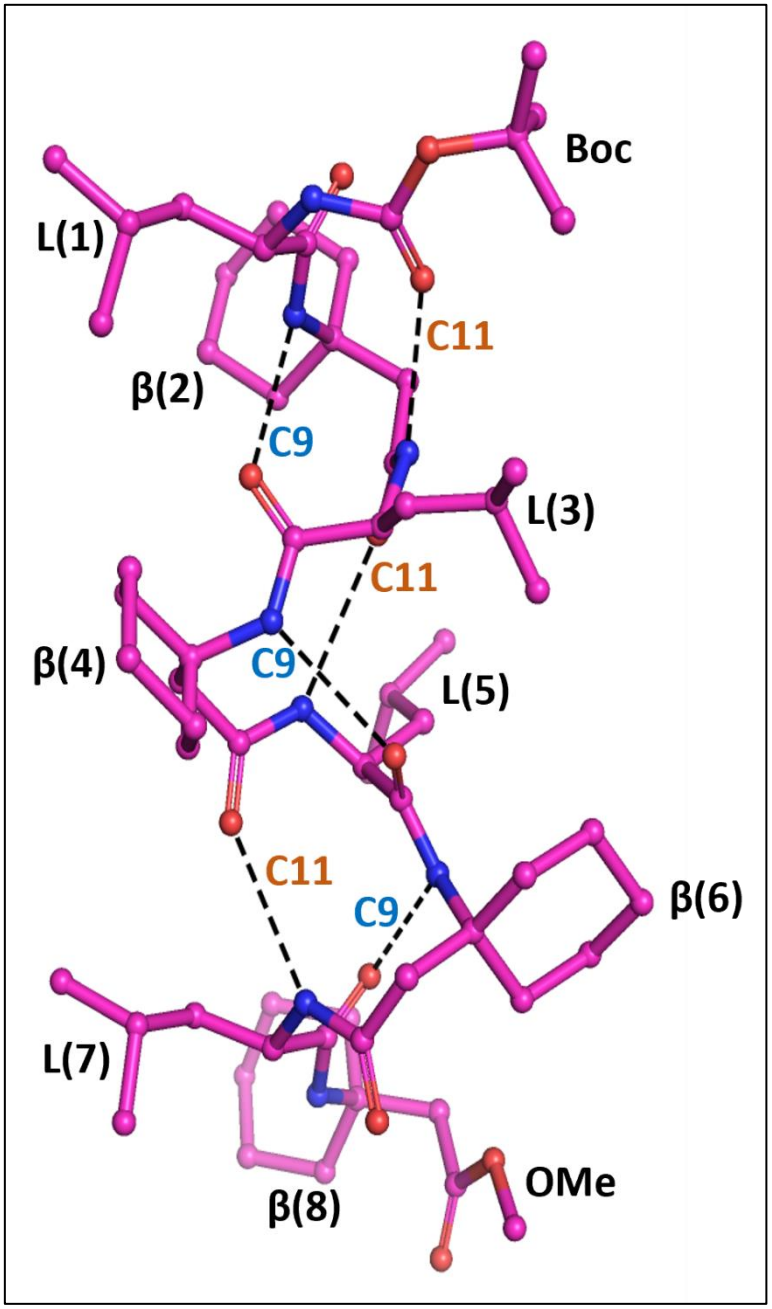

4.2 Abstract

This study elucidates the conformational characteristics of α/β hybrid peptide, Boc-^{L}Leu-β^{3,3}Ac$_6$c-^{L}Leu-β^{3,3}Ac$_6$c-^{L}Leu-β^{3,3}Ac$_6$c-^{L}Leu-β^{3,3}Ac$_6$c-OMe (**P2**) through X-ray crystallography. The octapeptide **P2** adopts a folded helical conformation stabilized by repeating mixed types of C_{11}/C_9 intramolecular H-bonds. The chiral ^{L}Leu residues seem to take φ, and ψ values around ±65.3(12.4)°, and ±154.9(5)° while the *β*-residues (*β*^{3,3}Ac$_6$c) seem to take phi (φ), theta (θ) and psi (ψ) values around (77(6)°, 58(6) and -91(6)°). The φ and ψ values in this range suggest that the ^{L}Leu residues likely fall within regions typical for β-sheet-like secondary structure and the β-residues exhibit more conformational diversity, particularly in the ψ angle, indicating they might be involved in a more flexible region of the peptide. The larger spread in ψ angle suggests that the β-residues may have greater conformational flexibility compared to the ^{L}Leu residues suggesting that the β-residues are able to accommodating structural changes or transitions better than Leu. The β^{3,3}Ac$_6$c (2-8) residues are able to fit well in helical conformation. Four molecules are present in the triclinic space group due to symmetry breaking. The self-assembly of peptide **P2** forms channels filled with solvent molecules (Dioxane and ethanol) that present interesting patterns in the crystal.

Keywords: Amino acids, α/β hybrid peptides, hydrogen bonds, helices, conformations, x-ray crystallography.

4.3 Introduction

This chapter presents the structural characteristics of α/β hybrid peptide (s) Boc-[Leu-$\beta^{3,3}Ac_6c]_4$-OMe containing dimeric repeating units of one chiral L-α-amino acid (Leucine) and one achiral β-amino acid ($\beta^{3,3}Ac_6c$) shown in Figure 4.1 a in solid state studied by single crystal X-ray crystallography. Earlier, similar structures of the tetrapeptide and pentapeptide were solved and reported by Wani et. al., 2017.(31) Hence, by repeating these α and β dimers, we want to see if the structural features observed in previously reported tetrapeptide and pentapeptide are retained or changed when we increase the length of these α/β hybrid peptides.

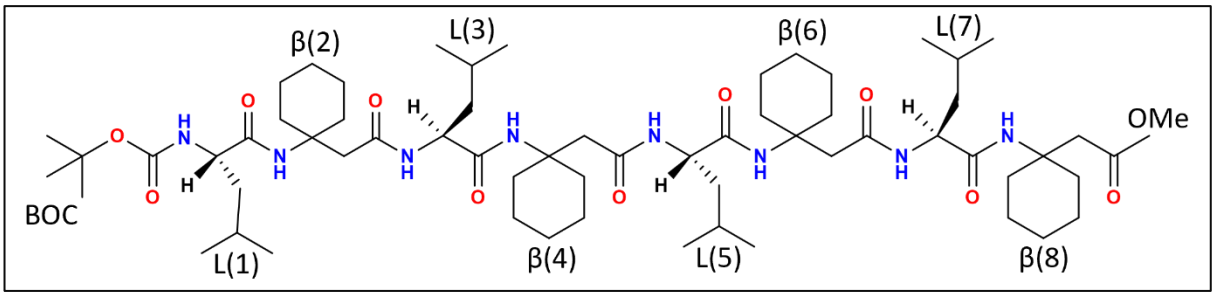

Figure 4.1: Scheme of peptide **P2** (Boc-[Leu-$\beta^{3,3}Ac_6c]_4$-OMe).

4.4 Literature review

The previous study by Wani et. al., 2017(31) and Vasudev et. al., 2008(8) reported C_{11}/C_9 helical folding in α/β hybrid peptides containing 1-amino cyclohexane acetic acid ($\beta^{3,3}Ac_6c$), a homolog of the conformationally constrained amino acid 1-amino-cyclohexane-1-carboxylic acid, Ac_6c. Research in this area is aimed at how alternating sequences of L- and β-residues facilitate unique folding behaviors.1,3,3–7 For instance, 1-amino-cyclohexane acetic acid (Ac_6c) or its derivatives are acknowledged to influence backbone torsion angles and foster helical motifs such as the C_{11}/C_9 helix. From our previously published data by Shankar et. al., 2022(111) we replaced the

leucine residue in the backbone peptide with an achiral amino acid glycine. They studied the effect of conformationally flexible achiral glycine residue C_{11}/C_{12} helix on the backbone conformation in α/β-hybrid peptides through x-ray crystallography analysis. Those studies aimed to explore the hydrogen-bonded conformations and examine the effect of β, β-di-substitution in an β-amino acid on the conformation of peptides.

In brief, the study of previous work by Wani et. al., 2017(31), was related to α/β hybrid peptides (tetrapeptide; Boc-[Leu-$\beta^{3,3}Ac_6c]_2$-OMe and pentapeptide; Boc-[Leu-$\beta^{3,3}Ac_6c]_2$-Leu-OMe) that contain α-amino acids (like L-amino acids) and β-amino acids have been studied for the unique structural properties of their helical folding and enhanced stability compared to their natural counterparts through x-ray crystallography method. The studies typically test the ability of β-amino acids to disrupt or stabilize specific secondary structures, such as C_{11}/C_9 helices or C_{12}-helices, which are very far from the standard α-helices found in proteins. The inclusion of β-amino acids containing rigid cyclohexane-based macrocycles increases conformational stability. Studies have been interested in the functions of the residues in generating well-characterized secondary structures. Such studies involve hydrogen bonding networks, torsion angles as well as steric contribution from the cyclohexane-containing β-residues.

In the present study, we extensively investigate the crystal structure of octapeptide containing 1-amino cyclohexane acetic acid ($\beta^{3,3}Ac_6c$) using single crystal x-ray crystallography. The crystal structure of long α/β hybrid peptide incorporating conformationally constrained β, β-disubstituted β-amino acid ($\beta^{3,3}Ac_6c$). β-Amino acid contains amino and carboxyl groups separated by two carbon atoms in the backbone. The insertion of additional atoms in between the flanking peptide units enhances the

number of degrees of torsional freedom resulting in an expansion of energetically-accessible conformational space. The chemical structure of a β-amino acid residues with torsion angles are shown in Figure 4.2.

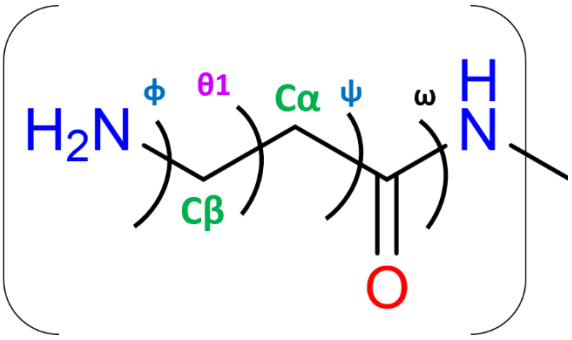

Figure 4.2: The chemical structure of β-amino acid residues showing its backbone torsion angles.

4.5 Methodology

4.5.1 Single crystal x-ray crystallography

The single crystals of octapeptide **P2**: (Boc-[Leu-$\beta^{3,3}$Ac6c]$_4$-OMe) were grown by a slow evaporation method using a dioxane/water (4:1) mixture. Clear, light hexagonal plate-shaped crystals were grown within 15 days. Initially, initially due to the poor quality of the crystals, we could not solve the structure for a long time. We repeated the data collection by selecting different crystals, but the structure could not be solved. Finally, a good quality crystal with a dimension of 0.9 x 0.6 x 0.2 mm^3, was used to collect the data at a cryogenic temperature of 100 K. The intensity data was collected on a Bruker Kappa Apex II diffractometer (*Mo Kα* = 0.71073 Å) using φ and ω scans. The peptide, **P2** subjected to structural solution and refinement using the Olex 2-1.5 (http://www.olexsys.org) program suite(82). SHELXT(83) program was used to solve the structure and refine it. Mercury 2024.2.0. (104)

(https://www.ccdc.cam.ac.uk/solutions/csd-system/components /mercury/) was used to create the hydrogen-bond distances, torsion angles (φ, θ, ψ, and ω), and crystal packing diagrams. The structures alignment was done by using chimera software(86) (Version 1.18) and the figures of molecules alignment/superimposed view were prepared using PyMol(112) (The PyMOL Molecular Graphics System, Version 2.3.2, Schrodinger, LLC.), and all figures are compiled together using GIMP version 2.10.34 (GNU Image Manipulation Program).(105)

The peptide **P2** structure cif file was submitted to The Cambridge Crystallographic Data Centre (CCDC) (Advancing Structural Science | CCDC (cam.ac.uk))(84) with CCDC number. The joint Cambridge Crystallographic Data Center and Fachinformationszentrum Karlsruhe http://www.ccdc.cam.ac.uk/structures Access Structures service provides these data free of charge.

4.6 Results and Discussion

4.6.1 Single crystal X-ray diffraction study

The octapeptide **P2** crystallized in the P1 space group with four molecules in the asymmetric unit. The crystal x-ray diffraction data and structure refinement parameters details of peptide **P2** are given in Table 4.1.

Table 4.1: Crystal x-ray diffraction data and structure refinement parameters of octapeptide **P2**.

Parameters	**octapeptide (P2)**
Empirical formula	$(C_4H_8O_2)_4\ (CH_4O)_4\ (H_2O)_2$
Formula weight	1278.61
Crystal habit	Plate
Crystal size [mm^3]	0.9 x 0.6 x 0.2
Crystallizing solvent	Water: Dioxane
Temperature (K)	100.15
Wavelength	0.71073
Crystal system	Triclinic
Space group	P1
a [Å]	9.9361(5)
b [Å]	10.0827(5)
c [Å]	84.853(5)
α [°]	89.242(3)
β [°]	88.749(3)
γ [°]	60.437(3)
Volume [$Å^3$]	7392.3(7)
Z	4
Density [g/cm3] [calc.]	1.149
F (000)	2790.0
Radiation	Mo K/α
Θ Range [°]	2.88 to 52.868
Scan type	ω/φ
Independent reflections	44360
Measured reflections	53752
Observed reflections with *I* >= *2σ(I)*	475893
R*int*	0.0478
Δ*ρmax* / Δ*ρmin* [e $Å^{-3}$]	0.67/-0.51
Goodness-of-fit on F2	1.021
Final *R* / *wR2* [%]	0.1007/0.2616
restraints/parameters	403/3384
Flack parameter	0.3 (7)
CCDC No.	

4.6.2. Molecular Structure

The solved molecular structures of peptide P2 are shown in Figure 4.3(a-d). In peptide **P2**, the amino group of $\beta^{3,3}$-Ac_6c (2), (4), (6), and (8) residues in all four molecules (mol-A to mol-D) occupy axial orientation. The cyclohexyl rings of all β-

residues are in stable chair conformation. All four molecules of the peptide take helical conformation which are stabilized by C9/C11 type H-bonds.

The superimpose view of all four molecules of octapeptide P2 is shown in Figure 4.3 e. The four molecules aligned with each other very well with slight differences at sidechain residues and N-terminus and C-terminus. All molecules mol-B, mol-C, and mol-D were aligned to mol-A with their RMSD value of about 0.593 Å, 0.528 Å, and 2.083 Å respectively.

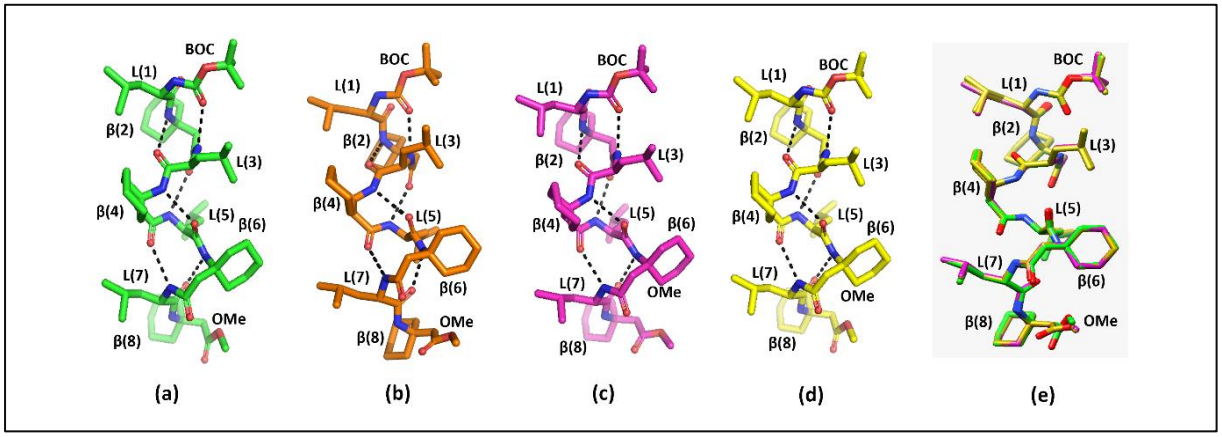

Figure 4.3: The solid-state molecular conformations of octapeptide **P2** showing four independent molecules. (a) Molecule-A; (b) Molecule-B; (c) Molecule-C; (d) Molecule-D; and (e) Superimposed view of all four molecules A-D. The repeating C_{11}/C_9 type intramolecular H-bonds in all four individual molecules were shown by black dashed lines. All the hydrogen atoms have been removed for the sake of clarity.

The torsion angles of all four molecules have been shown using Ramachandran plot (Figure 4.4). When we observe the torsion angles of the octapeptide **P2**, the β(8) residue shows a slight difference in conformation compared to all other β(2), β(4) and β(6) residues in the peptide molecules mol-A, mol-B, mol-C, and mol-D shown in, which may be due to constraining of H-bonding dioxane molecules as observed in the crystal structure. The φ and ψ values along with their standard deviation (SD) for α-

└Leucine residues Leu (1), (3), (5), and (7) for all four molecules are within the allowed region of the Ramachandran plot with φ and ψ values around -65.3(12.4)°, and +154.9(5)° respectively, which is β-sheet like conformation.

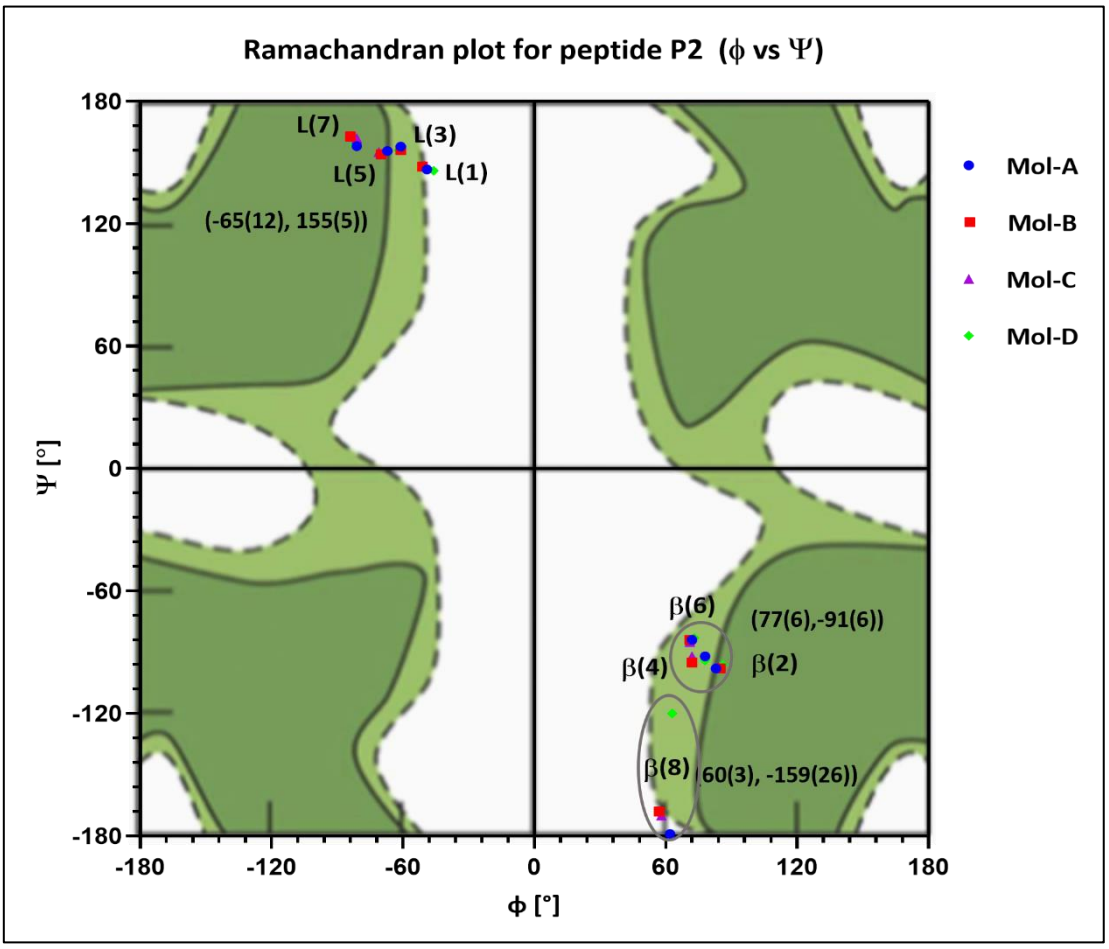

Figure 4.4: Ramachandran plot for all four molecules (mol A-D) of octapeptide **P2**. The green-colored area shows the allowed regions (continuous lines) and the generously allowed regions (dotted lines) for Gly residue in peptides/proteins (adapted from Ramakrishnan, 2001).(113,114) Each point corresponds to a specific residue, and their positions indicate the dihedral angles of peptide residue. The dihedral angles of *β* residues are also shown for comparison. Mol-A is shown in blue color, mol-B is shown in red color, mol-C is shown in purple color and mol-D is shown in green color.

The torsion angles of all β-amino acids from all four molecules β (2-8), lie in the fourth quadrant of the Ramachandran plot. The β(2-6) residues formed clusters with φ and ψ values around +77(6)° and -91.5(5.8) whereas all β(8) residues among four

molecules had slightly different values of φ and similar ψ values around +60(2.9) and -159(26.6). The difference observed for β(8) residues may be due to their environmental factors/packing constrains in the crystal lattice. The dihedral angles (φ and θ) of β-amino acids β(2), (4), (6), and (8) from all four molecules lie in the first quadrant of the plot. φ and θ values are around +73(9.3) and +58(5.6) shown in Figure 4.5.

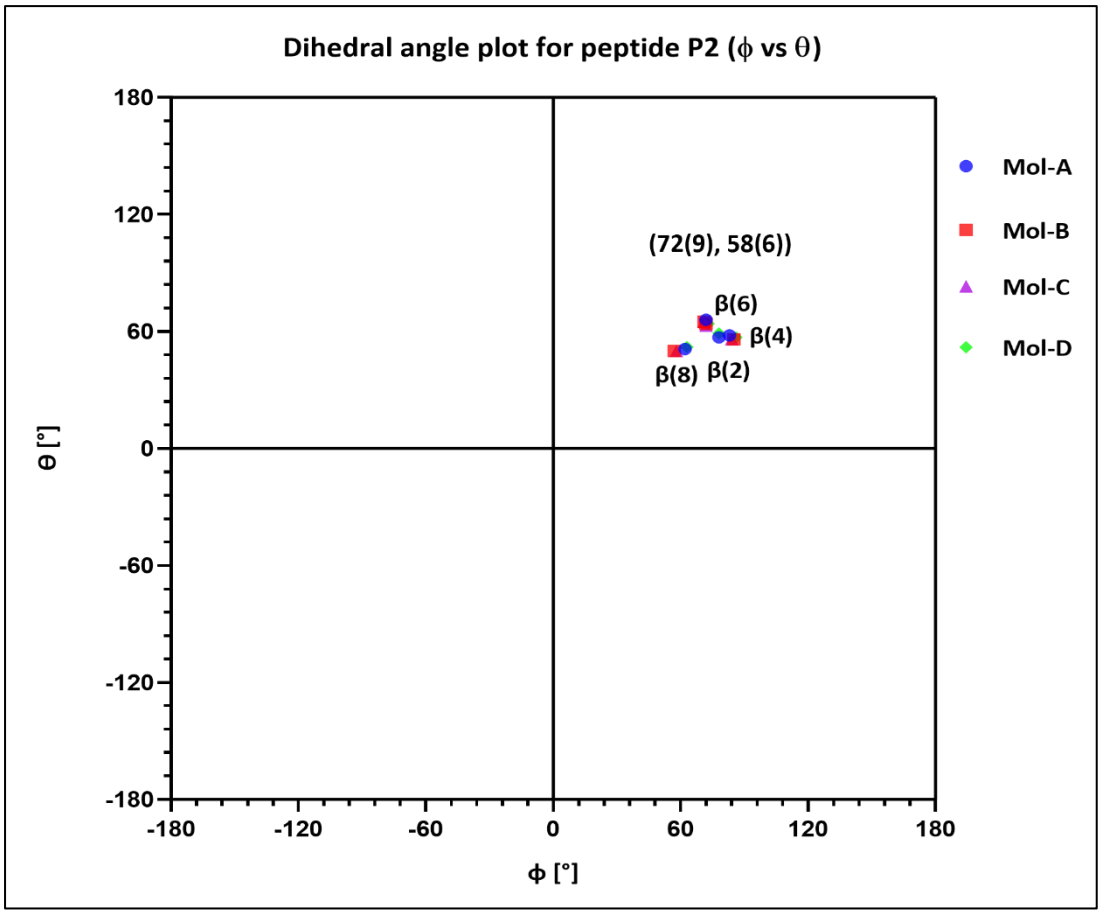

Figure 4.5: Dihedral angles plot for all β-residue of four molecules (mol-A to mol-D) of octapeptide **P2**. The green-colored area shows the allowed regions (continuous lines) and the generously allowed regions (dotted lines) for Gly residue in peptides/proteins (adapted from Ramakrishnan, 2001). (113,114)The dihedral angles of *β* residues are also shown for comparison. Mol-A is shown in blue colour, mol-B is shown in red colour, mol-C is shown in purple colour, and mol-D is shown in green colour.

4.6.3. Crystal Packing Studies of Peptide P2

In the crystal packing studies of the peptide **P2**, while packing, the four molecules mol-A, mol-B, mol-C, and mol-D were packed in the present cell with *c*-axes of 85 Å and not the half-length 45 Å cell along the *c*-axis, which we had anticipated. Along with the unique solvent interface between mol-B and mol-C, the finer differences between interfaces of mol-A/mol-B and mol-C/mol-D may be breaking the symmetry among the four observed molecules in the present crystal structures. Hence, we do not get a higher symmetrical space group with one molecule asymmetric unit. Rather, we get four molecules in the present triclinic crystal system with the *P*1 space group, as shown in Figure 4.6. The dimension of each of the four molecules was calculated and shown in Table 4.2.

The intramolecular and intermolecular H-bonding distances and their angles were calculated for all four molecules mol A-D of peptide **P2** and are listed in Table 4.3 and Table 4.4, respectively. All four molecules (mol-A to mol-D) in the peptide **P2** are taking helical conformation stabilized by repeating C_{11}/C_9 type of H-bonds which are crucial for stabilizing the molecular structures in peptides. In α-helical structure, the C_{11} type of intramolecular H-bond forms between β-amino acid residue and α-amino acid i to i+3 manner, and the C_9 type of intramolecular H-bond also forms between β-amino acid residue and α-amino acid i to i+1 manner (Figure 4.9). The N-H of L(3), L(5), and L(7) groups are forming C_{11} type of intramolecular H-bond repeats with C=O of Boc, β(2), β(4) groups respectively in the backbone structure of all four molecules (mol-A to mol-D) and N-H of β(2), β(4) and β(6) groups are forming C_9 type of intramolecular H-bond repeats with C=O of L(3), L(5) and L(7) groups respectively in the backbone structure of all four molecules mol-A to mol-D contribute to maintaining stable helical secondary structure. The crystal packing pattern of four molecules of octapeptide **P2**

in a crystal unit cell along the a-axis shown in Figure 4.7. Mol-A and mol-B are bound together by a dioxane molecule in a tail-to-tail manner whereas mol-B and mol-C interact in a head-to-head manner. Mol-C and mol-D interact similarly to mol-A and mol-B. The same arrangement of molecules inside the crystal unit cell pattern is shown in the cartoon representation shown in Figure 4.7b. Similarly, the crystal packing pattern viewed along the a-direction and b-direction are shown in Figure 4.7c,.

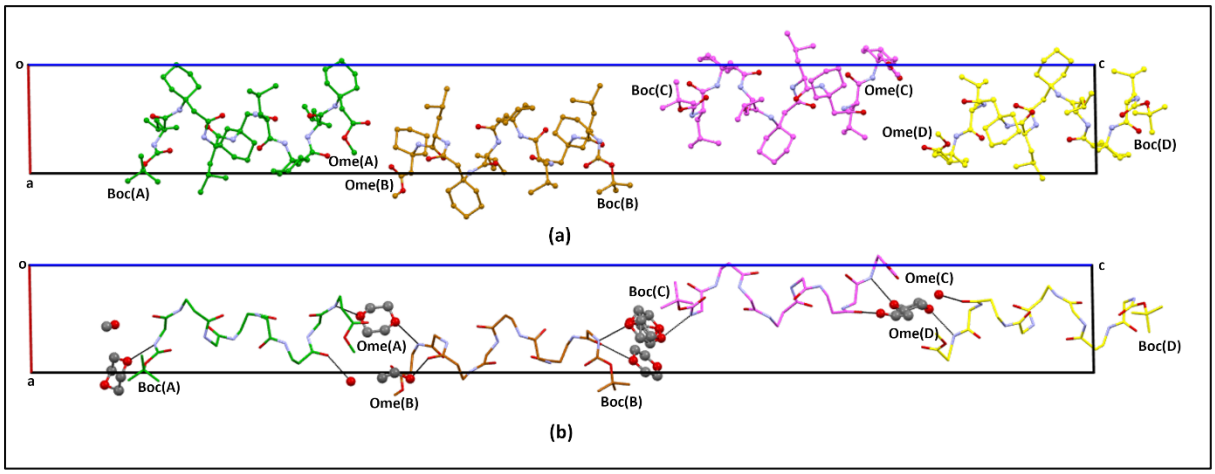

Figure 4.6: The crystal packing octapeptide **P2** viewed along the b-direction. (a) All four molecules A-D are shown in the ball and stick model with respective colour codes (mol-A (green), mol-B (orange), mol-C (magenta), and mol-D (yellow)). All solvent molecules and hydrogens were removed for the sake of clarity; (b) The same view was shown along with solvent molecules. All four molecules shown in the stick model and all sidechains of the backbone have been deleted for sake of clarity. All solvent molecules are shown in the ball and stick model. All hydrogens have been removed for the sake of clarity. The putative H-bonds have been shown in black dashed lines.

Also, the N-H of β(8) and L(1) forming intermolecular H-bonds with solvent molecules (Dioxane and ethanol) help in overall crystal packing and solvent-mediated stabilization of peptides.

Table 4.2: Data for crystal cell dimensions and cell origin of each molecule of octapeptide P2.

Peptide	**Dimension (Å)**

Mol-A	
Cell Basis Vector 1 (a)	11.040000200271606 0 0
Cell Basis Vector 2 (b)	0 11.365999698638916 0
Cell Basis Vector 3 (c)	0 0 19.977996826171875
Cell Origin: x = 8.061817169189453; y = 2.575385332107544; z = 80.86487579345703	
Mol-B	
Cell Basis Vector 1 (a)	10.944999754428864 0 0
Cell Basis Vector 2 (b)	0 11.577999830245972 0
Cell Basis Vector 3 (c)	0 0 20.23299789428711
Cell Origin: x = 5.526697158813477; y = 2.9047629833221436; z = 60.07504653930664	
Mol-C	
Cell Basis Vector 1 (a)	10.9660005569458 0 0
Cell Basis Vector 2 (b)	0 11.535999774932861 0
Cell Basis Vector 3 (c)	0 0 20.307998657226563
Cell Origin: x = 10.111132621765137; y = 2.842677116394043; z = 38.02681350708008	
Mol-D	
cell Basis Vector 1 (a)	11.059999585151672 0 0
Cell Basis Vector 2 (b)	0 11.38700008392334 0
Cell Basis Vector 3 (c)	0 0 19.937000274658203
Cell Origin: x = 7.567444801330566; y = 2.478381395339966; z = 17.238279342651367	
Whole peptide P2 dimension along with solvent molecules	
Cell Basis Vector 1 (a)	15.919000446796417 0 0
Cell Basis Vector 2 (b)	0 14.101000308990479 0
Cell Basis Vector 3 (c)	0 0 87.81100034713745
Cell Origin: x = 7.788802146911621; y = 2.8312554359436035; z = 47.974884033203125	

Table 4.3: Hydrogen bond distances and angles for peptide P2. The standard deviations are shown in parentheses.

Type of H-bond	Donor	Acceptor	D----A (°)	H----A (°)	<DH---A (°)
Mol-A					
Intramolecular (C_{11})	NH (L3)	CO (Boc)	2.95(1)	2.153	150.1
Intramolecular (C_9)	NH ($\beta^{3,3}Ac_6c$ (2))	CO (L3)	3.01(1)	2.286	139.7
Intramolecular (C_{11})	NH (L5)	CO ($\beta^{3,3}Ac_6c$ (2))	3.019(9)	2.261	143.8
Intramolecular (C_9)	NH ($\beta^{3,3}Ac_6c$ (4))	CO (L5)	3.00(1)	2.326	133.2
Intramolecular (C_{11})	NH (L7)	CO ($\beta^{3,3}Ac_6c$ (4))	3.06(1)	2.262	151.6
Intramolecular (C_9)	NH ($\beta^{3,3}Ac_6c$ (6))	CO (L7)	2.99(1)	2.306	134.6
Intermolecular	NH ($\beta^{3,3}Ac_6c$ (8))	O1 (dioxane-E)	2.96(1)	2.136	155.2
Mol-B					
Intermolecular	NH (L1)	O1 (dioxane-G)	2.95(2)	2.2	143
Intramolecular (C_{11})	NH (L3)	CO (Boc)	2.97(1)	2.17	150.4
Intramolecular (C_9)	NH ($\beta^{3,3}Ac_6c$ (2))	CO (L3)	3.00(1)	2.273	140.5
Intramolecular (C_{11})	NH (L5)	CO ($\beta^{3,3}Ac_6c$ (2))	3.04(1)	2.273	145.5
Intramolecular (C_9)	NH ($\beta^{3,3}Ac_6c$ (4))	CO (L5)	2.98(1)	2.296	134
Intramolecular (C_{11})	NH (L7)	CO ($\beta^{3,3}Ac_6c$ (4))	2.99(1)	2.182	151.5
Intramolecular (C_9)	NH ($\beta^{3,3}Ac_6c$ (6))	CO (L7)	2.95(1)	2.262	135.1
Intermolecular	NH ($\beta^{3,3}Ac_6c$ (8))	O4 (dioxane-E)	2.96(1)	2.13	156.8
Mol-C					
Intermolecular	NH (L1)	O4 (dioxane-G)	3.06(3)	2.2	166.8
Intramolecular (C_{11})	NH (L3)	CO (Boc)	3.00(1)	2.187	152.6
Intramolecular (C_9)	NH ($\beta^{3,3}Ac_6c$ (2))	CO (L3)	3.01(1)	2.282	139.7
Intramolecular (C_{11})	NH (L5)	CO ($\beta^{3,3}Ac_6c$ (2))	3.04(1)	2.266	147.6
Intramolecular (C_9)	NH ($\beta^{3,3}Ac_6c$ (4))	CO (L5)	2.99(1)	2.337	131.7
Intramolecular (C_{11})	NH (L7)	CO ($\beta^{3,3}Ac_6c$ (4))	2.98(1)	2.18	151.2
Intramolecular (C_9)	NH ($\beta^{3,3}Ac_6c$ (6))	CO (L7)	2.95(1)	2.276	133.3
Intermolecular	NH ($\beta^{3,3}Ac_6c$ (8))	O1 (dioxane-H)	2.96(1)	2.124	157.8
Mol-D					
Intermolecular	NH (L1)	O1 (dioxane-J)	2.98(2)	2.13	165.4
Intermolecular	NH (L1)	O1 (methanol-K)	3.34(3)	2.581	150
Intramolecular (C_{11})	NH (L3)	CO (Boc)	2.93(1)	2.128	151.4
Intramolecular (C_9)	NH ($\beta^{3,3}Ac_6c$ (2))	CO (L3)	3.01(1)	2.27	141
Intramolecular (C_{11})	NH (L5)	CO ($\beta^{3,3}Ac_6c$ (2))	3.01(1)	2.256	143.9
Intramolecular (C_9)	NH ($\beta^{3,3}Ac_6c$ (4))	CO (L5)	3.00(1)	2.311	134.5
Intramolecular (C_{11})	NH (L7)	CO ($\beta^{3,3}Ac_6c$ (4))	3.06(1)	2.249	152.5
Intramolecular (C_9)	NH ($\beta^{3,3}Ac_6c$ (6))	CO (L7)	2.977(9)	2.276	136.7
Intermolecular	NH ($\beta^{3,3}Ac_6c$ (8))	O4 (dioxane H)	2.95(1)	2.131	154.9

Table 4.4: Torsional angles observed for peptide **P2**. The standard deviations are shown in parentheses.

Residue	φ [°]	Θ [°]	ψ [°]	ω [°]
molecule A				
Leu (1)	-49(1)	--	146.6(9)	-169.7(9)
$\beta^{3,3}$Ac$_6$c (2)	83(1)	58(1)	-98(1)	168.1(9)
Leu (3)	-61(1)	--	157.8(8)	-175.8(9)
$\beta^{3,3}$Ac$_6$c (4)	78(1)	57(1)	-92(1)	166.7(9)
Leu (5)	-67(1)	--	155.7(8)	-172.4(9)
$\beta^{3,3}$ Ac$_6$c (6)	72(1)	66(1)	-84(1)	163.8(9)
Leu (7)	-81(1)	--	158.1(9)	178.2(9)
$\beta^{3,3}$ Ac$_6$c (8)	62(1)	51(1)	-179(1)	--
molecule B				
Leu (1)	-51(1)	--	148.3(9)	-166.9(9)
$\beta^{3,3}$ Ac$_6$c (2)	85(1)	56(1)	-98(1)	167.6(9)
Leu (3)	-61(1)	--	156.2(8)	-175.2(9)
$\beta^{3,3}$ Ac$_6$c (4)	72(1)	64(1)	-95(1)	167.9(8)
Leu (5)	-70(1)	--	154.0(8)	-170.9(9)
$\beta^{3,3}$ Ac$_6$c (6)	71(1)	65(1)	-84(1)	164.6(9)
Leu (7)	-84(1)	--	162.8(9)	-172.7(9)
$\beta^{3,3}$ Ac$_6$c (8)	57(1)	50(1)	-168(1)	--
molecule C				
Leu (1)	-50(1)	--	148.4(9)	-167(1)
$\beta^{3,3}$ Ac$_6$c (2)	84(1)	56(1)	-97(1)	168.5(9)
Leu (3)	-61(1)	--	156.8(8)	-175.2(9)
$\beta^{3,3}$ Ac$_6$c (4)	72(1)	63(1)	-92(1)	165.0(8)
Leu (5)	-71(1)	--	155.2(8)	-171.0(9)
$\beta^{3,3}$ Ac$_6$c (6)	71(1)	65(1)	-85(1)	164.4(9)
Leu (7)	-81(1)	--	161.9(9)	-175.3(9)
$\beta^{3,3}$ Ac$_6$c (8)	58(1)	50(1)	-170(1)	--
molecule D				
Leu (1)	-46(1)	--	146(1)	-170(1)
$\beta^{3,3}$ Ac$_6$c (2)	86(1)	57(1)	-96(1)	166.4(9)
Leu (3)	-62(1)	--	156.1(8)	-175.3(8)
$\beta^{3,3}$ Ac$_6$c (4)	78(1)	59(1)	-94(1)	167.2(8)
Leu (5)	-67(1)	--	155.6(8)	-174.3(8)
$\beta^{3,3}$ Ac$_6$c (6)	73(1)	64(1)	-83(1)	163.6(9)
Leu (7)	-82(1)	--	158.5(8)	179.8(9)
$\beta^{3,3}$ Ac$_6$c (8)	63(1)	52(1)	-120(1)	--

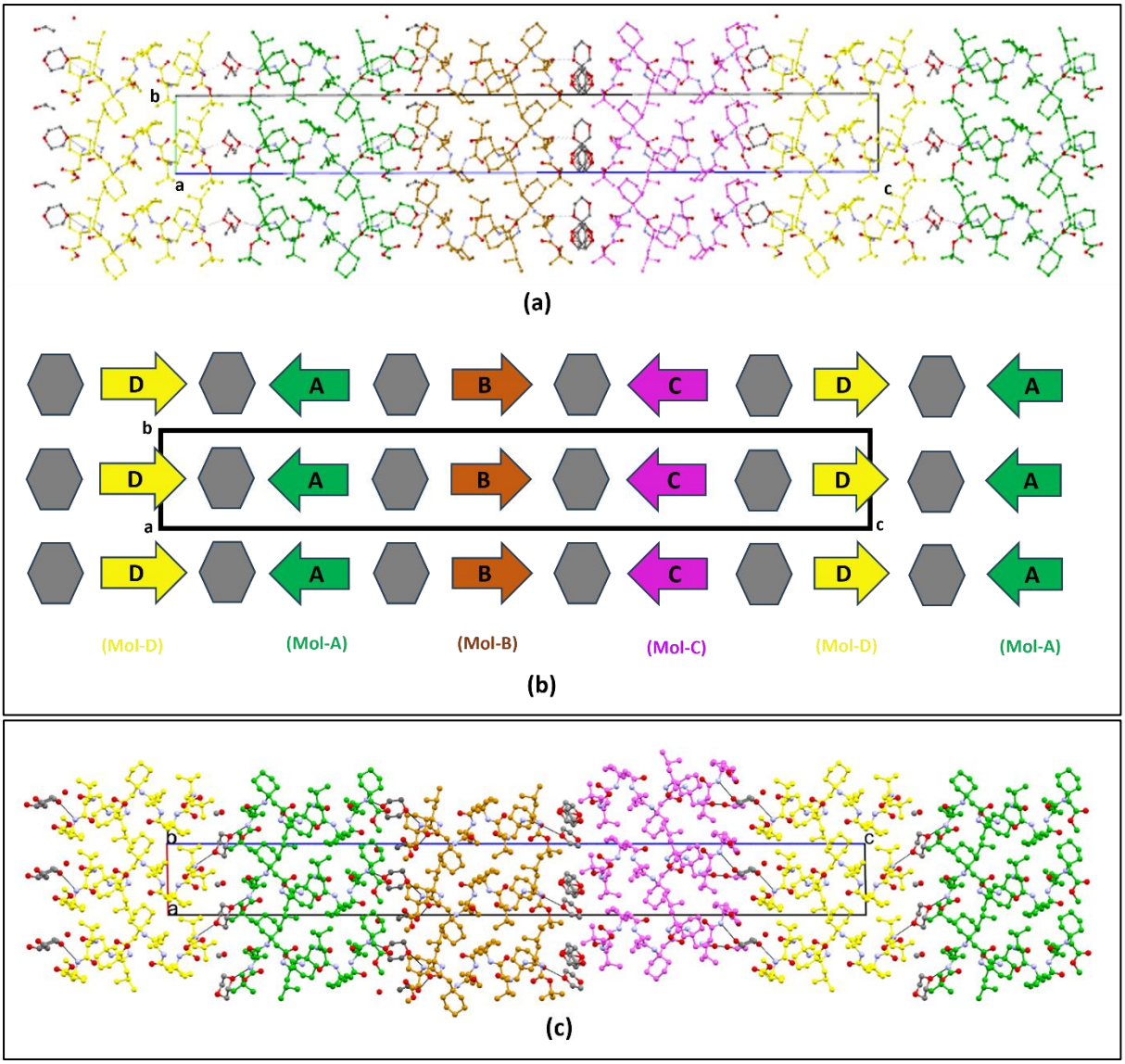

Figure 4.7 Crystal packing of four molecules of octapeptide **P2**. (a) Interactions between four molecules mol-A to mol-D and solvent molecules, are shown viewed along the a-axis. All the molecules, including solvent molecules, are shown in the ball and stick model with their colour codes. Mol-A and mol-B interact with dioxane in a tail-to-tail manner, whereas mol-B and mol-C interact in a head-to-head manner. Mol-C and mol-D interact similarly to mol-A and mol-B; (b) The same arrangement of molecules inside the crystal unit cell is shown in the cartoon representation. All the molecules are shown in arrow representation similar to the molecule's colour and labelled accordingly, whereas solvent dioxane molecules are shown in in grey colour; (c) Same viewed along the b-direction. All the molecules were shown in the stick model with their colours mol-A to mol-D (green, orange, magenta, and yellow, respectively), whereas all the solvent molecules were shown in the ball and stick model for a better appearance. All hydrogens have been deleted for the sake of clarity. The putative hydrogen bonds have been shown in black dashed lines.

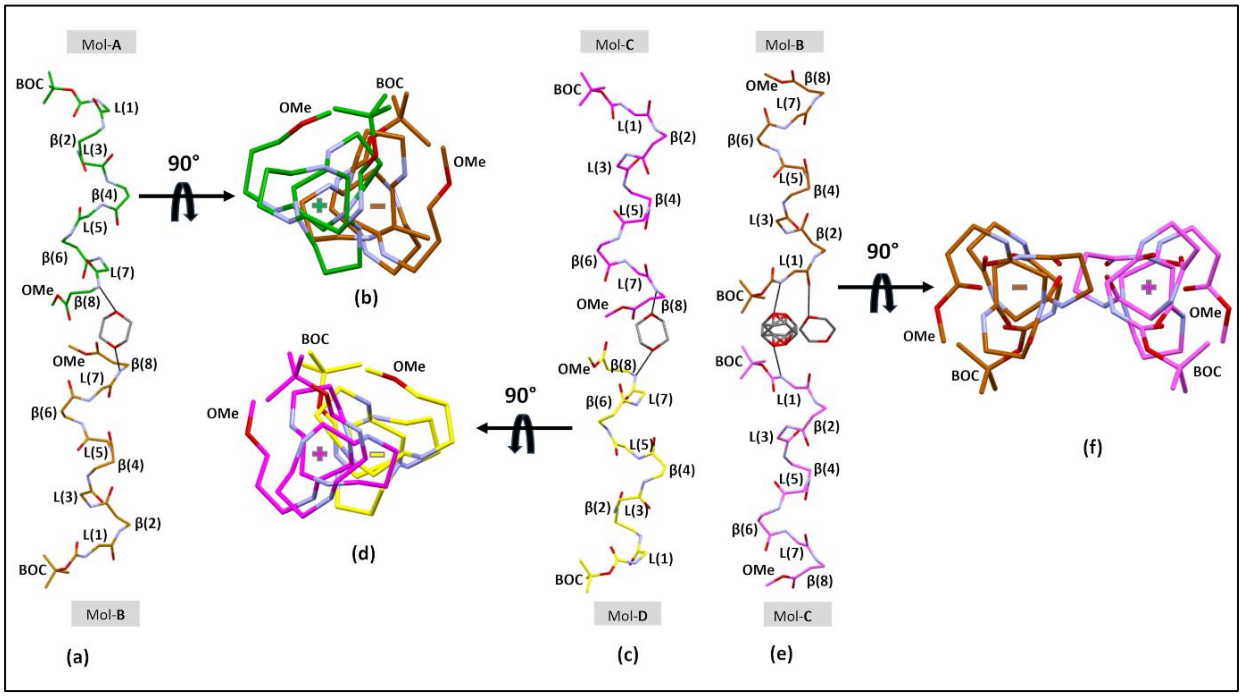

Figure 4.8: Packing of the helices of molecules (A-D) octapeptide **P2** viewed along the *c*-axis (all four molecules (A-D) shown in stick model in their respective colour; side chains in the backbone structures and all hydrogens have been removed for sake of clarity. The arrows indicate the direction of the helix axis from the N-terminus to the C-terminus. The (+) sign indicates that the helix-axis direction from N to C terminal is pointing inwards into the plane of the paper, whereas (−) indicates that it is pointing outwards towards the viewer; side, and top view, respectively, (a) The symmetry-related interconnected helices of mol-A and mol-B (green and orange) side view; (b) same from a top view; (c) the symmetry-related interconnected helices of mol-C and mol-D (magenta and yellow) side view; (d) same from a top view; (e) The symmetry-related interconnected helices of mol-B and mol-C (orange and magenta) side view; (f) same from the top view. The putative H-bonds are shown in black-colored dashed lines.

The mol-A exhibits both C_{11}/C_9 type intramolecular and intermolecular H-bonds in its structure. The repetitive N-H groups consistently form intramolecular H-bonds with C=O groups at various positions stabilizing the structure. The solvent-mediated intermolecular interaction with the dioxane molecule also helps stabilize the structure. Similar to mol-A, mol-B also forms N-H(C_{11}) and N-H(C_9) types of Intramolecular H-bonds among backbone groups and significant solvent dioxane-mediated intermolecular interaction. Mol-C also exhibits consistent C_{11}/C_9 type intramolecular H-bonds. Another H-bond involves solvent interaction with a dioxane molecule. Mol-D

also repeats a similar C_{11}/C_9 type intramolecular H-bond pattern and intermolecular H-bond with solvent molecules dioxane including a unique interaction with ethanol. The dimensions of each molecule (mol A-D) were measured and listed in Table 4.2. All four molecules are roughly 11 Å thick, 11.45 Å wide and about 20.2 Å long. The dimensions of unit cell is *a* = 15.919Å, *b* = 14.010Å, and *c* = 87.818Å respectively. From the dimensions, the *c*-axis is significantly longer (*c*=87.818Å) than the individual molecule dimensions reflecting the presence of solvent molecules as well as the elongated packing of octapeptide along c-axis. The inclusion of solvent molecules can cause lattice expansion along one or more axes, which is reflected in this crystal structure.

In octapeptide **P2**, the mol-A and mol-B helices are aligned in a tail-to-tail manner helped by the solvent dioxane molecule which interfaces the two helical peptide molecules mol-A and mol-B. In mol-A, the N-H of β(8) is interfacing with the cyclic

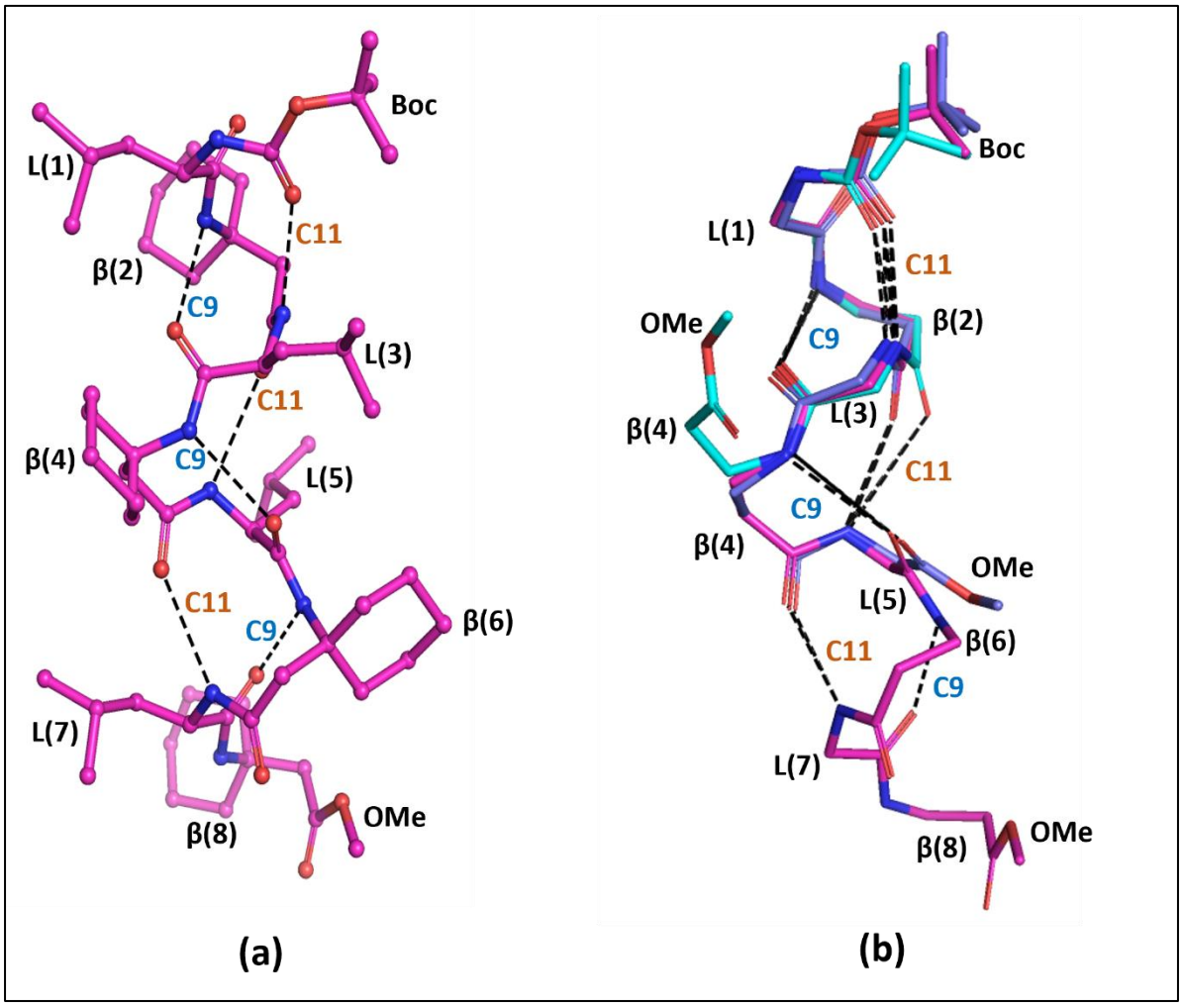

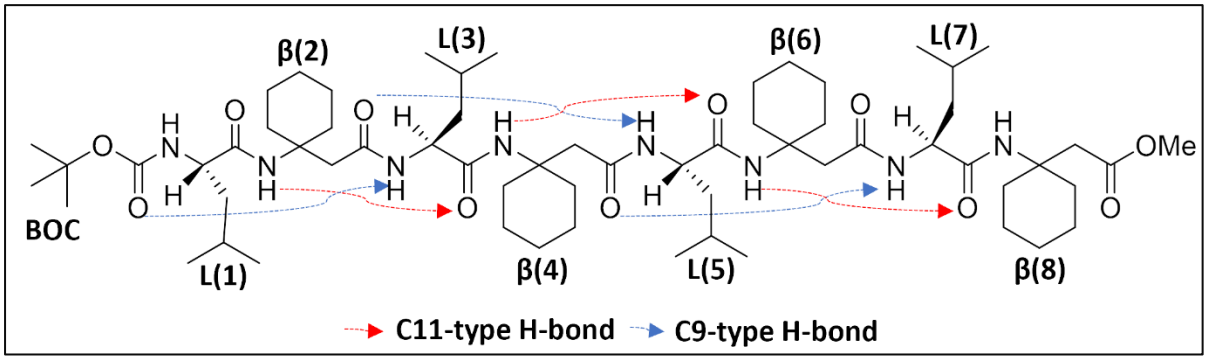

Figure 4.9: (a) The molecular structure of octapeptide **P2** is shown in the ball and stick model. All the C_{11}/C_9 type intramolecular H-bonds are shown in black dashed lines and labeled accordingly; (b) The superimposed view of Octapeptide P4 with previously published tetrapeptide (shown in orange color) and pentapeptide (shown in green color) in stick model. All side chain residues from backbone structures were removed for clarity. The repeating C_{11}/C_9 type intramolecular H-bonds are shown in black dashed lines and labeled accordingly; (c) The chemical structure of octapeptide P4 with its C_{11}/C_9 type intramolecular H-bonds pattern shown in red and green color dashed arrows respectively.

ether of the solvent dioxane molecule. In contrast, the other cyclic ether oxygen of the solvent dioxane molecule is involved in making an H-bond with β(8) N-H of mol-B (Figure 4.8a). The interaction between mol-B and mol-C happens in a head-to-head manner interfaced by a solvent disorder dioxane molecule as shown in Figure 4.8c. Here, the main chain N-H of Leu(1) is H-bonded to the cyclic ether oxygen of solvent dioxane molecule, while the other cyclic ether oxygen of solvent dioxane molecule is H-bonded to the main chain N-H of residue Leu(1) of mol-C. The interaction between mol-C and mol-D is in a tail-to-tail fashion mediated by H-bonding with a cyclic ether oxygen of solvent dioxane molecule which is sandwiched between them (Figure 4.8c). The interaction between mol-B and mol-C is similar to that observed between mol-A and mol-B. When the head-to-head interaction is taking place, there are two solvent dioxane molecules at the interface. When tail-to-tail interaction takes place, there are dioxane, ethanol, and water solvent molecules close to the interface. The interface between mol-B and mol-C is unique. However, the interface between mol-A and mol-B is similar to that between mol-C and mol-D. The difference in their interface along with finer differences among molecules may be responsible for breaking the symmetry between them and hence **P2** crystallizes with 4 molecules in the asymmetric unit of *P*1 space group rather than a higher symmetry space group.

The superimpose aligned view of octapeptide **P2** with previously published tetrapeptide and pentapeptide containing similar α-L-amino acid and β3,3Ac6c repeats with their C_{11}/C_9 type of intramolecular H-bonding repeats is shown in Figure 4.9b. This comparison study confirms that such repeat can indeed lead to helical folds stabilized by a similar type of C_{11}/C_9 type of H-bonding patterns as observed in shorter peptides and holds true even on length elongation of the peptides as shown by **P2**

(Figure 4.9 a-b). It is the first observation of this kind of helix formation with C_{11}/C_9 type intramolecular H-bonds in an octapeptide, which may be used as a design principle.

4.7 Conclusions

The study produces greater clarity in the preferences of β-amino acids like $\beta^{3,3}Ac_6c$ regarding their (ϕ,θ, ψ) torsion angles, especially when flanked by chiral α-L-amino acid like ^{L}Leu.

This study also confirms that α-L-amino acid and $\beta^{3,3}Ac_6c$ repeats form stable helical structures stabilized by a similar type of C11/C9 type of H-bonding patterns, as reported for smaller peptides (tetra/pepta-peptides) by us. It is the first observation of this kind in such a long octapeptide **P2**. The insight gained from this study may be used as a design principle in new peptide designs for getting specific folds or designing peptides with new functions.

CHAPTER-5

Effect of N-terminus chirality in the conformational changes of some α and γ hybrid tripeptides

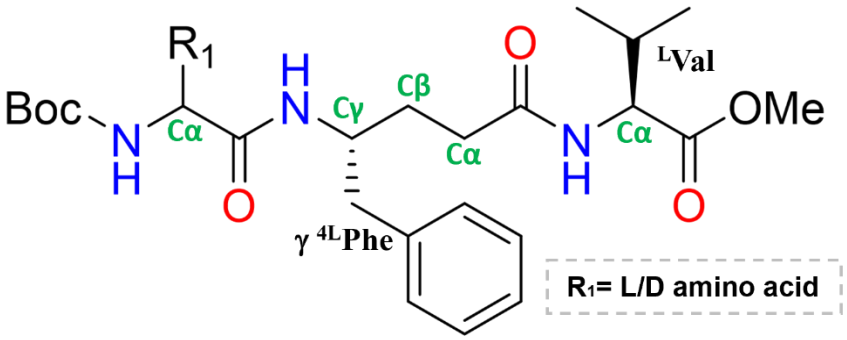

α/γ hybrid peptide

5.1. Graphical Abstract

Stable β-turns: Hybride Boc-protected tripeptides containing α and γ-amino acids, with generic Boc-^{D}X/^{L}P-γ4^{L}F-V-Ome sequence, display folded hairpin structure without forming any intramolecular hydrogen bonds. The folding in these tripeptides seems to be invariant of the sequence changes at the first position of the tripeptide.

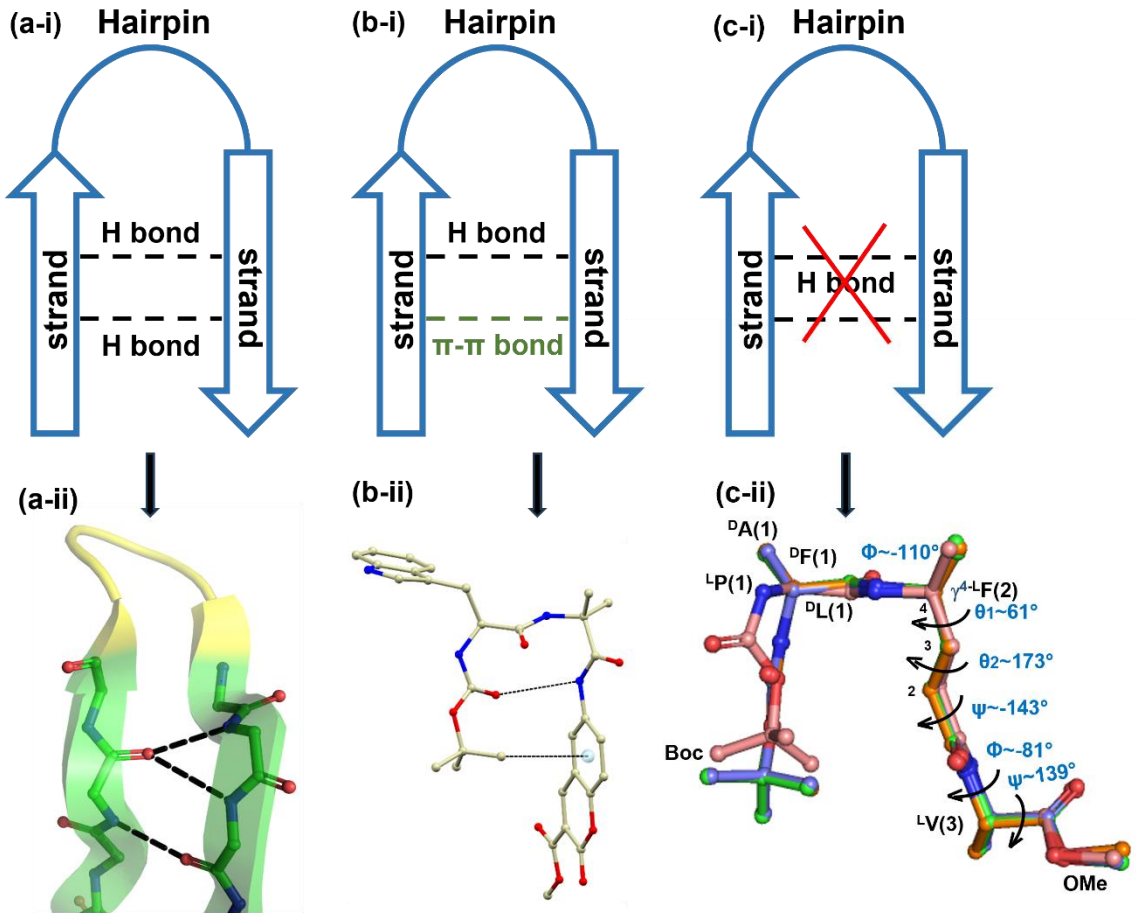

5.2. Abstract

In this chapter, we investigate the influence of chirality on the conformational properties of α/γ hybrid tripeptides with Boc-X-γ^{4L}Phe-^{L}Val-OMe sequence, where X is L/D amino acid. Using single-crystal X-ray diffraction analysis, we have studied the structural preferences of five tripeptides (P3–P7) and their sensitivity to N-terminal chirality of amino acid, their backbone torsion angles, and their potential for forming any intermolecular H-bonding. The findings indicate that **P3**–**P5** with X=D-amino acids mostly take on β-turn conformations, while **P6**, ^{L}pro has a distinct polyproline-like conformation, showing the effect of proline residues on folding behaviour. The research also exhibits the ability of these sequences to form β-hairpin structures and get stabilized in the absence of any intramolecular H-bonds. Rather, supramolecular interactions, such as π–π stacking and van der Waals forces, contribute to the structural stability and lipid bilayer type crystal packing of the tripeptides in the solid state. The effect of chirality is clear, as changes in D- and L-amino acid conformations affect hydrogen-bonding schemes, producing different crystal packing structures. Furthermore, apart from chirality at the N-terminus, the conformation of γ4-^{L}phenylalanine amino acid contributes to β-hairpin formation as its shows invariant conformation in these peptides.

In summary, this research enhances our knowledge of short peptide folding mechanisms and self-assembly, with implications for biomaterials and drug design. The work implies that engineering tripeptides with targeted sequence changes can induce stable β-hairpin folds, widening their scope of applications in nanotechnology and molecular recognition systems.

Keywords: Tripeptides, β-hairpin, hydrogen bonds, α/γ hybrid peptides, supramolecular interactions, crystal packing, self-assembly, X-ray crystallography.

5.3. Introduction

Tripeptides have also become central models for the study of β-hairpin formation and stabilization, which are critical motifs in protein structure. In these motifs, two anti-parallel β-strands joined by a loop, are stabilized mainly by intramolecular H-bonds.(115–120) Recent studies suggest that β-hairpin loops can also be formed and stabilized without conventional hydrogen bonding, broadening our knowledge of peptide folding mechanisms. The tripeptide self-assembly has been studied extensively, and the knowledge gained shows that certain sequences can form β-hairpin conformations that are stabilized through intramolecular H-bonds. An example is the tripeptide Boc-Leu-Val-Ac_{12}c-OMe, which contains a bulky 1-aminocyclododecane-1-carboxylicacid (Ac_{12}c) residue. The molecular arrangement shows a fascinating supramolecular twisted parallel β-sheet that folds into a helical structure in the crystal state. This disposition highlights the role of certain amino acid residues and their side chains in β-hairpin folding and stabilization via hydrogen-bonding networks.(121) Chirality is responsible for self-assembly and structure formation of tripeptides. Experiments have shown that a change in the chirality of the N-terminal amino acid residue in tripeptides like ^{D}Val-^{L}Phe-^{L}Phe(^{D}V^{L}F^{L}F) and ^{D}Phe-^{L}Phe-^{L}Val (^{D}F^{L}F^{L}V) triggers hydrogelation at physiological pH, a characteristic not exhibited by their all L-analogues. Notably, the inversion of phenylalanine residues yields different nanostructures; ^{D}V^{L}F^{L}F produces nano tapes, while ^{D}F^{L}F^{L}V generates twisted fibres. These findings highlight how chirality influences hydrogen bonding patterns and, consequently, the morphology of β-hairpin structures.(116) In addition to conventional H-bonds, β-hairpin structures can be stabilized by other interactions. Studies of hybrid αγ polypeptides have shown the presence of mixed C_{12}/C_{10} helices with alternating directionality

of hydrogen bonds. For instance, the hybrid αγ peptide Boc-Leu-Gpn-Leu-Aib-OMe, which includes gabapentin (Gpn) and amino isobutyric acid (Aib), takes on a helical conformation stabilized by atypical hydrogen bonding patterns. This indicates that β-hairpin loops can be stabilized by non-conventional hydrogen bonds, broadening the design and functionality of peptides.(117) In addition, the introduction of backbone-expanded amino acid residues, including β- and γ-amino acids, into tripeptides has been found to affect β-hairpin stability. These residues can introduce conformational flexibility, enabling the generation of stable β-hairpin structures even without traditional hydrogen bonds. This flexibility enables the investigation of various folding patterns and stabilization mechanisms, expanding the possible applications of tripeptide-based materials in biotechnology and medicine.(122) In short, tripeptides are general models for β-hairpin loop formation and stabilization. Although intramolecular H-bonds play a central role in stabilizing these structures, other interactions and modifications, including chirality changes and backbone-expanded residues, provide other means of stabilization. These findings not only advance our knowledge of peptide folding kinetics but also open the door to the design of new biomaterials with engineered structural and functional properties.

Through single-crystal X-ray crystallographic research, this chapter reveals how L- and D-amino acids comprising peptides interact with one another to stabilize overall conformations in specific ways and pack in the crystal lattice. This understanding may help advance peptide-based drug design and material development and, more importantly, influences the stereochemical underpinning in biological systems. We have also discussed the crystallographic studies of α/γ hybrid tripeptides containing non-coded amino acids. Some of the key aspects of the research in this direction

include exploring the unusual folding patterns, how the supramolecular networks assist these structures in maintaining those forms, and how changes in the torsion angle affect peptide dynamics.

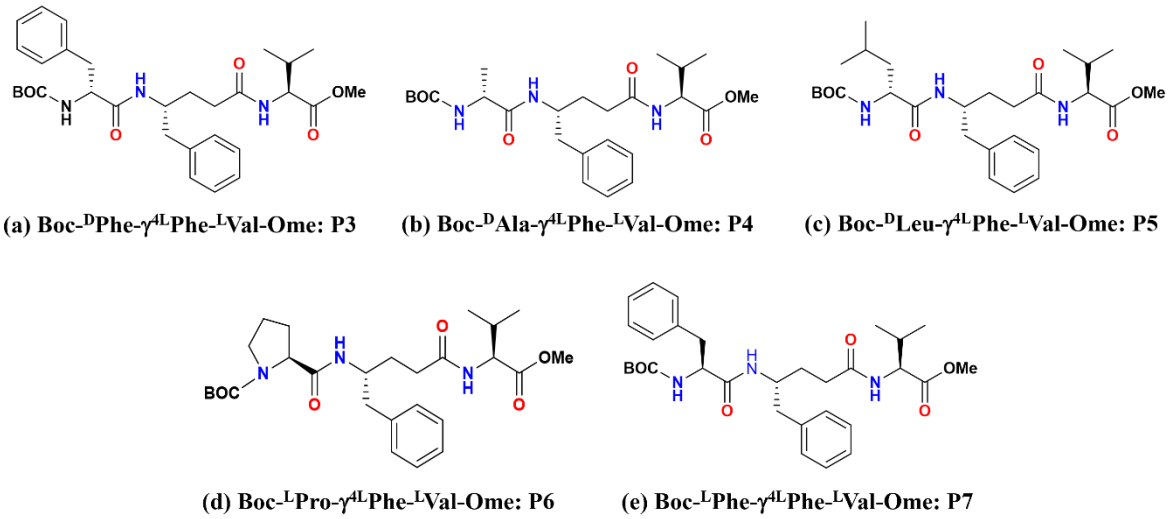

Figure 5.1: Scheme of tripeptides (**P3**-**P7**). (a) Boc-^{D}Phe-γ^{4L}Phe-^{L}Val-OMe, **P3**; (b) Boc-^{D}Ala-γ^{4L}Phe-^{L}Val-OMe, **P4**; (c) Boc-^{D}Leu-γ^{4L}Phe-^{L}Val-OMe, **P5**; (d) Boc-^{D}Pro-γ^{4L}Phe-^{L}Val-OMe, **P6**; and (e) Boc-^{L}Phe-γ^{4L}Phe-^{L}Val-OMe, **P7**.

5.4. Literature Review

The study of tripeptides, particularly those incorporating D-phenylalanine (^{D}Phe), L-phenylalanine (^{L}Phe), and L-valine (^{L}Val), has been a subject of interest due to their unique structural and conformational properties. These investigations provide insights into peptide behaviour, stereochemistry, and potential applications in drug design, nanotechnology and material science.(123–126) Initial research focused on understanding the fundamental conformations of tripeptides. Studies on sequences like Gly-Gly-X (where X represents various amino acids) revealed that glycine residues confer significant flexibility, allowing the peptide backbone to adopt multiple conformations. This flexibility is crucial for accommodating various side chains and influences the overall stability and function of the peptide. The introduction of D-amino

acids into peptide sequences has been explored to understand their impact on peptide conformation and stability. For instance, the synthesis and structural analysis of peptides containing both D- and L-proline residues demonstrated that heterochiral sequences can adopt multiple conformations.(127) These studies highlighted that the presence of D-amino acids can lead to distinct folding patterns, influencing the peptide's biological activity and resistance to enzymatic degradation.(128) N-(Benzyloxycarbonyl)glycylglycyl-L-norvaline: This tripeptide, containing a nonproteinogenic amino acid norvaline (an isomer of valine), was found to adopt an extended conformation. The crystal structure revealed a network of N–H···O and O–H···O hydrogen bonds, stabilizing the packing and influencing the overall molecular arrangement.(129) Research into peptides with sequences containing $^{D/L}$-proline such as Piv-^{D}Pro-^{L}Pro-^{D}Xxx-NHMe (where Xxx represents various amino acids) showed that these heterochiral sequences could adopt multiple conformations in the solid state. The presence of both D- and L-proline residues was found to influence the peptide's folding and intermolecular interactions, contributing to conformational diversity.(128)(119,130–132) Understanding the structural nuances of tripeptides, especially those incorporating both D- and L-amino acids, has significant implications including Drug Design where Incorporating D-amino acids into peptide-based therapeutics can enhance stability against enzymatic degradation, potentially leading to more effective drugs with longer half-lives and in material science, these tripeptides' unique packing and self-assembly properties can be harnessed in the design of novel biomaterials with specific structural characteristics.(133,134) The Boc-^{L}Phe-γ^{4L}Phe-^{L}Val-OMe, **P7** compound from our current work has already been reported for its antimicrobial activity.(135)

5.5. Methodology

Single crystals of tripeptides Boc-^{D}Phe-γ^{4L}Phe-^{L}Val-OMe, **P3**, Boc-^{D}Ala-γ^{4L}Phe-^{L}Val-OMe, **P4**, Boc-^{D}Leu-γ^{4L}Phe-^{L}Val-OMe, **P5,** and Boc-^{L}Pro-γ^{4L}Phe-^{L}Val-OMe, **P6,** Boc-^{L}Phe-γ^{4L}Phe-^{L}Val-OMe, **P7** (P3-P7**)** suitable for X-ray diffraction, were grown by slow evaporation from methanol/water mixtures with different ratios for compounds **P3**-**7** listed in x-ray diffraction parameters list Table 5.1. Needle-shaped crystals with a maximum size of about 1nm were used to collect the data. The X-ray intensity data for tripeptide crystals, **P3**-**7**, were collected at room temperature on a Bruker Kappa APEX II diffractometer with graphite monochromated *Mo K*α (*λ*=0.71073Å) radiation from a sealed tube generator.(136) They were subjected to structural solution and refinement using the Olex 2-1.5 (http://www.olexsys.org) program suite.(82) Absorption corrections were made using the SADABS program.(101,102) The structures were determined by direct phase determination using SHELXL.(103) Refinements of non-hydrogen atoms for all five structures (**P3-P6**) were carried out with a full matrix anisotropic least-square method using SHELXT.(83) In tripeptide **P3**, one solvent dioxane molecule was observed from different Fourier maps during the refinement. All the hydrogen atoms were fixed geometrically in the idealized positions and refined as riding over the heavier atoms to which they are bonded. The hydrogen atoms attached to nitrogen atoms were located from different Fourier maps and refined isotopically and the final refinement was using the Olex 2-1.5 (http://www.olexsys.org) program suite.(82) All hydrogen-bond distances, torsion angles (φ, θ, ψ, and ω), and crystal packing diagrams were created by using Mercury 2024.2.0. 8 software (https://www.ccdc.cam.ac.uk/solutions/csd-system/components /mercury/),(104) The important crystallographic parameters are listed in Table 5.1 and 5.2. The structures alignments were done by using chimera software (Version 1.18)(86) and the figures of molecules alignment/ superimposed view were prepared using PyMol (The PyMOL

Molecular Graphics System, Version 2.3.2, Schrodinger, LLC.),(112) and all figures are compiled together using GIMP version 2.10.34 (GNU Image Manipulation Program).(105)

All the relevant crystallographic data collection parameters and structure refinement details for the five tripeptides (**P3**-**P7**) are summarized in Tables 5.1 and Table 5.2. The CIF files were generated and submitted to the Cambridge Crystallographic Data Centre (CCDC) (Advancing Structural Science | CCDC (cam.ac.uk))(84) with CCDC number containing, CCDC-1455264 **P3**, CCDC-1456694 **P4**, CCDC-1877122 **P5**, CCDC-1877707 **P6**, and CCDC-1877796 **P7**.

5.6. Results and Discussion

5.6.1 Single crystal X-ray diffraction

We described the crystallographic characterization of the tripeptides (**P3**-**P7)** Boc-^{D}Phe-γ^{4}-^{L}Phe-^{L}Val-OMe, **P3**, Boc-^{D}Ala-γ^{4}-^{L}Phe-^{L}Val-OMe, **P4**, Boc-^{D}Leu-γ^{4}-^{L}Phe-^{L}Val-OMe, **P5,** and Boc-^{D}Pro-γ^{4}-^{L}Phe-^{L}Val-OMe, **P6,** and Boc-^{L}Phe-γ^{4}-^{L}Phe-^{L}Val-OMe, **P7**. The solved peptides or trip images are shown in Figure 5.2. The measured hydrogen-bond distances and backbone torsion angle parameters for the peptides P3-7 are listed in Tables 5.3-4, respectively. The Ortep view image and molecular confirmation are shown in Figures 3.2 and 3.3, respectively.

Table 5.1: single crystal X-ray diffraction data and structure refinement parameters of tripeptides **P3**-**5**.

Parameters	P3	P4	P5
Empirical formula	$C_{31}H_{43}N_3O_6$	$C_{25}H_{39}N_3O_6$	$C_{28}H_{44}N_3O_6$
Formula weight	553.68	477.59	518.66
Crystal habit	Needle	Needle	Needle
Temperature/K	293	296	296
Wavelength (Å)	0.71073	0.71073	0.71073
Crystal size[mm]	0.86×0.08×0.08	0.6×0.15×0.12	0.9×0.09×0.07 mm
Crystal solvent	Methanol/Water	Methanol/Water	Methanol/Water
Crystal system	Triclinic	Monoclinic,	Monoclinic
Space group	*P1*	*$P2_1$*	*C2*
a/Å	5.1571 (10)	5.108 (3)	18.863 (9)
b/Å	9.762 (2)	27.778 (18)	5.148 (2)
c/Å	16.624 (3)	9.607 (6)	32.319 (15)
α/°	95.432 (14)	90	90
β/°	96.408 (13)	102.089(6)	104.464 (13)
γ/°	102.952 (13)	90	90
Volume/$Å^3$	804.3 (3)	1333.1 (14)	3039 (2)
Z	1	2	4
Density [g/cm^3][calc.]	1.143	1.190	1.134
F(000)	298	516	1124
Radiation type	Mo Kα	Mo Kα	Mo Kα
T_{min}, T_{max}	0.738, 1	0.480, 0.745	0.662,0.745
θ Range[°]	2.35 to 25.45	2.617 to 25.683	2.2–22.1
Scan type	ϕ/ω	ϕ/ω	ϕ/ω
Independent reflections	6872	4588	4880
Measured reflections	13209	9371	16367
Observed reflections with I > 2σ (I)]	3781	2976	3008
R_{int}	0.033	0.076	0.051
Δρmax/ Δρmin (e Å−3)	0.11, −0.13	0.11, −0.17	0.25/ −0.26
Goodness-of-fit on F^2	0.97	0.99	1.00
Final *R/ wR2*[%]	0.044/ 0.116	0.043/ 0.105	0.059/0.173
Restraints/ parameters	87/ 492	1/ 314	6/363
Absolute structure parameter	0.1 (7)	0.0 (10)	−0.2 (7)
CCDC No.	1456694	1877122	1877707

Table 5.2: Crystal x-ray diffraction data and structure refinement parameters of tripeptides **P6** and **P7**.

Parameters	**P6**	**P7**
Empirical formula	$C_{27}H_{41}N_3O_6$	$C_{31}H_{43}N_3O_6 \cdot C_4H_8O_2$
Formula weight	503.63	641.78
Crystal habit	Needle	Needle
Temperature/K	298	100
Wavelength (Å)	0.71073	0.71073
Crystal size [mm]	0.34 × 0.19 × 0.16	0.7 × 0.24 × 0.2
Crystal solvent	Methanol/Water	Methanol/Dioxane
Crystal system	Monoclinic	Triclinic
Space group	*$P2_1$*	*P1*
a/Å	5.645 (3),	5.1030(3)
b/Å	28.944 (17)	13.4312(10)
c/Å	9.135 (5)	13.5881(10)
α/°	90	95.190(5)
β/°	103.982 (10)	90.742(4)
γ/°	90	97.366(4)
Volume/Å^3	1448.4 (15)	919.564(11)
Z	2	1
Density [g/cm][calc.]	1.155	1.159
F(000)	544	346
Radiation type	Mo Kα	Mo Kα
T_{min}, T_{max}	0.654, 0.745	0.789, 1
θ Range[°]	25.840-2.297	3.012 to 27.496
Scan type	ϕ/ω	ϕ/ω
Independent reflections	4785	7428
Measured reflections	14148	15204
Observed reflections with I > 2σ(I)]	1517	5344
R_{int}	0.069	0.027
Δρmax/ Δρmin (e Å^{-3})	0.26, −0.15	0.16, −0.18
Goodness-of-fit on F^2	0.847	1.023
Final *R/ wR2* [%]	0.065/0.216	0.045/ 0.1192
Restraints/ parameters	24/331	3/421
Absolute structure parameter	−0.9 (10)	0.4 (5)
CCDC No.	1877796	1455264

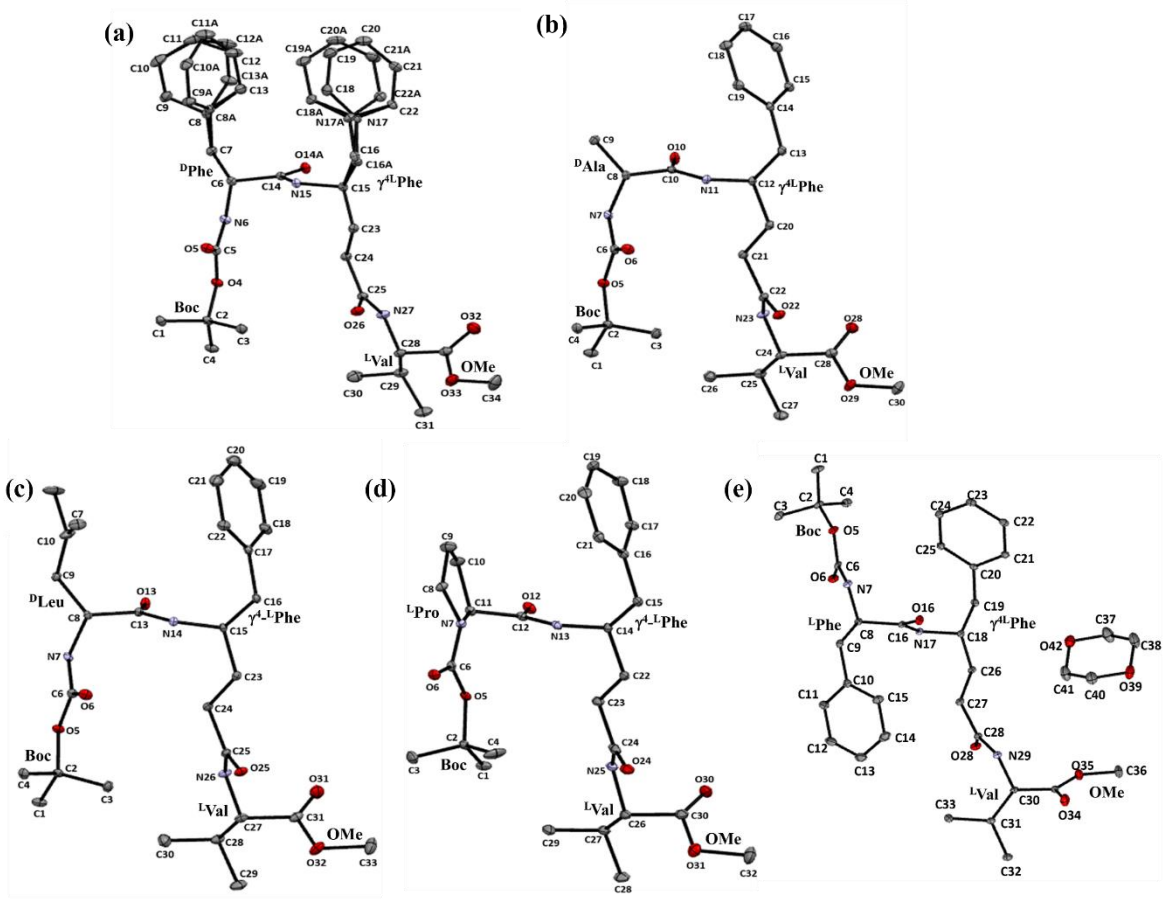

Figure 5.2. The ORTEP diagram of peptide with ellipsoid probability of 20% for (a) **P3**; (b) **P4**; (c) **P5**; (d) **P6**; (e) **P7**. All N and O atoms have been shown in blue and red colours, respectively. All H-atoms have been removed for the sake of clarity.

5.6.2. Molecular structures of tripeptides (P3-7)

All tripeptide structures (P3-P7) have been designed and synthesized using similar backbone sequences except the first amino acid Boc-X-γ^4-^{L}Phe-^{L}Val-OMe, where X is

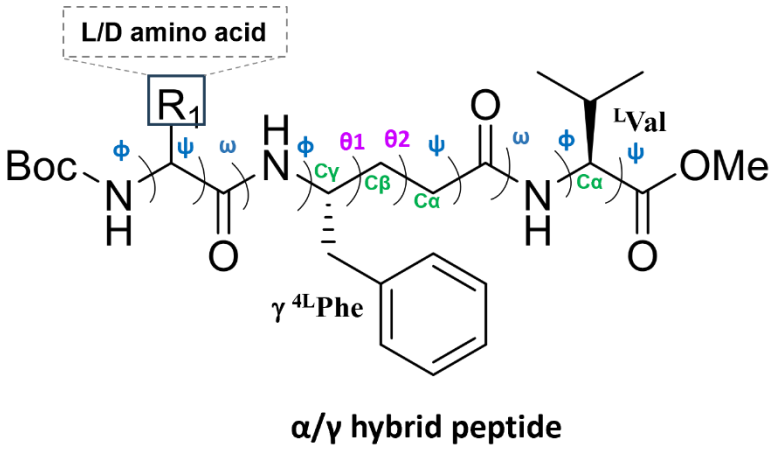

Figure 5.3: The scheme of tripeptide backbone.

L/D amino acids shown in Figure 5.3 and all individual tripeptides molecular structures are listed in Figure 5.4(a-e). All tripeptides have N-terminus Boc and C-terminus OMe protective functional groups. The first amino acid in the backbone is either L or D amino acids, the second position was substituted with $^{\gamma 4L}$phe amino acids. While ^{L}Val residue is at the third position.

P3 shows a β-hairpin structure where the two phenyl rings of side chains of ^{D}Phe (1) and γ4^{L}Phe(2) are positionally disordered such that they form T-type π-π interactions leading to stable conformation without forming any intramolecular H-bonded interactions by the main chain atoms (Figure 5.4a). It appeared that the π-π interactions may be the primary force behind stabilization of the β-hairpin structure. Hence, another peptide **P4** was designed where ^{D}Phe(1) was replace with ^{D}Ala(1) residue (containing short sidechain) to break the π-π interaction and to see if **P4** retains β-hairpin structure. Surprisingly, **P4** also shows similar backbone conformation as that observed in **P3** (Figure 5.4b). Similarly, in **P5**, where we increased the sidechain length by mutating ^{D}Ala(1) to ^{D}Leu(1), the overall structure of the peptide remained the same (Figure5.4c). From the literature knowledge, we know that both ^{L} and ^{D}pro residues are capable of making stable β-hairpin loop conformations.(127)

Hence, we designed peptide **P6** with ^{L}pro(1) mutation which also showed similar overall fold for the peptide as observed for **P3**-**P5**. Since the side chain of residue at N-terminal first position points outwardly in P2-P5, without presenting any steric clash with any main-chain or side chain of neighbouring residues, it was speculated that the overall fold may be affected by the chirality at the N-terminal first residue. Hence, in **P7** was designed where ^{D}Phe(1) was mutated to ^{L}Phe(1) of **P3**. This change led to complete change of the overall conformation of the peptide which now showed zig-zag fold instead of β-hairpin fold (Figure 5.4e).

The superimposed view of all the peptides is shown in Figure 5.4f. It clearly shows that all peptides align very well with each other except **P7,** which shows altered conformation for the N-terminal first residues. However, it is interesting to note that the other two residues, γ4LPhe(2) and LVal(2) of P7, maintain their conformations despite the chirality change at the N-terminal first position and align well with the rest of the peptides **P3**-**P6**. Where all D-amino acids along with L-pro are aligning with each other very well with RMSD varying from 0.06 to 0.30 Å Total 12 pairs of atoms are aligning in this alignment, as L-Phe has total 11 pairs of atoms due to its different conformation. All the backbone dihedral angles for tripeptides (**P3**-**P7**) are calculated and listed in Table 5.3.

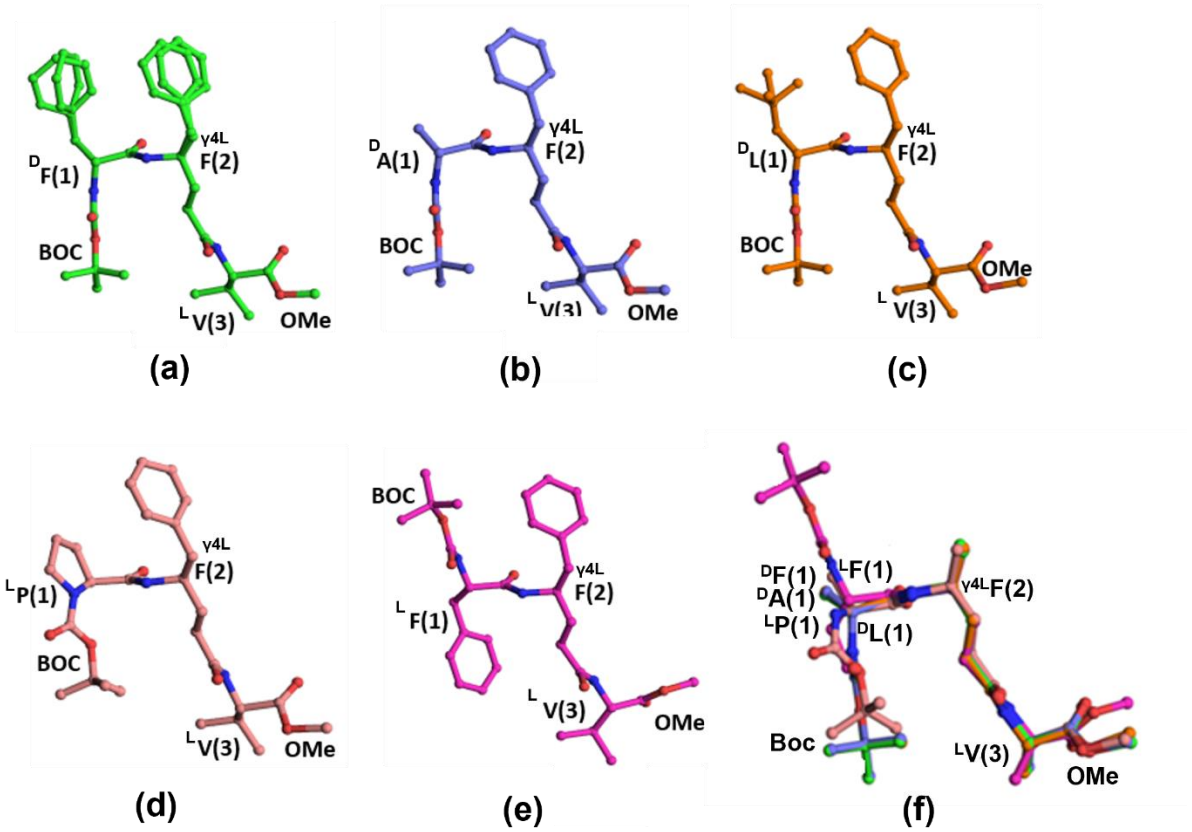

Figure 5.4. Molecular structure of tripeptides. (a) **P3**; (b) **P4**; (c) **P5**; (d) **P6**; (e) **P7**; and **(f)** Superimposed view of all tripeptides **P3**-**P7**. All side chain residues and H-atoms have been removed for sake of clarity.

Table 5.3. Torsion angles (deg) observed in **P3** - **P7**.

Residue	φ [°]	Θ_1 [°]	Θ_2 [°]	ψ [°]	ω [°]
Peptide P3					
Boc	-	-	-	-	-172.2(3)
^{D}Phe (1)	95.2(3)	-	-	-96.5(3)	168.0(3)
γ^{4}-^{L}Phe (2)	-111.1(3)	62.7(4)	171.8(3)	-139.2(3)	-178.9(3)
^{L}Val (3)	-84.8(5)	-	-	141.7(4)	-
Peptide P4					
Boc	-	-	-	-	-167.9(3)
^{D}Ala (1)	94.0(4)	-	-	-98.3(3)	172.8(3)
γ^{4}-^{L}Phe (2)	-115.7(3)	63.3(4)	171.4(3)	-139.5(4)	-179.4(3)
^{L}Val (3)	-79.0(5)	-	-	139.8(4)	-
Peptide P5					
Boc	-	-	-	-	-170.7(4)
^{D}Leu (1)	91.8(5)	-	-	-101.2(4)	169.2(4)
γ^{4}-^{L}Phe (2)	-110.0(5)	62.7(5)	171.1(4)	-141.8(4)	-179.9(4)
^{L}Val (3)	-81.6(6)	-	-	137.2(6)	-
Peptide P6					
Boc	-	-	-	-	19(1)
^{L}Pro (1)	-85(1)	-	-	-11(1)	-175.0(9)
γ^{4}-^{L}Phe (2)	-102(1)	61(1)	-179(1)	-151(1)	-177(1)
^{L}Val (3)	-80(2)	-	-	139(1)	-
Peptide P7					
Boc	-	-	-	-	172.8(2)
^{L}Phe (1)	-100.45(3)	-	-	104.3(3)	-177.3(2)
γ^{4}-^{L}Phe (2)	-123.2(3)	59.3(3)	169.0(2)	-126.7(2)	-175.6(2)
^{L}Val (3)	-132.1(3)	-	-	83.0(3)	-

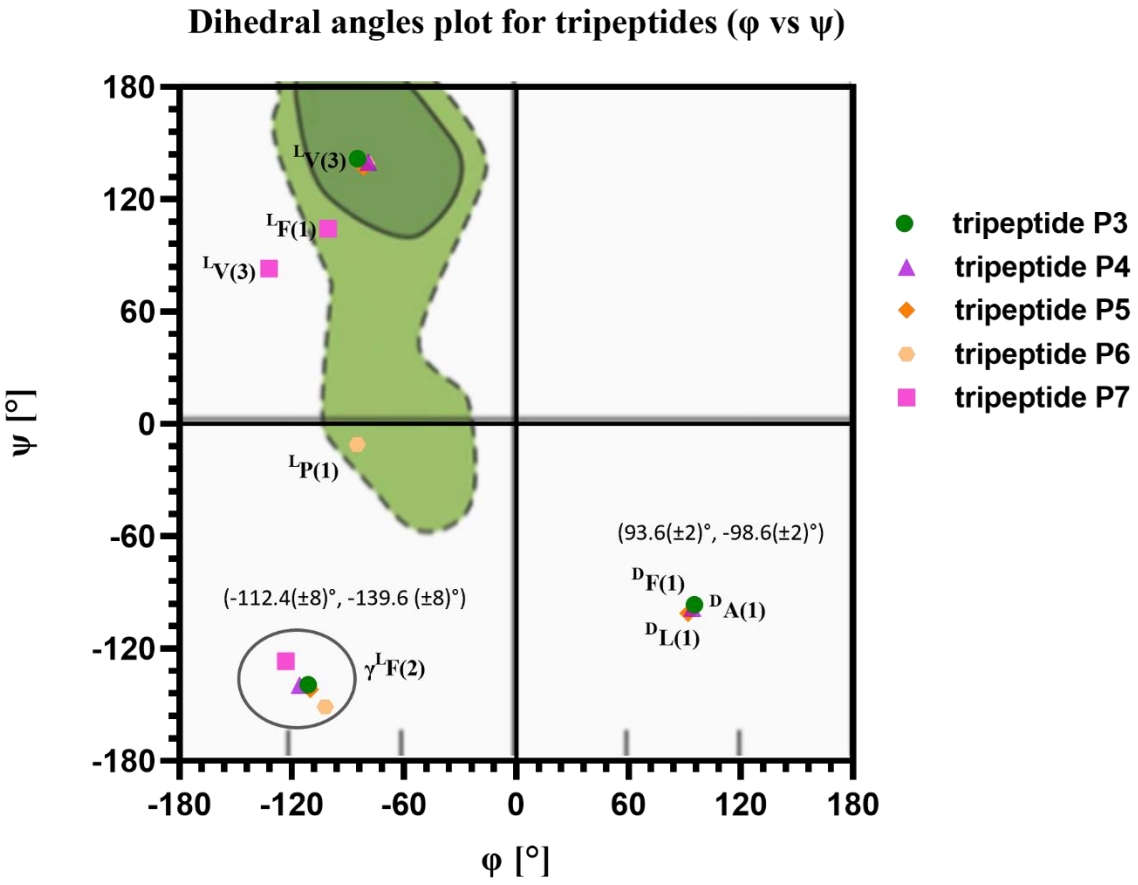

Figure 5.5. The Dihedral angles plot (φ vs ψ) for peptides **P3**-**P7.** All peptides have been labeled with individual color codes. The green-colored area shows the allowed regions (continuous lines) and the generously allowed regions (dotted lines) for Proline residues in peptides/proteins (adapted from Ramakrishnan, 2001).(88,106) Each point corresponds to a specific residue in all tripeptides, and their positions indicate the dihedral angles of peptide **P3-P7**.

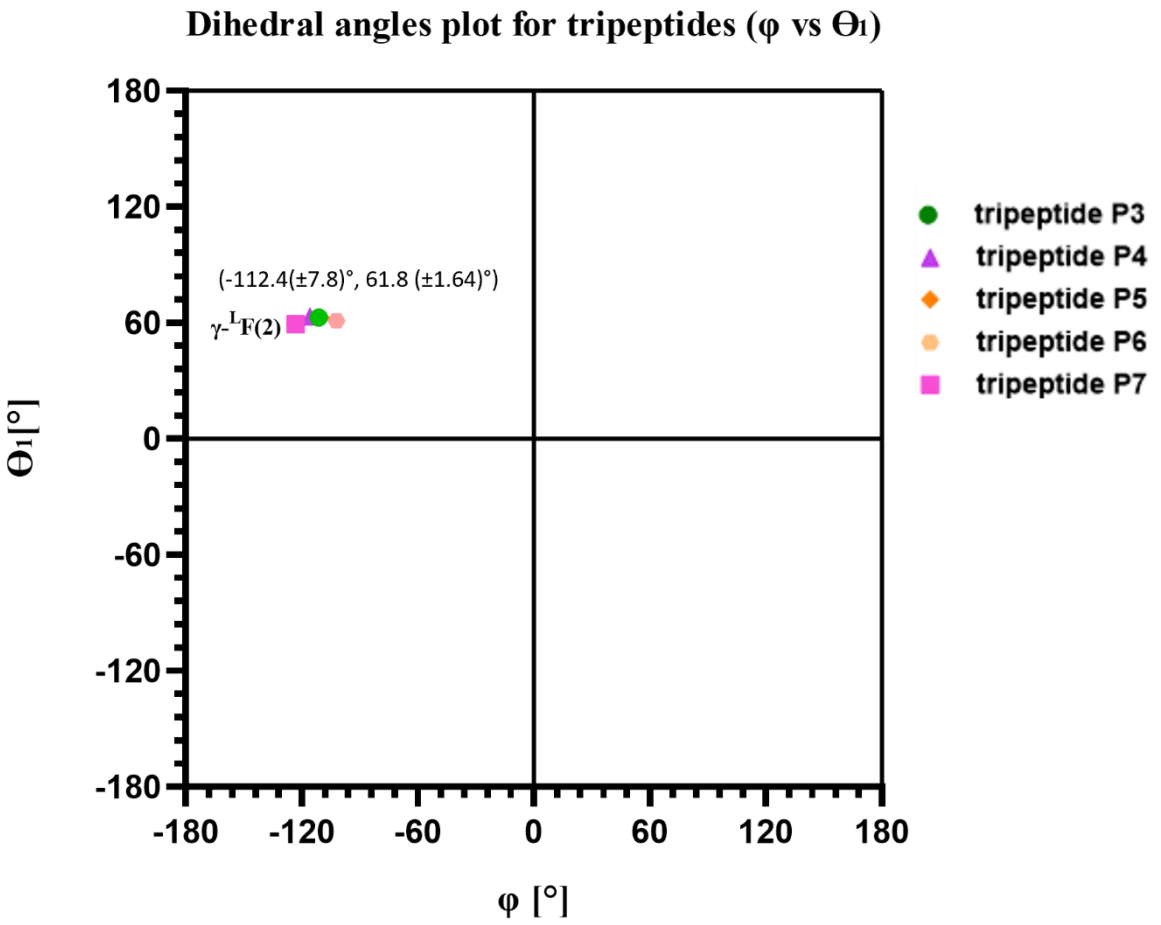

Figure 5.6: The Dihedral angles plot (φ vs θ_1) for peptides **P3**-**P7.** All peptides are labelled with individual colour codes. (33,34)Each point corresponds to a specific γ^4-^{L}Phe residue in all tripeptides, and their positions indicate the dihedral angles of peptide **P3-P7**.

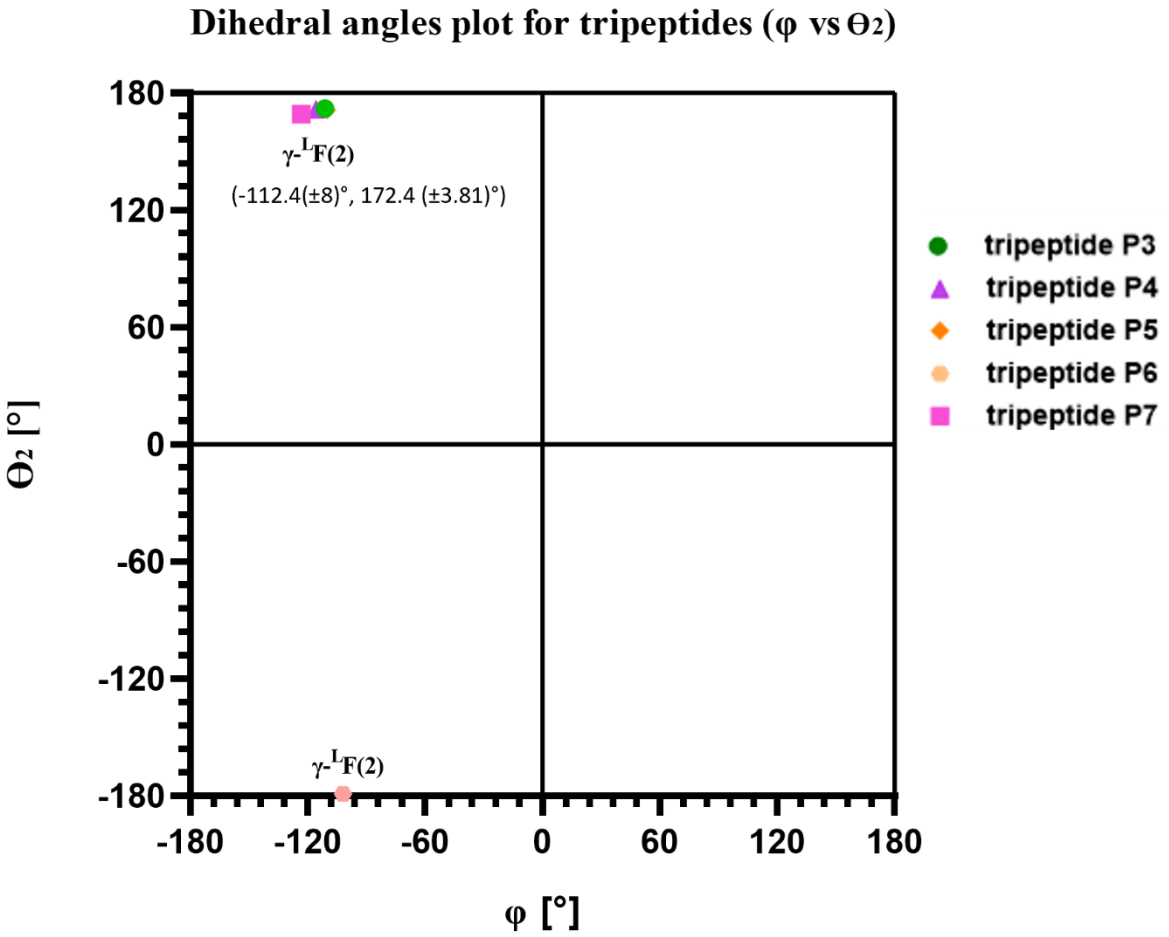

Figure 5.7: The Dihedral angles plot (φ vs θ_2) for peptides **P3**-**P7.** All peptides are labelled with individual colour codes. (33,34)Each point corresponds to a specific γ^4-^{L}Phe residue in all tripeptides, and their positions indicate the dihedral angles of peptide **P3-P7**.

All torsional dihedral angles (φ, θ_1, θ_2, and ψ) for peptides **P3**-**P7** were calculated and shown in a Ramachandran plot (dihedral plot) along with proline residue. The plots confirm that different residues adopt specific backbone conformations depending on their chirality, steric bulk, and sequence position within the tripeptide.

It is very clear from the analysis that the γ^4 ^{L}Phe(2), which is the middle residue of all the tripeptides, shows the most stable conformation in all five peptides with φ = -112.4 ± 7.8º, Θ1 = 61.8 ± 1.8º, Θ2 = 172.5 ± 3.8º, ψ= -139.6 ± 8.7º values irrespective of variations at the first position among these peptides. The φ torsion around -112º keeps

the side chain phenyl ring of γ4-LPhe(2) optimally oriented such that it is facing towards the outer surface of the β-hairpin and avoids any clashes with the main-chain backbone. The Θ1=61.8º is in staggered gauche conformation which is a stable conformation. Values lower than this may cause clashes with the N-terminal residue, and higher values may reduce the optimal van der Waal's contacts, which this residue and the C-terminal ^{L}Val(3) make with the folded N-terminal residues. The Θ2 value of 173º is a stable trans-conformation, which is optimum as the gauche-conformation may cause steric clashes with the main-chain backbone. The ψ value of -139.6 º is a normal stable extended conformation. It may be noted that the standard deviation in the values of Θ1 and Θ2 in these peptides is less compared to that of ϕ and ψ, which may be understood from the fact that the γ-Phe has no substitutions at γ^2 an γ^3 positions which put less packing contains compared to ϕ and ψ values which are constrained by the side chain's steric or main chain carbonyl's H-bonding interactions.

As can be seen from Figure 5.5 all the Val(3) residues are in the extended β-sheet-like conformation with φ around -81.4 ± 2.5º and ψ around 139.4 ± 1.5º in peptides **P3**-**P6**. However, In P7, we find that the (φ, ψ) values, which remain in the extended conformation are significantly different (-132º, 83º) compared to other peptides. The packing constraints may be responsible for such differences as the zig-zag shape of **P7** is dramatically different compared to other peptides (**P3**-**P6**), which form β-hairpin, due to the chirality change at the N-terminal first position in these tri-peptides.

All D-residues at the N-terminus, including ^{D}Phe, ^{D}Ala, and ^{D}Leu exhibit extended β-hairpin conformation with average φ and ψ values of about 93.7 ±1.7° and 98.7 ± 2.4 and are lying in the 4th quadrant of the Ramachandran plot. This falls in the forbidden region of the normal Ramachandran plot of L-amino acids. However, it should be noted that the allowed region of the D-amino acids in this plot is expected to be a mirror

image of that of the L-amino acids, which has also been shown by theoretical studies by Towse et al. 2014.(137) Hence, accessing these conformations is only possible due to chirality changes. The low standard deviation values for (ϕ,ψ) suggest that the structures have stable conformations. Substituting L-Phe(1) at the N-terminus first position as in P7, which has (φ= -100.5°, ψ= 104.5°), exactly the opposite sign that observed for D-amino acids at this position, forces breaking of the β-hairpin structure and it rather takes a zig-zag fold (Figure 5.4). Interestingly, the ^{L}Pro(1) as in **P6** with (φ= -85°, ψ= -11°), which is in the generously allowed region for Proline residues in the Ramachandran plot, falls intermediate between that of aliphatic L and D amino acids (Figure 5.5). This conformation still allows the formation of the β-hairpin as observed in **P6**, which is well-known for proline residues. The average omega(ω) value in all peptides P3-P7 is 174.05 ± 4.15° suggesting stable trans conformation. In summary, the torsional angles data strongly suggests that tripeptides **P3**-**P5** form β-strand-like conformations, while **P6** likely adopts a turn-like structure, which is essential for hairpin loop formation. This distribution supports the hypothesis that these tripeptides together adopt a β-hairpin conformation, a common motif in protein secondary structures, but without forming any H-bonds, which is not reported so far in the literature.

5.6.3. Crystal Packing Studies

The H-bond distances and angles of peptides **P3**-**P7** are listed in Table 5.4.

Table 5.4. Hydrogen bond parameters for **P3**-**P7**. The standard deviations are shown in parentheses.

Type	Donor (D)	Acceptor (A)	D---A (Å)	H---A (Å)	<DH---A (°)
Peptide P3					
Intermolecular	NH (^{D}phe (1))	CO (Boc)[a]	3.011(4)	2.18	161

Intermolecular	NH (γ^{4L}Phe (2))	CO (^{D}phe (1))^{b}	2.932(4)	2.15	151
Intermolecular	NH (^{L}val (3))	CO (γ^{4L}Phe (2))^{a}	3.061(4)	2.21	171
Peptide P4					
Intermolecular	NH (^{D}Ala (1))	CO (Boc)^{a}	2.965(5)	2.16	156
Intermolecular	NH (γ^{4L}Phe (2))	CO (^{D}Ala (1))^{b}	2.913(4)	2.12	154
Intermolecular	NH (^{L}val (3))	CO (γ^{4L}Phe (2))^{a}	3.023(5)	2.17	170
Peptide P5					
Intermolecular	NH (^{D}Leu (1))	CO (Boc)^{d}	3.043(6)	2.22	161
Intermolecular	NH (γ^{4L}Phe (2))	CO (^{D}Leu (1))^{c}	2.925(5)	2.16	147
Intermolecular	NH (^{L}val (3))	CO (γ^{4L}Phe (2))^{c}	3.055(6)	2.21	169
Peptide P6					
Intermolecular	NH (γ^{4L}Phe (2))	NH (^{D}pro (1))	2.833(12)	2.44	109
Intermolecular	CH (BOC)	CO (Boc)	3.02(2)	2.45	118
Intermolecular	CH (BOC)	CO (Boc)	2.946(19)	2.42	115
Intermolecular	CH (^{D}pro (1))	CO (Boc)^{b}	3.406(12)	2.53	149
Intermolecular	CH (γ^{4L}Phe (2))	CO (^{D}pro (1))	2.866(12)	2.49	103
Intermolecular	CH (γ^{4L}Phe (2))	CO (^{D}pro (1))^{a}	3.424(13)	2.57	146
Intermolecular	CH (OMe)	CO (γ^{4L}Phe (2))	2.68(3)	2.23	107
Peptide P7					
Intermolecular	NH (^{L}Phe (1))	CO (Boc)^{a}	2.976(3)	2.11	167
Intermolecular	NH (γ^{4L}Phe (2))	CO (^{L}Phe (1))^{b}	2.897(3)	2.08	155
symmetry operations: a:1+x,y,z; b:-1+x,y,z; c: x,-1+y,z; d: x,1+y,z.					

The peptide **P3** has a disordered phenyl ring at the first position in its backbone showing a pi-pi interaction with the phenyl moiety of γ4-^{L}Phe(2). The pi-pi interactions observed are both parallel staggered and T-type as the two consecutive phenyl moieties are each positionally disordered with occupancies of about 50% in two conformations observed in the crystal structures (Figure 5.8 a and d). In parallel staggered geometry, the centroid-to-centroid distances between disordered Phe rings vary from 4.6 - 5.0 Å, with dihedral angles between planes varying between 34º-39º. In T-type geometry, the centroid-centroid distances are between 4.8-5.2 Å with dihedral angles between planes varying between 46º-49º.

The crystal packing of **P3** is shown in Figure 5.8 (a,b and d). The packing is stabilized by three intermolecular H-bonds can be seen in the view along the c-axis shown in Figure 5.8 (a,b and d). The C=O of Boc H-bonds with translational symmetry related

N-H of ^{D}Phe(1)' at 3.01Å with an angle of about 161° at the same time the N-H of γ4-LPhe(2) H-bonds with symmetry-related C=O of ^{D}Phe(1)' at h-bond distance of about 2.932Å and the angle of about 151°. Additionally, the C=O of γ4-^{L}Phe(2) and N-H of symmetry related ^{L}Val(3)' show H-bonding at a distance of about 3.061Å and an angle of 171°. These interactions help the molecules propagate along the a-direction in the crystal. The π-π interactions and van der Waal's interactions among Boc and main chain γ4-^{L}Phe(2) of symmetry-related molecules help them propagate along the b-direction in the crystal lattice (Figure 5.8 b and c). The hydrophobic interactions among phenyl moieties of ^{D}Phe(1), γ4-^{L}Phe(2), the side chain of Val(3), and OMe moieties help the propagation of molecules along the c-direction in the crystal (Figure 5.8 b and c).

The crystal packing of **P4** is shown in Figure 5.10. **P4**, molecules form H-bonded dimers such that NH of ^{D}Ala(1) is H-bonded with C=O of Boc′ of symmetry-related molecules at a distance of about 2.965 Å and H-bond angle of about 156°. Similarly, the C=O of ^{D}Ala(1) is H-bonded with NH of γ4-^{L}Phe(2)′ of symmetry-related molecule at a distance of 2.913 Å and the H-bond angle of about 154° and NH of LVal(3) is H-bonded with the C=O of γ4-^{L}Phe(2)′ of symmetry-related molecule at a distance of about 3.023 Å and has a near-linear H-bond angle of about 170° ensuring strong directional bonding. These H-bonds help in the propagation of molecules along a-direction in the crystals (Figure 5.9 a,b and d). The hydrophobic interactions among the phenyl moieties of γ4-^{L}Phe, OMe, Boc, and side chains of ^{D}ala(1) and ^{L}Val(3) help in the propagation of molecules along the b-direction in the crystal lattice (Figure 5.9c). Similarly, the hydrophobic interactions among Boc, the main chain of γ4-^{L}Phe(2), and side chains of DAla(1) and γ4-LPhe(2) help in the propagation of molecules along the c-direction in the crystal (Figure 5.9c).

Since **P3** crystallizes in the *P*1 space group. When compared with the approximate calculated dimensions of different peptides observed in these crystal structures, as shown in Table 5.5.

Table 5.5: Calculations of molecular dimensions of each peptide (P3-P7).

Compound	Thickness (Å)	Length (Å)	Width (Å)
P3	4.05	14.81	9.39
P4	3.66	12.83	8.97
P5	4.26	13.31	9.12
P6	4.85	13.35	8.50
P7 (without solvent mol)	4.14	15.90	8.86
P7 (with solvent mol)	5.12	15.90	10.95

The a, b and c dimensions of the unit cell approximately represent the thickness, width and length of the β-hairpin formed by **P3**. For **P4**, the dimensions of the a and c axes are similar to the dimensions of the a and b axes, respectively of **P3**. This implies that the thickness of the β-hairpin of **P3** and **P4** are also similar, as the γ4-Phe(2) is present in both of them, even though there is a change of residues at the N-terminal first position. Only their third dimension (c= 16.624 Å, for **P3** and b=27.778 Å for **P4**) are different. The longer b dimension of **P4** is due to the 2-fold screw axis along the b-direction of the monoclinic lattice, which increases the length of the axis approximately two times its molecular length of about 12.83Å. Comparing the packing of **P3** and **P4**, it may be noted that their H-bonding pattern is conserved along the a-direction in their respective crystal structures which is also reflected in their similar dimension of the a-axis in their respective unit cells (Table 5.1). Perhaps the change in the side chains at the N-terminal first position of the two peptides *i.e.* ^{D}Phe(1) in **P3** and ^{D}Ala(1) in **P4**,

may be responsible for breaking the symmetry in their respective crystalline arrangements. Hence, while **P3** crystallizes in the *P*1 space group, **P4** crystallizes in the $P2_1$ space group.

The molecular interactions and crystal packing of **P5** is shown in Figure 5.10. **P5** also shows H-bonded molecular dimer formation, similar to that observed for **P3** and **P4** (Figure 5.10a). The H-bonded molecules stack along the b-direction in the crystal (Figure 5.10b). The hydrophobic interactions between side-chains of ^{D}Leu(1) and γ4-^{L}Phe(2) as well as the Boc and main chain of γ4-^{L}Phe(2) help the molecules to pack as layers along the a-direction in the crystal lattice. At one end, the hydrophobic interactions between the side chains of Val(3) and OMe moieties in binding of the layers together.While at the other end the interactions between Leu and Phe sides chains, which form leucin-zipper interaction running along a-axis, help the above molecular layers bind together and propagate along the c-direction in the crystal. This packing arrangement mimics lipid bilayers in the crystal, where one layer propagating along the a-direction interacts with neighbouring layers separated along the c-direction. The presence of Leu(1) and its interactions with other neighbouring molecules breaks the symmetry as observed for **P3**, which crystallizes in P1 space group and **P5** crystallizes in *C*2 space group. The b-axis of the unit cell in **P5** remains similar to that of the a-axis dimension of **P3** and **P4** (about 5.1 Å) , which represents the thickness of the β-hairpin. However, there is a doubling of its a and b-axis unit cell length compared to the b and c-axis length, respectively, of the **P3** crystal lattice to accommodate 4 molecules in the unit cell.

In **P6**, due to the presence of a Pro(1) residue, the main chain free NH is lost as it is used for cyclization of the side chain in Pro(1). This, along with the steric hindrance presented by the Pro(1) side chain, there is no H-bonded dimer formation similar to

that observed in **P3**, **P4** and **P5**, where the main chain NH was observed to be involved in H-bonding with symmetry-related neighbouring molecules. Although there is still stacking of the β-hairpin shaped **P6** molecules along the a-direction of the crystal lattice, due to the lack of any H-bonds along this direction, the squeezing effect that H-bonds produce is lacking. The molecules interact purely by van der Waal's interaction along a-direction, which, along with the steric hindrance by the side chain of Pro(1), most likely leads to the elongation of the molecular stacking axis (here a-axis) to 5.65 Å instead of ~ 5.11 to 5.16 Å observed for **P3**-**P5** (Table 5.1). The molecules form layers along the c-direction in the crystal due to hydrophobic interactions between Boc and the main chain of γ4-Phe(2) and between the phenyl moiety of γ4-Phe(2) and the side-chain of Pro(1). These layers interact by hydrophobic interactions among side chains of γ4-Phe(2), Pro(1), Val(3) and OMe moiety at the C-terminus along the b-direction in the crystal. Overall, the crystal lattice of **P6** is isomorphous with that of **P4**, as they have almost the same crystal parameters, and they both have the same $P2_1$ space group (Table 5.1). Their b-dimension is almost double the molecular length as two molecules are accommodated along the b-direction due to the 2-fold screw axis in the monoclinic crystal lattice.

IIn the case of Peptide P7, there are two intermolecular H-bonds present, which is shown in Figure 5.9a. The same crystal packing view is shown in Figure 5.9b. The N-H of ^{L}Phe(1) and C=O of Boc' with a h-bond distance of about 2.976 Å, and the angle was about 167° suggests highly directional h-bonding, enhancing packing strength and another C=O of ^{L}Phe(1) and N-H of ^{L}Phe(2)' with H-bond about 2.897 Å indicate a compact and well-packed arrangement in the crystal which are relatively strong due to their short H-bond distances and the angle was about 155°. There are no direct h-

bonds see along the axis-a (Figure 5.9c) The solvent dioxane molecules were helped in filling the space between molecules during crystal packing.

Overall crystal packing studies in similar tripeptides P3-7, peptides P3-5 have the shortest hydrogen bonds, leading to tight packing arrangements and the peptides P5-7 have slightly longer interactions, suggesting a more open lattice. Due to weak h-bond interactions in peptide P6, it has more flexible packing motifs may adopt a less rigid, possibly layered arrangement in the crystal lattice, compared to all other tripeptides.

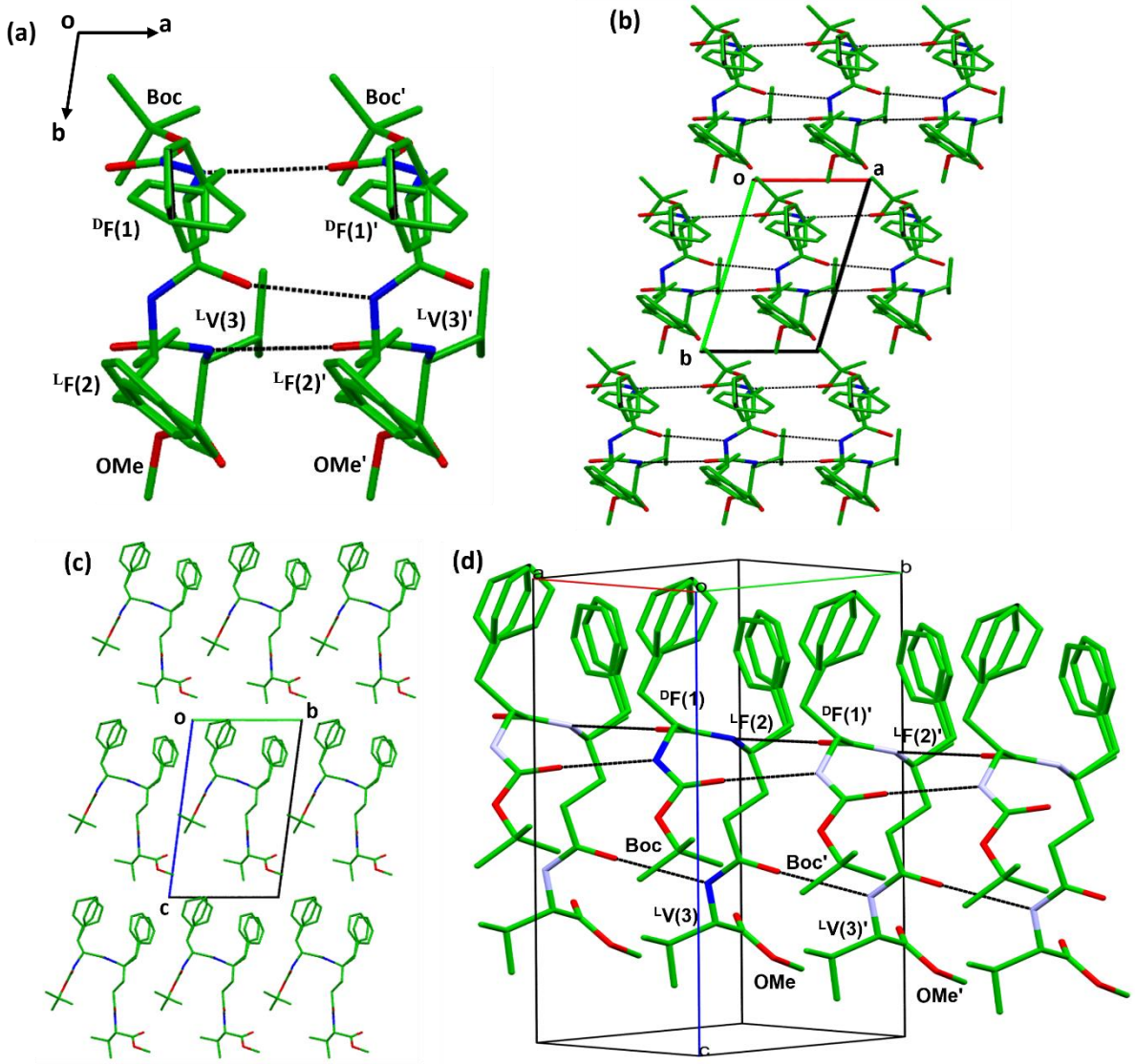

Figure 5.8: Crystal packing view in stick model for tripeptide Boc-^{D}Phe-γ^{4}-^{L}Phe-^{L}Val-OMe, **P3**. (a) The intermolecular interactions between two molecules of peptide **P3** in crystal (one mol shown in green and another mol in light green color) are shown. The two molecules labeled and the parallel molecule labeled using prime; (b) The same viewed along the c-axis; (c) The interaction pattern in crystal packing along the a-axis, and (d) The intermolecular interaction pattern between molecules inside crystal packing. Dash lines in black color show the putative H-bonds. All N-atoms are shown in blue color while all O are shown in red color. All H-atoms were removed for the sake of clarity.

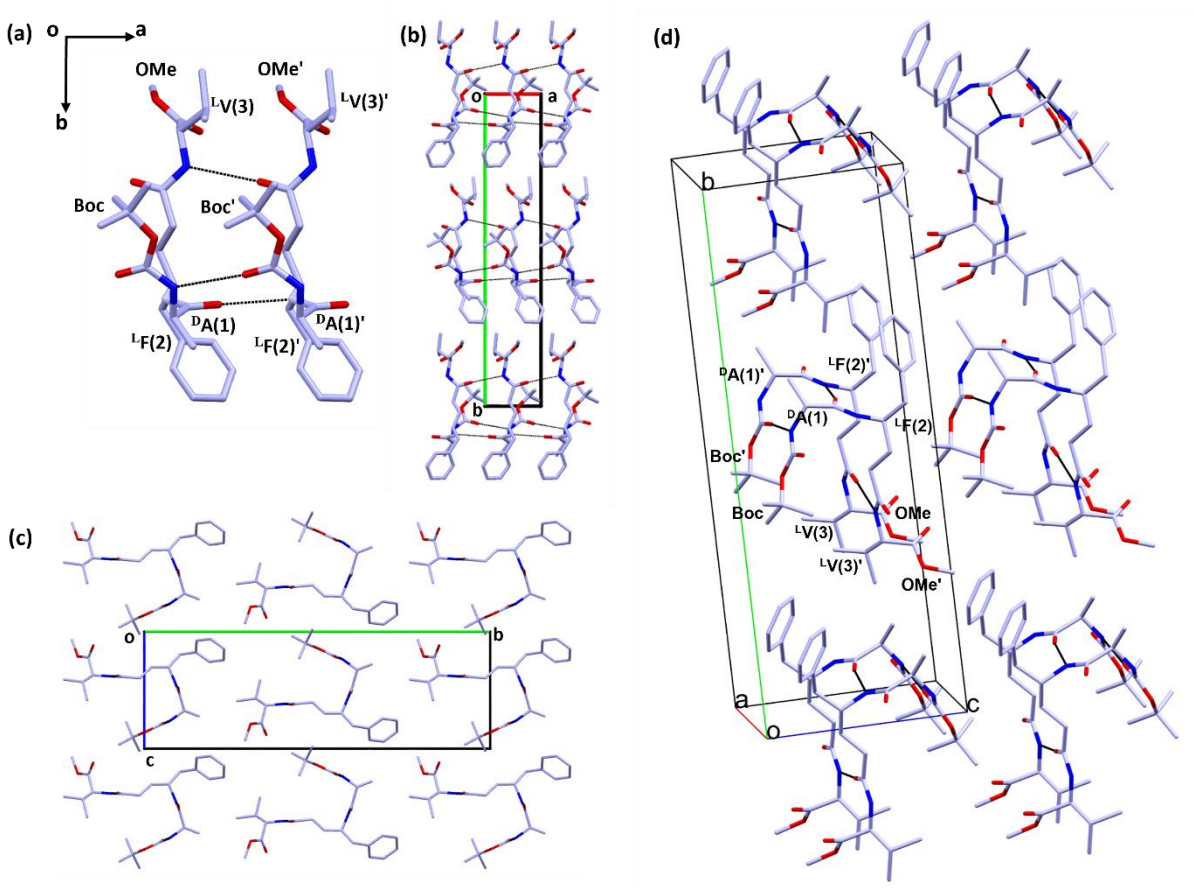

Figure 5.9: Crystals packing of **P4**. (a) The intermolecular H-bonded dimer formation by molecules of **P5** in crystal lattice. The some of the residues of both molecules have been labeled and the translational symmetry related molecule has been labeled using prime; (b) The crystal packing viewed along the c-axis; (c) The same viewed along the a-axis, (d) The intermolecular interaction pattern between molecules inside crystal viewed approximately along a-direction. The putative H-bonds are shown by dash lines in black colour. All C, N and O atoms have been shown in light-blue, blue and red colours, respectively. All H-atoms have been removed for the sake of clarity.

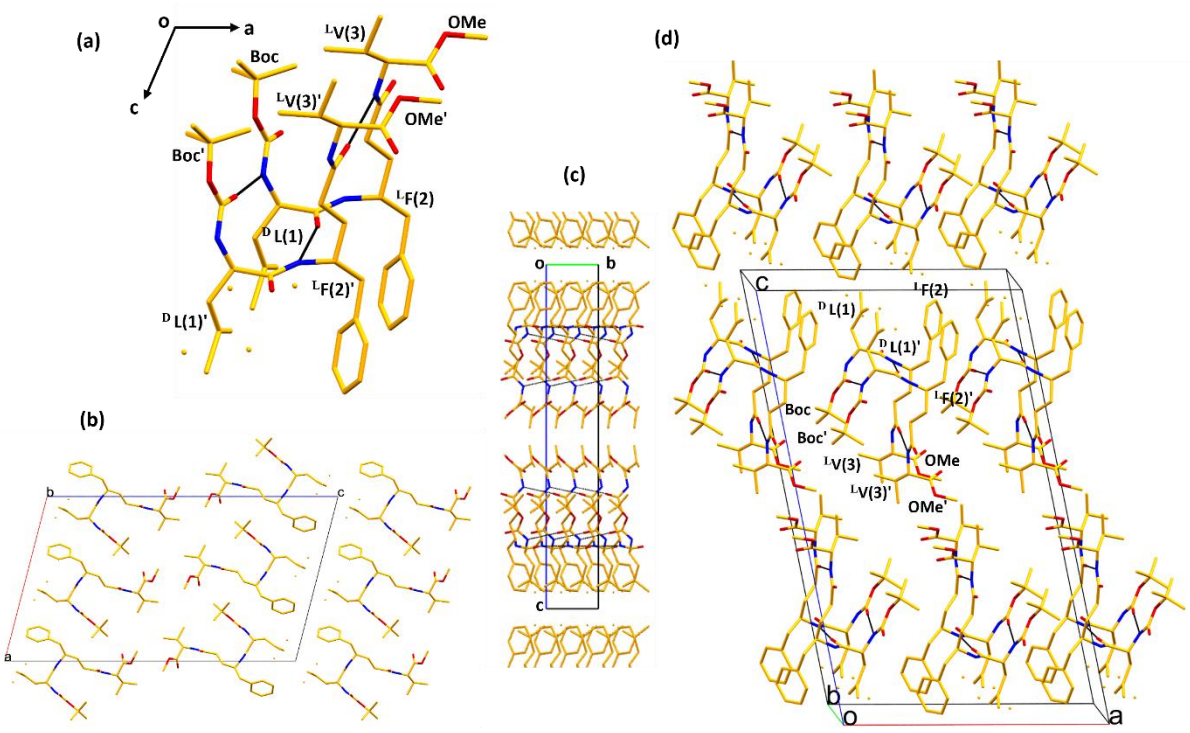

Figure 5.10: Crystals packing of **P5**. (a) The intermolecular H-bonding between two molecules of **P5** in crystals viewed approximately along the b-axis. Some of the residues are labelled, and the symmetry-related molecule's residues are labelled using prime; (b) The crystal packing viewed along the b-axis; The same when viewed along the (c) a-axis and (d) b-axis. The putative H-bonds are shown by dash lines in black colour. All C, N and O atoms have been shown in yellow, blue and red colours, respectively. All H-atoms have been removed for the sake of clarity.

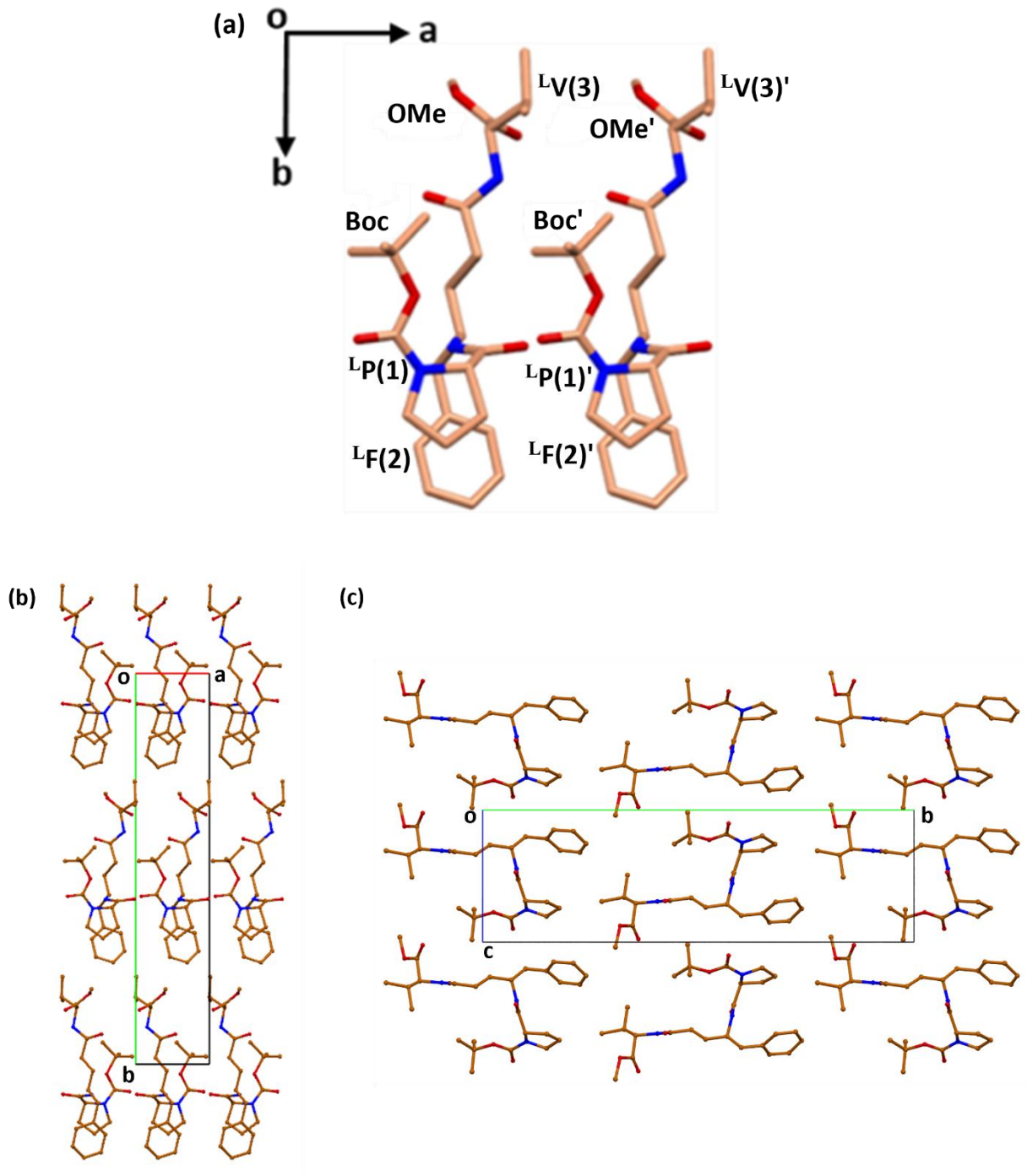

Figure 5.11: Crystals packing of **P6**. (a) The weekly interacting two molecules of **P6** without forming any H-bonds**,** viewed approximately along the c-axis. Some of the residues of **P6** are labelled, and the translation symmetry-related molecule is labelled using a prime (b) The crystal packing viewed along the c-axis; (c) The same view along the a-axis. All C, N and O atoms have been shown in brown, blue and red colours, respectively. All H-atoms have been removed for the sake of clarity.

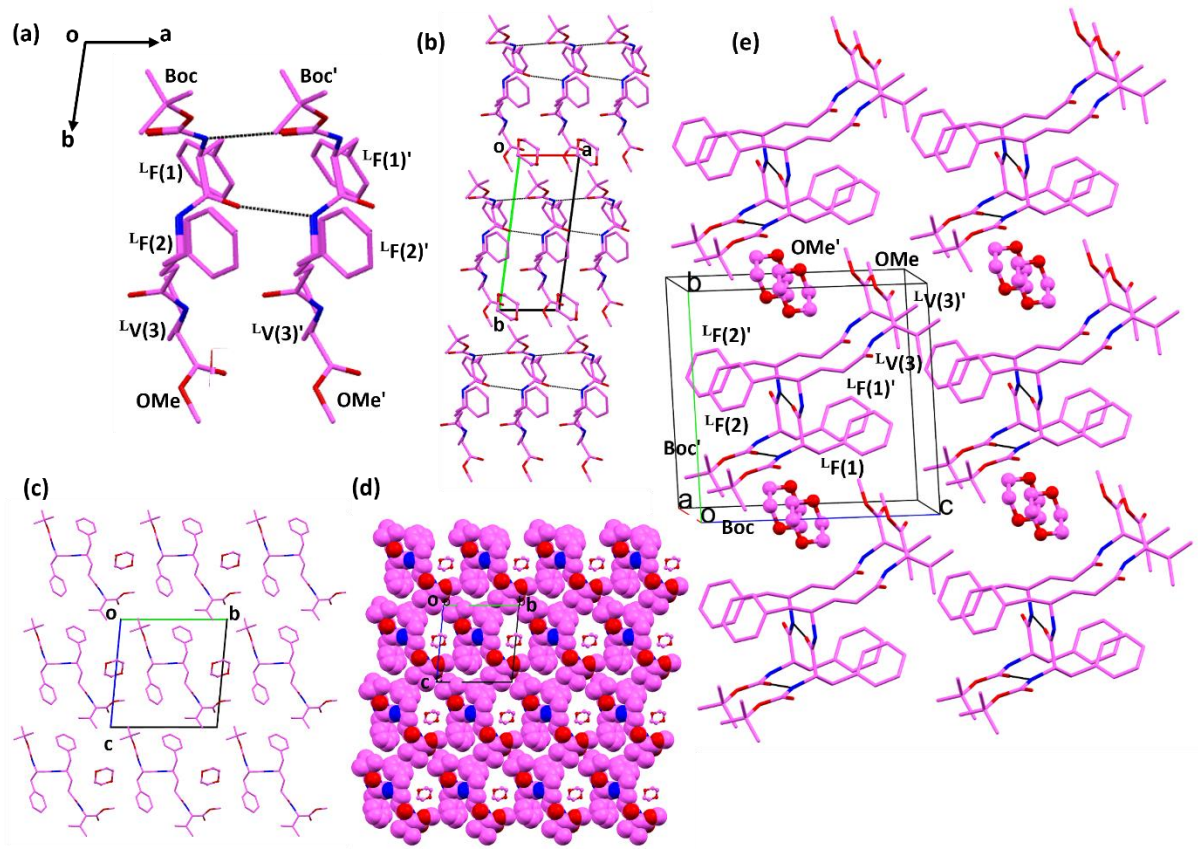

Figure 5.12: Crystals packing of **P7**. (a) The H-bonded two molecules of **P7** form dimers in crystalline state. The residues of both molecules are labelled. The translation symmetry-related molecule has been labelled using prime. Note that these dimers form only two H-bonds whereas three H-bonds were observed in **P3**-**P5** (b) The crystal packing viewed along the c-axis; (c) The same viewed along the a-axis. (d) The where **P7** molecules are shown as CPK model and the solvent molecules are shown in the ball and stick model. Note the channel formed by the self-assembly of P7, which is occupied by solvent molecules (dioxane) (e). The crystal packing is viewed approximately along the a-axis. P7 molecules are shown in stick models, and the solvent molecules are shown in ball and stick models. Dash lines in black colour show the putative H-bonds. All C, N and O atoms have been shown in magenta, blue and red colours, respectively. All H-atoms have been removed for the sake of clarity.

5.7. Conclusions

We have discovered a tri-peptide-based β-hairpin turn that is stable without any forming any intra-molecular H-bonded interactions normally observed in natural or non-canonical amino-acid based petides. This fold remains stable even with changes in the sequence of the tri-peptide by varying the first amino acid in the sequence. The chirality of the first amino acid seems to be critical for the β-hairpin formation. The rigidity of γ4-^{L}Phe conformation also seems to play an important role in the formation an maintenance of these β-hairpin turns.

5.8. Future Perspectives

It will be interesting to see if the β-hairpin structures observed in the solid state also hold true in the solution state. Solution state NMR studies may takeun up in the future. It would also be interesting if these β-turns could be incorporated into much bigger peptides by incorporating resides on both its N and C-termini to demonstrate their use for introducing such β-turns in longer peptides to form super secondary structures. This may form part of future studies.

.

1. Gellman SH. Foldamers: A Manifesto. Acc Chem Res. 1998;31(4):173–80.

2. Saraogi I, Hamilton AD. Recent advances in the development of aryl-based foldamers. Chem Soc Rev. 2009;38(6):1726–43.

3. Vasudev PG, Chatterjee S, Narayanaswamy S, Padmanabhan B. Structural chemistry of peptides containing backbone expanded amino acid residues: Conformational features of β, γ, and hybrid peptides. Chem Rev. 2011;111(2):657–87.

4. Hill DJ, Mio MJ, Prince RB, Hughes TS, Moore JS. A field guide to foldamers. Chem Rev. 2001;101(12):3893–4011.

5. Guichard G, Huc I. Synthetic foldamers. Chemical Communications. 2011;47(21):5933–41.

6. W.S. Horne, L.M. Johnson, T.J. Ketas, P.J. Klasse, M. Lu, J.P. Moore, & S.H. Gellman, Structural and biological mimicry of protein surface recognition by α/β-peptide foldamers, Proc. Natl. Acad. Sci. U.S.A. 106 (35) 14751-14756.

7. Seebach D, Gademann K, Schreiber J V., Matthews JL, Hintermann T, Jaun B, et al. 'Mixed' β-Peptides: A Unique Helical Secondary Structure in Solution. Helv Chim Acta. 1997;80(7):2033–8.

8. Vasudev PG, Chatterjee S, Ananda K, Shamala N, Balaram P. Hybrid αγ Polypeptides: Structural Characterization of a C 12 /C 10 Helix with Alternating Hydrogen-Bond Polarity . Angewandte Chemie. 2008;120(34):6530–2.

9. Sharma GVM, Thodupunuri P, Sirisha K, Basha SJ, Reddy PG, Sarma AVS. Design and synthesis of peptides with hybrid helix-turn-helix (HTH) motif and their conformational study. Journal of Organic Chemistry. 2014;79(18):8614–28.

10. R.S. Roy,I.L. Karle,S. Raghothama,& P. Balaram, α,β hybrid peptides: A polypeptide helix with a central segment containing two consecutive β-amino acid residues, Proc. Natl. Acad. Sci. U.S.A. 101 (47) 16478-16482.

11. Dong H, Sharma M, Zhou HX, Cross TA. Glycines: role in α-helical membrane protein structures and a potential indicator of native conformation. Biochemistry. 2012 Jun 19;51(24):4779-89.

12. Sharma GV, Yadav TA, Choudhary M, Kunwar AC. Design of β-amino acid with backbone-side chain interactions: stabilization of 14/15-helix in α/β-peptides. J Org Chem. 2012 Aug 17;77(16):6834-48.

13. Gellman SH. Minimal model systems for β sheet secondary structure in proteins. Curr Opin Chem Biol. 1998;2(6):717–25.

14. Seebach D, Beck AK, Bierbaum DJ. The World of b - and g -Peptides Comprised of Homologated Proteinogenic Amino Acids and Other Components 2 . From the Biopolymer Poly (b-hydroxybutyric acid ester) to b -Peptides ± from Organic Synthesis to Departure into a New World 3 . Earlier Work o. Chem Biodivers. 2004;1:1111–239.

15. Baldauf C, Günther R, Hofmann HJ. Helices in peptoids of α- and β-peptides. Phys Biol. 2006;3(1).

16. Dieter S and James G. *Accounts of Chemical Research* 2008; *41*(10):1366-1375.

17. Datta S, Roy A. Antimicrobial Peptides as Potential Therapeutic Agents: A Review. Int J Pept Res Ther. 2021;27(1):555–77.

18. Fülöp F, Martinek TA, Tóth GK. Application of alicyclic β-amino acids in peptide chemistry. Chem Soc Rev. 2006;35(4):323–34.

19. Young HS and Samuel H. Gellman. *Journal of the American Chemical Society* 2018;*140* (4),1394-1400.

20. Cabrele C, Martinek TA, Reiser O, Berlicki Ł. Peptides containing β-amino acid patterns: challenges and successes in medicinal chemistry. J Med Chem. 2014 Dec 11;57(23):9718-39.

21. Baldauf C, Günther R, Hofmann HJ. Helix formation in alpha,gamma- and beta,gamma-hybrid peptides: theoretical insights into mimicry of alpha- and beta-peptides. J Org Chem. 2006 Feb 3;71(3):1200-8.

22. Shahmohammadi S, Fülöp F. E ffi cient Synthesis of New Fluorinated β -Amino Acid. 2020;1–11.

23. Kiss L, Mándity IM, Fülöp F. Highly functionalized cyclic β-amino acid moieties as promising scaffolds in peptide research and drug design. Amino Acids. 2017;49(9):1441–55.

24. Sharma GVM, Venkateshwarlu G, Katukuri S, Ramakrishna KVS, Sarma AVS. Design and synthesis of novel oxetane β3-amino acids and α, β-peptides. Tetrahedron. 2015;71(14):2158–67.

25. Sharma GVM, Sridhar T, Veena B, Purushotham Reddy P, Reddy SV, Bruneau C, et al. Synthesis and conformational studies of α/β2,3-peptides derived from alternating β2,3-amino acids and L-Ala repeats. New Journal of Chemistry. 2015;39(5):3295–309.

26. Legrand B, André C, Moulat L, Wenger E, Didierjean C, Aubert E, et al. Unprecedented Chain-Length-Dependent Conformational Conversion Between 11/9 and 18/16 Helix in α/β-Hybrid Peptides. Angewandte Chemie. 2014;126(48):13347–51.

27. Kudo F, Miyanaga A, Eguchi T. Biosynthesis of natural products containing β-amino acids. Nat Prod Rep. 2014;31(8):1056–73.

28. Sleebs BE, Nguyen NH, Hughes AB. Diastereoselective synthesis of cyclic β2,3-amino acids utilizing 4-substituted-1,3-oxazinan-6-ones. Tetrahedron. 2013;69(30):6275–84.

29. Lee, M. R., Raman, N., Gellman, S. H., Lynn, D. M., & Palecek, S. P. (2017). Incorporation of β-Amino Acids Enhances the Antifungal Activity and Selectivity of the Helical Antimicrobial Peptide Aurein 1.2. ACS chemical biology, 12(12), 2975–2980.

30. Liang Y, Strieth-Kalthoff F, Bellotti P, Glorius F. Catalytic one-carbon homologation of α-amino acids to β-amino aldehydes. Chem Catalysis. 2021;1(7):1427–36.

31. Wani NA, Raghothama S, Singh UP, Rai R. C11/C9Helical Folding in αβ Hybrid Peptides Containing 1-Amino-cyclohexane acetic acid (β3, 3-Ac6c). Chemistry - A European Journal. 2017;23(35):8364–70.

32. Shankar S, Jyothi D, Rahim J ur, Pal PC, Singh UP, Rai R. Conformation of Achiral α/β Hybrid Peptides Containing Glycine and 1-Aminocyclohexaneacetic Acid. ChemistrySelect. 2022;7(10):1–7.

33. Beke T, Csizmadia IG, Perczel A. On the flexibility of β-peptides. *Journal of Computational Chemistry*, 2004;*25*(2):285-307.

34. Conlon JM, Kolodziejek J, Nowotny N. Antimicrobial peptides from ranid frogs: Taxonomic and phylogenetic markers and a potential source of new therapeutic agents. Biochim Biophys Acta Proteins Proteom. 2004;1696(1):1–14.

35. Koehbach J, Craik DJ. The Vast Structural Diversity of Antimicrobial Peptides. Trends Pharmacol Sci. 2019;40(7):517–28.

36. Appella, D.H., Christianson, L.A., Karle, I.L., Powell, A.D., & Gellman, S.H. (1996). β-Peptide Foldamers: Robust Helix Formation in a New Family of β-Amino Acid Oligomers. Journal of the American Chemical Society, 118, 13071-13072.

37. Sang P, Cai J. Unnatural helical peptidic foldamers as protein segment mimics. Chem Soc Rev. 2023;52(15):4843–77.

38. degrado-schneider-1998-the-design-of-efficient-α-helical-c-capping-auxiliaries.pdf.

39. Schneider JP, Lombardi A, DeGrado WF. Analysis and design of three-stranded coiled coils and three-helix bundles. Fold Des. 1998;3(2):29–40.

40. Goodman CM, Choi S, Shandler S, DeGrado WF. Foldamers as versatile frameworks for the design and evolution of function. Nat Chem Biol. 2007;3(5):252–62.

41. Sahu, D., Zhao, Z., Tsen, F., Cheng, C. F., Park, R., Situ, A. J., Dai, J., Eginli, A., Shams, S., Chen, M., Ulmer, T. S., Conti, P., Woodley, D. T., & Li, W. (2012). A potentially common peptide target in secreted heat shock protein-90α for hypoxia-inducible factor-1α-positive tumors. Molecular biology of the cell, 23(4), 602–613.

42. Martinek TA, Fülöp F. Peptidic foldamers: Ramping up diversity. Chem Soc Rev. 2012;41(2):687–702.

43. Socolich M, Lockless SW, Russ WP, Lee H, Gardner KH, Ranganathan R. Evolutionary information for specifying a protein fold. Nature. 2005;437(7058):512–8.

44. Seebach D, Matthews JL. β-peptides: A surprise at every turn. Chemical Communications. 1997;1(21):2015–22.

45. Seebach, D., & Gardiner, J. (2008). Beta-peptidic peptidomimetics. Accounts of chemical research, 41(10), 1366–1375.

46. Koert U. β-peptides: Novel secondary structures take shape. Angewandte Chemie (International Edition in English). 1997;36(17):1836–7.

47. Ni TW, Tofanelli MA, Ackerson CJ. Structure Determination by Single Crystal X-ray Crystallography. Vol. 9, Frontiers of Nanoscience. Elsevier; 2015. 103–125 p.

48. Li J, Sun J. Application of X-ray Diffraction and Electron Crystallography for Solving Complex Structure Problems. Acc Chem Res. 2017;50(11):2737–45.

49. Hatcher LE, Warren MR, Pallipurath AR, Saunders LK, Skelton JM. Watching photochemistry happen: Recent developments in dynamic single-crystal X-ray diffraction studies. Struct Bond. 2020;185:199–238.

50. Xiao Y, Wu C, Zhou L, Commins P, Li L, Naumov P, et al. Current trends and advancements in crystallization and single-crystal structural analysis of small molecules. Coord Chem Rev. 2024;517(April).

51. Gorfman S. Sub-microsecond X-ray crystallography: Techniques, challenges, and applications for materials science. Crystallogr Rev. 2014;20(3):210–32.

52. Glusker, Jenny P and Lewis, Mitchell and Rossi M. Crystal Structure Analysis for Chemists and Biologists. Vol 16. John Wiley & Sons Ltd.; 1996.

53. Aravinda S, Shamala N, Roy RS, Balaram P. Non-protein amino acids in peptide design. Proceedings of the Indian Academy of Sciences: Chemical Sciences. 2003;115(5-6 SPEC. ISS.):373–400.

54. Bucci R, Contini A, Clerici F, Beccalli EM, Formaggio F, Maffucci I, et al. Fluoro-aryl substituted α,β 2,3 -peptides in the development of foldameric antiparallel β-sheets: A conformational study. Front Chem. 2019;7(APR):1–11.

55. Choi, S. H., Guzei, I. A., Spencer, L. C., & Gellman SH. crystallographic-characterization-of-12-helical-secondary-structure-in-β-peptides-containing-side. ACS Publications; 2010. p. 13879–85.

56. Adessi C, Soto C. Converting a Peptide into a Drug: Strategies to Improve Stability and Bioavailability. Curr Med Chem. 2005;9(9):963–78.

57. Patgiri A, Joy ST, Arora PS. Nucleation E ff ects in Peptide Foldamers. 2012;

58. Han D, Li A, Zhu L, Zhuang C, Zhao Q, Zou Y. Peptide inhibitors targeting Ras and Ras-associated protein–protein interactions. Eur J Med Chem. 2024;279(August):116878.

59. Banta S, Wheeldon IR, Blenner M. Protein engineering in the development of functional hydrogels. Annu Rev Biomed Eng. 2010;12:167–86.

60. Coles SJ, Gale PA. Changing and challenging times for service crystallography. Chem Sci. 2012;3(3):683–9.

61. De Zotti M, Biondi B, Park Y, Hahm KS, Crisma M, Toniolo C, et al. Antimicrobial lipopeptaibol trichogin GA IV: Role of the three Aib residues on conformation and bioactivity. Amino Acids. 2012;43(4):1761–77.

62. Kabsch W. Integration, scaling, space-group assignment and post-refinement. Acta Crystallogr D Biol Crystallogr. 2010;66(2):133–44.

63. Guichard G, Huc I. Synthetic foldamers. Chemical Communications. 2011;47(21):5933–41.

64. Albericio F, Chinchilla R, Dodsworth DJ, Nájera C. New trends in peptide coupling reagents. Org Prep Proced Int. 2001;33(3):203–303.

65. Humphrey JM, Chamberlin AR. Chemical synthesis of natural product peptides: Coupling methods for the incorporation of noncoded amino acids into peptides. Chem Rev. 1997;97(6):2243–66.

66. Charoen-In U, Ramasamy P, Manyum P. Comparative study on l-alaninium maleate single crystal grown by SankaranarayananRamasamy (SR) method and conventional slow evaporation solution technique. J Cryst Growth. 2010;312(16–17):2369–75.

67. P JW. research papers The ® ner things in X-ray diffraction data collection research papers. 1999;1718–25.

68. Powell HR. From then till now: changing data collection methods in single crystal X-ray crystallography since 1912. Crystallogr Rev. 2019;25(4):264–94.

69. Deschamps JR. X-ray crystallography of chemical compounds. Life Sci. 2010;86(15–16):585–9.

70. Fish PW. Electron diffraction and the Bragg equation. Phys Educ. 1971;6(1):7–9.

71. Pope CG. X-ray diffraction and the bragg equation. J Chem Educ. 1997;74(1):129–31.

72. Determination S. International Tables for Crystallography (2019). 2019;2019.

73. Ewald BYPP. The So-Called Correction of Bragg's Law. 1986;50(February):411–3.

74. Kabsch W. Evaluation of single-crystal X-ray diffraction data from a position-sensitive detector. J Appl Crystallogr. 1988;21(6):916–24.

75. Spingler B, Schnidrig S, Todorova T, Wild F. Some thoughts about the single crystal growth of small molecules. CrystEngComm. 2012;14(3):751–7.

76. Niwa S, Takeda K. Usefulness of oils for cleaning the host matrix and for cryoprotection of lipidic cubic phase crystals. J Appl Crystallogr. 2019;52(4):864–8.

77. Boulle A. DxTools: Processing large data files recorded with the Bruker D8 diffractometer. J Appl Crystallogr. 2017;50(3):967–74.

78. Otwinowski, Z., & Minor, W. (1997). Processing of X-ray diffraction data collected in oscillation mode. Methods in enzymology, 276, 307–326.

79. Tsymbarenko D, Grebenyuk D, Burlakova M, Zobel M. Quick and robust PDF data acquisition using a laboratory single-crystal X-ray diffractometer for study of polynuclear lanthanide complexes in solid form and in solution. Applied Crystallography. 2022 Aug 1;55(4):890-900.

80. Sheldrick GM. A short history of SHELX. Acta Crystallogr A. 2008;64(1):112–22.

81. Sheldrick GM. Crystal structure refinement with SHELXL. Acta Crystallogr C Struct Chem. 2015;71(Md):3–8.

82. Dolomanov O V., Bourhis LJ, Gildea RJ, Howard JAK, Puschmann H. OLEX2: A complete structure solution, refinement and analysis program. J Appl Crystallogr. 2009;42(2):339–41.

83. Sheldrick GM. SHELXT - Integrated space-group and crystal-structure determination. Acta Crystallogr A. 2015;71(1):3–8.

84. Allen FH. research papers The Cambridge Structural Database : a quarter of a million crystal structures and rising research papers. Acta Cryst. 2002;B58:380–8.

85. Spek AL. Single-crystal structure validation with the program PLATON. J Appl Crystallogr. 2003;36(1):7–13.

86. Pettersen EF, Goddard TD, Huang CC, Couch GS, Greenblatt DM, Meng EC, et al. UCSF Chimera - A visualization system for exploratory research and analysis. J Comput Chem. 2004;25(13):1605–12.

87. Cheng, R. P., Gellman, S. H., & DeGrado, W. F. (2001). beta-Peptides: from structure to function. Chemical reviews, 101(10), 3219–3232.

88. Ramakrishnan C. Ramachandran and his Map. Resonance. 2001;6(10):48–56.

89. Martinek TA, Fülöp F. Peptidic foldamers: Ramping up diversity. Chem Soc Rev. 2012;41(2):687–702.

90. Basuroy K, Karuppiah V, Shamala N, Balaram P. The structural characterization of folded peptides containing the conformationally constrained β-amino acid residue β 2,2Ac6c. Helv Chim Acta. 2012;95(12):2589–603.

91. Mándity IM, Wéber E, Martinek TA, Olajos G, Tóth GK, Vass E, et al. Design of peptidic foldamer helices: A stereochemical patterning approach. Angewandte Chemie - International Edition. 2009;48(12):2171–5.

92. Basuroy K, Karuppiah V, Balaram P. C11/C9 helices in crystals of αβ hybrid peptides and switching structures between helix types by variation in the α-residue. Org Lett. 2014;16(17):4614–7.

93. Sharma, G. V., Nagendar, P., Jayaprakash, P., Radha Krishna, P., Ramakrishna, K. V., & Kunwar, A. C. (2005). 9/11 mixed helices in alpha/beta peptides derived from C-

linked carbo-beta-amino acid and L-Ala repeats. Angewandte Chemie (International ed. in English), 44(36), 5878–5882.

94. Vasudev, P. G., Rai, R., Shamala, N., & Balaram, P. (2008). Conformations of beta-amino acid residues in peptides: X-ray diffraction studies of peptides containing the achiral residue 1-aminocyclohexaneacetic acid, beta3,3Ac6c. Biopolymers, 90(2), 138–150.

95. Basuroy, K., Rajagopal, A., Raghothama, S., Shamala, N., & Balaram, P. (2012). β-Turn analogues in model αβ-hybrid peptides: structural characterization of peptides containing β(2,2)Ac6c and β(3,3)Ac6c residues. Chemistry, an Asian journal, 7(7), 1671–1678.

96. Kiss, L., & Fülöp, F. (2014). Synthesis of carbocyclic and heterocyclic β-aminocarboxylic acids. Chemical reviews, 114(2), 1116–1169.

97. Martinek TA, Fülöp F. Peptidic foldamers: Ramping up diversity. Chem Soc Rev. 2012;41(2):687–702.

98. Appella DH, Christianson LA, Klein DA, Powell DR, Huang X, Barchi JJ, et al. Residue-based control of helix shape in β-peptide oligomers. Vol. 387, Nature. 1997. p. 381–4.

99. Mándity IM, Fülöp L, Vass E, Tóth GK, Martinek TA, Fülöp F. Building β-peptide H10/12 foldamer helices with six-membered cyclic side-chains: Fine-tuning of folding and self-assembly. Org Lett. 2010;12(23):5584–7.

100. Whitesides GM. Moving from structure to function. Abstracts of Papers of the American Chemical Society. 2001;221:U318–U318.

101. Chaudhary S, Rai RN, Jyothi D, Singh UP. Solid state synthesis, thermal, spectral, optical, crystal structure and atomic packing studies of 2-(3-Hydroxyphenyl)-2,3-dihydroquinazolin-4(1H)-one. Mater Lett. 2023 Jun 15;341:134253.

102. Krause L, Herbst-Irmer R, Sheldrick GM, Stalke D. Comparison of silver and molybdenum microfocus X-ray sources for single-crystal structure determination. J Appl Crystallogr. 2015;48(1):3–10.

103. Sheldrick GM. Crystal structure refinement with SHELXL. Acta Crystallogr C Struct Chem. 2015;71(Md):3–8.

104. MacRae CF, Sovago I, Cottrell SJ, Galek PTA, McCabe P, Pidcock E, et al. Mercury 4.0: From visualization to analysis, design and prediction. J Appl Crystallogr. 2020;53:226–35.

105. Solomon RW. Free and open source software for the manipulation of digital images. American Journal of Roentgenology. 2009;192(6):330–4.

106. Carugo O, Djinovic Carugo K. Half a century of Ramachandran plots. Acta Crystallogr D Biol Crystallogr. 2013;69(8):1333–41.

107. Basuroy K, Karuppiah V, Balaram P. C11/C9 helices in crystals of αβ hybrid peptides and switching structures between helix types by variation in the α-residue. Org Lett. 2014;16(17):4614–7.

108. Legrand B, André C, Moulat L, Wenger E, Didierjean C, Aubert E, et al. Unprecedented chain-length-dependent conformational conversion between 11/9 and 18/16 helix in α/β-hybrid peptides. Angewandte Chemie - International Edition. 2014;53(48):13131–5.

109. Ahmad Wani N, Gupta VK, Kant R, Aravinda S, Rai R. Conformation and crystal structures of 1-aminocyclohexaneacetic acid (β3,3Ac6c) in N-protected derivatives. Acta Crystallogr Sect E Struct Rep Online. 2014;70(11):272–7.

110. Basuroy K, Rajagopal A, Raghothama S, Shamala N, Balaram P. β-turn analogues in model αβ-hybrid peptides: Structural characterization of peptides containing β 2,2Ac 6c and β 3,3Ac 6c residues. Chem Asian J. 2012;7(7):1671–8.

111. Shankar S, Jyothi D, Rahim J ur, Pal PC, Singh UP, Rai R. Conformation of Achiral α/β Hybrid Peptides Containing Glycine and 1-Aminocyclohexaneacetic Acid. ChemistrySelect. 2022 Mar 15;7(10):e202104453.

112. Briggs P, Winn MD, Bailey S, Ashton A. Ccp4 Newsletter on Protein Crystallography. Ccp4AcUk. 2002;(4).

113. Ramakrishnan C. Ramachandran and his Map. Resonance. 2001;6(10):48–56.

114. Carugo O, Djinovic Carugo K. Half a century of Ramachandran plots. Acta Crystallogr D Biol Crystallogr. 2013;69(8):1333–41.

115. Garcia AM, Iglesias D, Parisi E, Styan KE, Waddington LJ, Deganutti C, et al. Chirality Effects on Peptide Self-Assembly Unraveled from Molecules to Materials. Chem. 2018;4(8):1862–76.

116. Marchesan S, Easton CD, Kushkaki F, Waddington L, Hartley PG. Tripeptide self-assembled hydrogels: Unexpected twists of chirality. Chemical Communications. 2012;48(16):2195–7.

117. Vasudev PG, Chatterjee S, Ananda K, Shamala N, Balaram P. Hybrid αγ polypeptides: Structural characterization of a C 12/C10 helix with alternating hydrogen-bond polarity. Angewandte Chemie - International Edition. 2008;47(34):6430–2.

118. Kopeček J, Yang J. Peptide-directed self-assembly of hydrogels. Acta Biomater. 2009;5(3):805–16.

119. Sheehan F, Sementa D, Jain A, Kumar M, Tayarani-Najjaran M, Kroiss D, et al. Peptide-Based Supramolecular Systems Chemistry. Chem Rev. 2021;121(22):13869–914.

120. Bende NS, Dziemborowicz S, Herzig V, Ramanujam V, Brown GW, Bosmans F, et al. The insecticidal spider toxin SFI1 is a knottin peptide that blocks the pore of insect voltage-gated sodium channels via a large β-hairpin loop. FEBS Journal. 2015;282(5):904–20.

121. Vasudev PG, Aravinda S, Shamala N. Crystal structure of a tripeptide containing aminocyclododecane carboxylic acid: A supramolecular twisted parallel β-sheet in crystals. Journal of Peptide Science. 2016;22(3):166–73.

122. Vasudev PG, Chatterjee S, Narayanaswamy S, Padmanabhan B. Structural chemistry of peptides containing backbone expanded amino acid residues: Conformational features of β, γ, and hybrid peptides. Chem Rev. 2011;111(2):657–87.

123. Anishetty S, Pennathur G, Anishetty R. Tripeptide analysis of protein structures. 2002;8:1–8.

124. Moulton B, Zaworotko MJ. From molecules to crystal engineering: Supramolecular isomerism and polymorphism in network solids. Chem Rev. 2001;101(6):1629–58.

125. Marchesan S, Vargiu A V., Styan KE. The Phe-Phe motif for peptide self-assembly in nanomedicine. Molecules. 2015;20(11):19775–88.

126. Görbitz CH. The structure of nanotubes formed by diphenylalanine, the core recognition motif of Alzheimer's β-amyloid polypeptide. Chemical Communications. 2006;(22):2332–4.

127. Mahalakshmi R, Balaram P. The use of D-amino acids in peptide design. D-Amino Acids: A New Frontier in Amino Acid and Protein Research - Practical Methods and Protocols. 2007;(January 2007):415–30.

128. Saha I, Chatterjee B, Shamala N, Balaram P. Crystal structures of peptide enantiomers and racemates: Probing conformational diversity in heterochiral pro-pro sequences. Biopolymers - Peptide Science Section. 2008;90(4):537–43.

129. Nicholas S, Rizzoli C. Crystal structure of the tripeptide N-(benzyloxycarbonyl) glycylglycyl-L-norvaline. Acta Crystallogr Sect E Struct Rep Online. 2015;71(3):o216–7.

130. Giri RS, Mandal B. Formation of supramolecular single and double helix-like structures from designed tripeptides. CrystEngComm. 2019;21(37):5618–25.

131. Yeh MY, Huang CT, Lai TS, Chen FY, Chu NT, Tseng DTH, et al. Effect of Peptide Sequences on Supramolecular Interactions of Naphthaleneimide/Tripeptide Conjugates. Langmuir. 2016;32(30):7630–8.

132. Xie Y, Wang X, Huang R, Qi W, Wang Y, Su R, et al. Electrostatic and aromatic interaction-directed supramolecular self-assembly of a designed fmoc-tripeptide into helical nanoribbons. Langmuir. 2015;31(9):2885–94.

133. Wang H, Feng Z, Xu B. D-amino acid-containing supramolecular nanofibers for potential cancer therapeutics. Adv Drug Deliv Rev. 2017;110–111:102–11.

134. Yao J, Shang X, Shao N, He H, Wei J, Huang Y, Shen T, Chen L, Zhou Y, Chen W. Enantiomer-Dependent Supramolecular Antibacterial Therapy for Drug-Resistant Bacterial Keratitis. Langmuir. 2025 Feb 11;41(5):3356-3366.

135. Wani NA, Singh G, Shankar S, Sharma A, Katoch M, Rai R. Short hybrid peptides incorporating β- and γ-amino acids as antimicrobial agents. Peptides (NY) [Internet]. 2017;97:46–53.

136. Afrasiabi Z, Sinn E, Lin W, Ma Y, Campana C, Padhye S. Nickel (II) complexes of naphthaquinone thiosemicarbazone and semicarbazone: Synthesis, structure, spectroscopy, and biological activity. J Inorg Biochem. 2005;99(7):1526–31.

137. Towse CL, Hopping G, Vulovic I, Daggett V, Fersht A. Nature versus design: The conformational propensities of D-amino acids and the importance of side chain chirality. Protein Engineering, Design and Selection. 2014;27(11):447–55.

7. List of all Publications (Including manuscripts under communication)

1. Chaudhary, Sumit, Rama Nand Rai, **Deeti Jyothi**, Umesh Prasad Singh, and Abhinav Kumar. "Solid-State Green Synthesis of Two (1: 1) Organic Intermolecular compounds; their Physico-chemical, Thermal, Single Crystal Growth, and Atomic Packing Studies." *Materials Chemistry and Physics* (2024): 129541. https://doi.org/10.1016/j.matchemphys.2024.129541.
2. Chatterjee, Abhishek, Tapasi Roy, **Deeti Jyothi**, Vineet Kumar Mishra, Umesh Prasad Singh, and Snehasikta Swarnakar. "Melatonin Inhibits AGS Cell Proliferation by Binding to the ATP Binding Site of CDK2 Under Hyperglycemic Conditions." *Cell Biochemistry and Biophysics* (2024): 1-14. https://doi.org/10.1007/s12013-024-01241-9.
3. Pal, Purna Chandra, Sayoni Nag, **Deeti Jyothi**, Sudesna Das, Krishna Das Saha, and Umesh Prasad Singh. "Swietenolide isolated from Swietenia macrophylla King in Hook seeds shows in vitro anti-colorectal cancer activity through inhibition of mouse double minute 2 (MDM2) homolog." *Natural Product Research* 38, no. 12 (2024): 2097-2104. https://doi.org/10.1080/14786419.2023.2233045.
4. Chaudhary, Sumit, R. N. Rai, **Deeti Jyothi**, and Umesh Prasad Singh. "Solid state synthesis, thermal, spectral, optical, crystal structure and atomic packing studies of 2-(3-Hydroxyphenyl)-2, 3-dihydroquinazolin-4 (1H)-one." *Materials Letters* 341 (2023): 134253. https://doi.org/10.1016/j.matlet.2023.134253.
5. Shankar, Sudha, **Deeti Jyothi**, Junaid ur Rahim, Purna Chandra Pal, Umesh Prasad Singh, and Rajkishor Rai. "Conformation of Achiral α/β Hybrid Peptides Containing Glycine and 1-Aminocyclohexaneacetic Acid." *ChemistrySelect* 7, no. 10 (2022): e202104453. https://doi.org/10.1002/slct.202104453.

Materials Chemistry and Physics 322 (2024) 129541

Contents lists available at ScienceDirect

Materials Chemistry and Physics

journal homepage: www.elsevier.com/locate/matchemphys

Solid-state green synthesis of two (1:1) organic intermolecular compounds; their physico-chemical, thermal, single crystal growth, and atomic packing studies

Sumit Chaudhary [a], Rama Nand Rai [a,*], Deeti Jyothi [b], Umesh Prasad Singh [b], Abhinav Kumar [c]

[a] Department of Chemistry, Institute of Science, Banaras Hindu University, Varanasi, 221005, India
[b] CSIR-Indian Institute of Chemical Biology 4, Raja, S.C, Mullick Road, Kolkata, 700032, India
[c] Department of Chemistry, Faculty of Science, University of Lucknow, Lucknow, 226 007, India

HIGHLIGHTS

- Two novel IMCs have been synthesized using solid-state green synthesis.
- Phase diagram study specifies the formation of 1:1 IMC along with two eutectics.
- ANDMAB is a racemic mixture and infers two crystal phases simultaneously.
- Both IMCs (ANDMAB and DMABCNBA) crystallize in triclinic $P\bar{1}$ space group.
- DMABCNBA crystal packing shows peculiar interaction likewise the graphite.

GRAPHICAL ABSTRACT

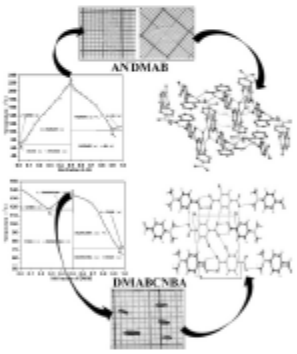

ARTICLE INFO

Keywords:
Solvent free reaction
Phase diagram
Intermolecular compound
Co-crystal
Crystal growth

ABSTRACT

The solid-state solvent free reaction method has been adopted for the one-pot synthesis of novel organic materials with utmost 100 % yield. To identify the composition forming the intermolecular compound (IMC), the solid-liquid equilibria of entire compositions have been studied by establishing the phase diagram of n, n-dimethylaminobenzaldehyde (DMAB) with anthranilamide (AN) and 2-chloro-4-nitro benzoic acid (CNBA). The structural changes and novelty of the IMCs to that of parents are studied using FTIR, NMR and X-ray diffraction. The studies of optical properties of intermolecular compounds using UV-vis absorption and fluorescence spectroscopy infer the significant fluorescence emission. The single crystals of both intermolecular compounds, ANDMAB and DMABCNBA, are grown from solution using slow evaporation technique. The single crystal X-ray diffraction studies reveal that IMC of AN and DMAB is a racemic mixture whereas IMC of DMAB and CNBA is a co-crystal, and both the crystals have crystallized in triclinic $P\bar{1}$ space group. The thermal stability and thermal

* Corresponding author.
E-mail address: rn_rai@yahoo.co.in (R.N. Rai).

https://doi.org/10.1016/j.matchemphys.2024.129541
Received 11 February 2024; Received in revised form 12 May 2024; Accepted 1 June 2024
Available online 2 June 2024

Cell Biochemistry and Biophysics
https://doi.org/10.1007/s12013-024-01241-9

ORIGINAL PAPER

Melatonin Inhibits AGS Cell Proliferation by Binding to the ATP Binding Site of CDK2 Under Hyperglycemic Conditions

Abhishek Chatterjee[1] · Tapasi Roy[1] · Deeti Jyothi[1] · Vineet Kumar Mishra[1] · Umesh Prasad Singh[1] · Snehasikta Swarnakar[1]

Received: 24 January 2024 / Accepted: 21 February 2024

Abstract

Cancer cells utilize glucose as their primary energy source. The aggressive nature of cancer cells is therefore enhanced in hyperglycemic conditions. This study has been adopted to investigate the therapeutic potential of melatonin against such aggressive proliferation of AGS cells–a human gastric cancer cell line, under hyperglycemic conditions. AGS cells were incubated with high glucose-containing media, and the effects of melatonin have been evaluated, therein. Cell proliferation, ROS generation, flow-cytometric analysis for cell cycle and apoptosis, wound healing, immunoblotting, zymography, reverse zymography assays, in-silico analysis, and kinase activity assays were performed to evaluate the effects of melatonin. We observed that melatonin inhibited the hyperglycemia-induced cell proliferation in a dose-dependent manner. It further altered the expression and activity of MMP-9 and TIMP-1. Moreover, melatonin inhibited AGS cell proliferation by arresting AGS cells in the G_0/G_1 phase after binding in the ATP binding site of CDK-2, thereby inhibiting its kinase activity. In association, a significant decrease in the expression of cyclin D1, cyclin E, CDK-4, and CDK-2 were observed. In conclusion, these findings suggest that melatonin has anti-gastric cancer potential. Melatonin could therefore be included in future drug designs for gastric cancer-hyperglycemia co-morbidity treatment.

✉ Snehasikta Swarnakar
snehasiktaiichidi@gmail.com

[1] Infectious Diseases and Immunology division, CSIR-Indian Institute of Chemical Biology, 4, Raja S.C. Mullick Road, Kolkata 700032 West Bengal, India

Natural Product Research

Formerly Natural Product Letters

ISSN: (Print) (Online) Journal homepage: https://www.tandfonline.com/loi/gnpl20

Swietenolide isolated from *Swietenia macrophylla* King in Hook seeds shows *in vitro* anti-colorectal cancer activity through inhibition of mouse double minute 2 (MDM2) homolog

Purna Chandra Pal, Sayoni Nag, Deeti Jyothi, Sudesna Das, Krishna Das Saha & Umesh Prasad Singh

To cite this article: Purna Chandra Pal, Sayoni Nag, Deeti Jyothi, Sudesna Das, Krishna Das Saha & Umesh Prasad Singh (14 Jul 2023): Swietenolide isolated from *Swietenia macrophylla* King in Hook seeds shows *in vitro* anti-colorectal cancer activity through inhibition of mouse double minute 2 (MDM2) homolog, Natural Product Research, DOI: 10.1080/14786419.2023.2233045

To link to this article: https://doi.org/10.1080/14786419.2023.2233045

Materials Letters 341 (2023) 134253

Contents lists available at ScienceDirect

Materials Letters

journal homepage: www.elsevier.com/locate/matlet

Solid state synthesis, thermal, spectral, optical, crystal structure and atomic packing studies of 2-(3-Hydroxyphenyl)-2,3-dihydroquinazolin-4(1H)-one

Sumit Chaudhary [a], R.N. Rai [a,*], Deeti Jyothi [b], Umesh Prasad Singh [b]

[a] Department of Chemistry, Institute of Science, Banaras Hindu University, Varanasi 221005, India
[b] CSIR-Indian Institute of Chemical Biology, Mullick Road, Kolkata 700032, India

ARTICLE INFO

Keywords:
Phase diagram
Solid state synthesis
Fluorescence
Optical
Single crystal growth
Single Crystal XRD

ABSTRACT

The environment friendly solid state synthesis is adopted for the synthesis of molecular complex, 2-(3-Hydroxyphenyl)-2,3-dihydroquinazolin-4(1H)-one, (ANHB) with utmost yield. The phase diagram (PD) of anthranilamide (AN) − 3-hydroxybenzaldehyde (HB) system gives the compositional behavior of composites in the entire range, and has identified the formation of two eutectics and a molecular complex. The novelty and structural behavior of ANHB was studied using FTIR, NMR, UV–vis, fluorescence, DSC and PXRD techniques. The various thermodynamic characterizations of eutectics and complex are done using the heat of fusion values obtained from DSC. The single crystal XRD (SCXRD) and atomic packing studies of grown ANHB crystal infer that ANHB crystallizes in centro-symmetric triclinic space group $P\bar{1}$ with two molecules in the asymmetric unit and four molecules in the unit cell. The synthesized complex shows fluorescence emission in visible region.

1. Introduction

Quinazolinone is naturally occurring alkaloid found in bioactive natural products with several biological activities [1], and its derivatives are potential pharmaceutical agents [2–6]. Due to significant importance, several methods have been used for cyclocondensation of anthranilamide with aromatic aldehydes in the presence of various catalysts [7–12]. Some methods show tedious limitations, such as, the use of excess solvents, expensive catalysts and particularly low yield. Therefore, the solvent free solid-state synthesis route has been adopted which has its own advantages being environment friendly, and economical. Furthermore, the study of PD provides the valuable information about the nature of binary composites in the entire compositions. The PD identifies the stoichiometry ratio of complex having novel behavior, and helps in synthesis of material with utmost 100% yield. The PD study has immense importance in crystal growth as it gives idea about nature of binary materials, melting temperature, change in behavior of compositional and stoichiometry composition forming the complex [13,14]. The investigations on PD, molecular complexation, particularly between medicinally known compounds, hydrogen bonded crystals are found to be worth to yield the promising materials [15,16].

Anthranilamide has three donor centers, nitrogen of the amine and nitrogen and oxygen of the amide group for bonding and has significantly used as a fluorescence label for the visualization of oligosaccharide [17]. 3-Hydroxybenzaldehyde belongs to orthorhombic crystal [18], and shows vasculoprotective potency and antibacterial activity [19,20].

With a view to synthesize the material via solid-state synthesis, AN (donor) and HB (acceptor) were selected. The compositions of eutectics and molecular complex were determined by the study of PD of the binary system. The synthesized ANHB complex was studied by spectral, thermal and XRD techniques. The single crystal of ANHB was grown from mixed solution and evaporation technique. The crystal structure and atomic packing of ANHB was studied by SCXRD. The studies of phase diagram, thermal properties, single crystal growth and SCXRD along with atomic packing are being communicated. However, the studies on the medicinal properties of the system are in progress.

2. Experimental

The purities of AN (98%) and HB (99%), procured from Sigma-Aldrich, Germany, were verified by melting points and NMR studies [21]. The PD of AN-HB system was established in temperature-composition curve [22]. The thermal behaviors were studied using DSC (Mettler DSC-4000). For spectral studies Perkin Elmer FTIR and JNM-ECZ500R/S1 500 MHz NMR were used. Rigaku Powder

* Corresponding author.
E-mail address: rnrai@bhu.ac.in (R.N. Rai).

https://doi.org/10.1016/j.matlet.2023.134253
Received 16 July 2022; Received in revised form 20 February 2023; Accepted 18 March 2023
Available online 21 March 2023

ChemistrySelect

Research Article
doi.org/10.1002/slct.202104453

Chemistry Europe
European Chemical Societies Publishing

www.chemistryselect.org

Organic & Supramolecular Chemistry

Conformation of Achiral α/β Hybrid Peptides Containing Glycine and 1-Aminocyclohexaneacetic Acid

Sudha Shankar,[a, b] Deeti Jyothi,[c] Junaid ur Rahim,[a, b] Purna Chandra Pal,[c] Umesh Prasad Singh,*[b, c] and Rajkishor Rai*[a, b]

The present work describes the conformation of achiral α/β hybrid peptides, Boc-Gly-$\beta^{2,3}$-Ac_6c-NHMe (**P1**), Boc-Gly-$\beta^{2,3}$-Ac_6c-Gly-OMe (**P2**), and Boc-Gly-$\beta^{2,3}$-Ac_6c-Gly-$\beta^{2,3}$-Ac_6c-OMe, (**P3**) using X-ray crystallography. Peptides **P1** and **P2** adopt C_{11} and C_{12} folded conformations, respectively. The directionality of the hydrogen bond observed in **P1** is opposite to that observed in peptide **P2**. In case of tetrapeptide **P3**, no such hydrogen bond is observed. Further, the solvent titration experiment establishes the similar intramolecular hydrogen bonding as observed in the crystals. In **P1** and **P2**, the amino group of $\beta^{2,3}$-Ac_6c occupies equatorial orientations, while in the case of peptide **P3**, it occupies axial and equatorial orientations for residues $\beta^{2,3}$-$Ac_6c(2)$ and $\beta^{2,3}$-$Ac_6c(4)$, respectively. The average (ϕ,θ,ψ) torsional preferences of $\beta^{2,3}$-Ac_6c in achiral α/β peptides are somewhat different from that of chiral α/β peptides.

The peptides containing β-amino acids have a strong propensity to fold into well-defined stable conformations.[1–5] The insertion of β-amino acid into α-peptide sequences facilitates varieties of folded structures.[6–11] The choice of β-amino acids determines the hydrogen bonding patterns in α/β-hybrid peptide sequences.[12–16] C_{11} and C_{14}/C_{15}-helical conformations have been observed in the crystal structure of octapeptide containing achiral α-aminoisobutyric acid (Aib) and *trans*-2-aminocyclopentanecarboxylic acid (ACPC).[17–19] C_{14}/C_{15} helical conformation has also been reported in the peptide containing Aib and acyclic β-amino acids.[20] The α/β-hybrid peptides containing alternating cis-2-aminocyclohexanecarboxylic acid, cis-2-aminocyclohex-4-enecarboxylic acid, and cis-2-aminocyclooctanecarboxylic acid (cis-ACOC) with alanine exhibited the C_{11}/C_9-helical conformation.[21–23] Legrand *et al.* reported the C_{11}/C_9 helix in the crystals of α/β- peptides containing α-amino acid and $\beta^{2,2,3}$-trisubstituted bicyclic amino acid, (*S*)1-aminobicyclo[2.2.2]octane-2-carboxylic acid.[24] The helical folds with C_{11} as well as C_{11}/C_9 hydrogen bonding patterns have been reported in α/β-hybrid peptides containing 1-(aminomethyl)cyclohexane carboxylic acid ($\beta^{2,3}$-Ac_6c)[25,26] and 1-aminocyclohexaneacetic acid ($\beta^{2,3}$-Ac_6c).[27–30] There are few examples of internally hydrogen-bonded conformations in peptides containing β,β-disubstituted-β-amino acid, $\beta^{2,2}$-Ac_6c.

Herein, we describe the synthesis and characterization of achiral α/β-hybrid peptides containing $\beta^{2,2}$-Ac_6c, Boc-Gly-$\beta^{2,2}$-Ac_6c-NHMe, **P1**; Boc-Gly-$\beta^{2,2}$-Ac_6c-Gly-OMe, **P2**; and Boc-(Gly-$\beta^{2,2}$-$Ac_6c)_2$-OMe, **P3** (Figure 1). The design of peptide **P1** is based on the previously reported peptide Piv-Pro-$\beta^{2,2}$-Ac_6c-NHMe,[27] in which Pro is replaced with Gly, while the design of **P2** and **P3** is based on the peptide sequence Boc-Leu-$\beta^{2,2}$-Ac_6c-Leu-$\beta^{2,2}$-Ac_6c-OMe,[30] in which Leu is replaced with Gly residue, which is the most conformationally flexible amino acid. In this study, we aimed to investigate the effect of conformationally flexible achiral glycine residue on the backbone conformation in α/β-hybrid peptides.

The peptides **P1**–**P3** were synthesized in the solution phase using EDC/HOBt (Schemes 1–3, Supporting Information) and the molecular conformation of α/β hybrid peptides **P1**–**P3** was determined by X-ray diffraction. Peptide **P1** was crystallized in orthorhombic space group *Pbca* with two molecules in the asymmetric unit, while **P2** and **P3** were crystallized in triclinic

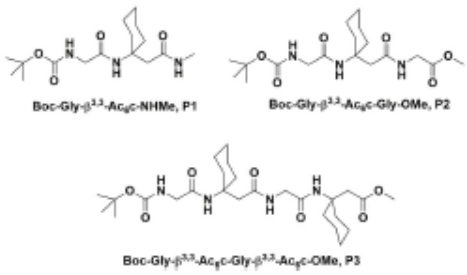

Figure 1. Chemical structure of Boc-Gly-$\beta^{2,2}$-Ac_6c-NHMe, **P1**; Boc-Gly-$\beta^{2,2}$-Ac_6c-Gly-OMe, **P2**, and Boc-Gly-$\beta^{2,2}$-Ac_6c-Gly-$\beta^{2,2}$-Ac_6c-OMe, **P3**.

[a] *Dr. S. Shankar, J. u. Rahim, Dr. R. Rai*
Natural Products & Medicinal Chemistry Division (NPMC), CSIR-Indian Institute of Integrative Medicine (CSIR-IIIM), Jammu-180001, India
E-mail: raj@iiim.res.in
[b] *Dr. S. Shankar, J. u. Rahim, Dr. U. P. Singh, Dr. R. Rai*
Academy of Scientific and Innovative Research (AcSIR), Ghaziabad-201002, India
[c] *D. Jyothi, P. C. Pal, Dr. U. P. Singh*
CSIR-Indian Institute of Chemical Biology (CSIR-IICB), Kolkata-700032, India
E-mail: umesh.singh@iicb.res.in

Supporting information for this article is available on the WWW under https://doi.org/10.1002/slct.202104453